BIOLOGICAL FIBRES

MECHANICAL PROPERTIES OF BIOLOGICAL MATERIALS
PRACTICALLY ONE DIMENSIONAL

Manuel Elices - Gustavo V. Guinea

Translated by John Morton.
The authors wish to express their appreciation to Dr. John Morton for his helpful collaboration on the translation.

ISBN: ?????
Depósito legal: M-?????-2019

Design and layout: Albatros Comunicación, S.L.

Index

1 CHAPTER Biological fibres. General concepts

1.1. INTRODUCTION

The vast majority of biological materials, and in particular all those with a structural (load bearing) function, are formed of fibres because, either on their own or as reinforcement in an organic or inorganic matrix, they constitute unidirectional elements, 1D (tendons for example) two-dimensional, 2D (membranes, such as the pericardium) or three-dimensional 3D (such as bone), with a variety of properties not yet achievable in artificial materials.

In this section the mechanical properties of biological materials which are essentially unidirectional (along the length of the fibres) are analysed. This assumption simplifies the mathematical treatment not only for the interpretation of the tests performed on the materials but also the modelling of their behaviour.

Fibres produced by animals or plants are much more complex than artifical fibres. This is hardly surprising since biological fibres are often multifunctional and possess hierachical structures. Plant fibres such as cotton, linen, hemp or wood fibres are **polysaccharides,** basically cellulose[1] materials, while animal-produced fibres, such as wool, silk and tendon are **polypeptides** amino acid polymers.

[1] In 1838, Anselme Payen suggested that the walls of many plant cells were formed of the same substance, which he called cellulose. Cellulose is a linear polymer of linked D-glucose units.

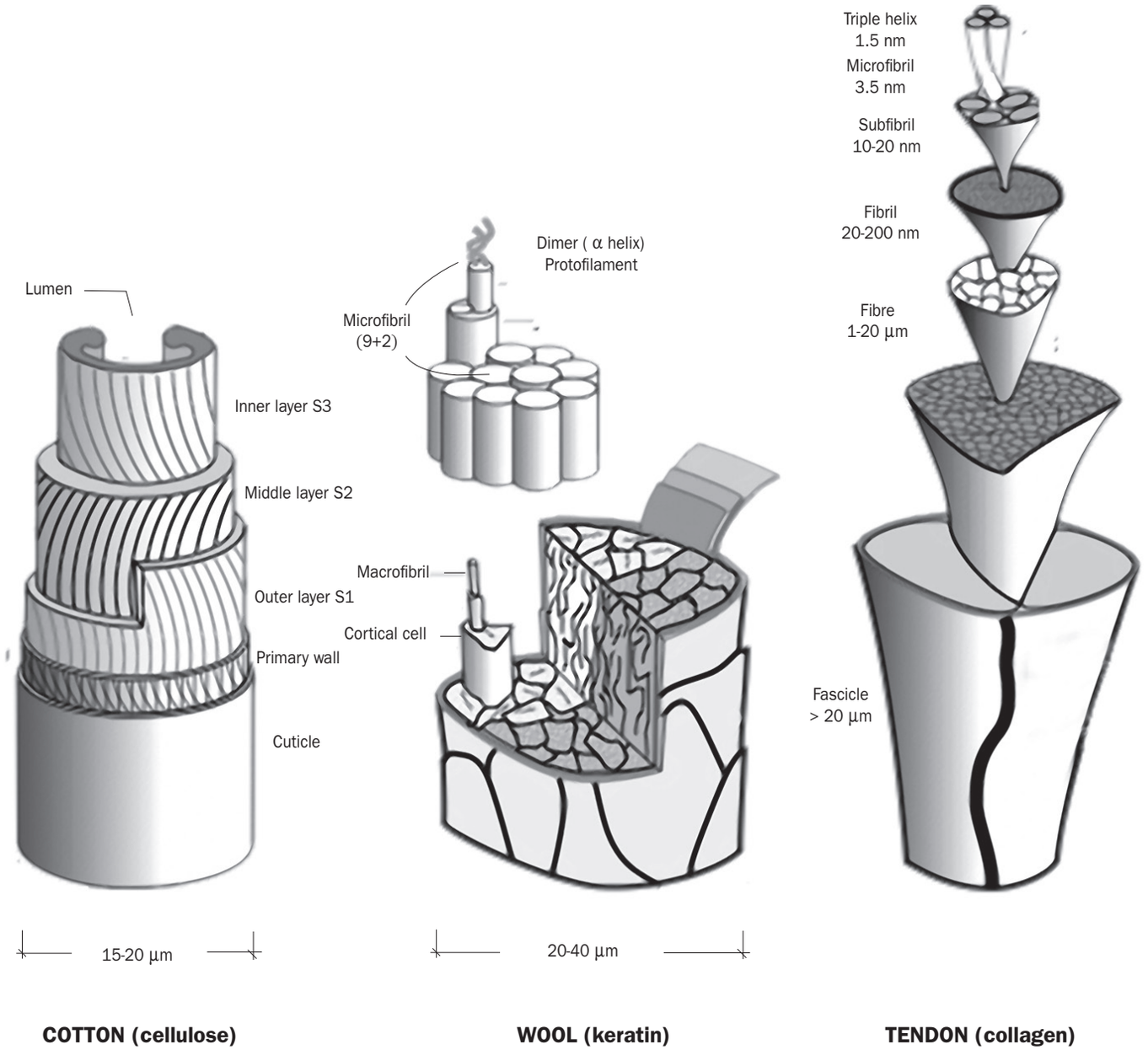

Fig. 1. *Hierarchical structure of several biological fibres*

The hierarchical structure of various fibres; cotton, wool and tendon are shown in figure 1. In biological materials, hierachical structures can encompass many orders of magnitude; in a muscle, from the diameter of a tropocollagen fibril (10^{-9} m) to the diameter of a tendon (10^{-2} m) or, in the case of a tree, from the diameter of a cellulose fibre (10^{-9} m) to the diameter of a giant sequoya (10 m). Stiffness, strength and other mechaniclal properties are controlled and optimised by the interaction between the various hierachical structures, to such an extent that it is very often difficult to distinguish between the material and the structure, which hugely complicates the development of models for the behaviour (constitutive equations) of these fibres.

Fibres produced from **plants** have the advantages of low cost, are biodegradable, are readily available, low density and reasonable mechanical properties. In plants they perform several functions, but principally they play a structural role –providing support to stems and leaves– which allows them to carry out their own functions and to withstand inclement weather. Another characteristic of vegetable fibres is their capacity to absorb moisture, since cellulose –which is hygroscopic– is a major component. This absorption changes their weight, dimensions and mechanical properties, as will be commented upon later.

Fibres from the **animal kingdom** can be considered, in a very simplified form, as being composed of proteins –aligned to the axis of the fibre– embedded in a proteic matrix. *Keratin* fibres are the principal component of skin, wool and bird feathers. Keratin is rich in cysteine –an amino acid containing sulphur– which produces the characteristic smell when these fibres are burned. Structures based on keratin can be very strong, such as rhinoceros horn, and very flexible, such as human hair. Silk fibres produced by silkworms and spiders also contribute structurally; they form the cocoons of the silkworms and the threads of spider webs, whose tenacity has not been surpassed by artificial fibres. *Collagen* fibres are the most abundant structural component of the extracellular matrix of vertebrates and invertebrates and principal ingredient of tendons and ligaments.

Biological fibres have many industrial applications, as well as being important in the textile sector. They are environmentally friendly, renewable and have sufficiently good mechanical properties for many applications –resistant to impact and low density– which make them useful, for example, in the automotive sector (*Mercedes-Benz* E Class cars use them in several components) and in geotextiles, to stabilise floors and banks. Silkworm fibres, whose principal destiny is the textile industry, is used in biomedicine for sutures and, recently, to make scaffolds in tissue engineering. Spider silk fibres are opening promising applications due to their extraordinary tenacity. Collagen fibres have numerous uses in medicine, bioengineering and in the cosmetics and food industries. Their excellent mechanical and biological properties place them at the forefront of future biomaterials.

The aim of this book is to describe the mechanical properties of biological fibres, and their possible applications for structural purposes.

In the first chapter a short summary of the principal natural fibres –polymers– both of vegetable and animal origin, is presented.

In order to characterise the mechanical behaviour of fibres, it is essential to test them, record the results and to know how to interpret them. The second chapters is dedicated to that end.

First, the most common mechanical tests are described in detail; tensile and torsion tests, the former being the more frequently employed.

The interpretation of the results is not without difficulty with these biological materials, because they can undergo large deformations and the response to a stimulus can depend upon time and the load history. This behaviour falls within the field of visco-elasto-plasticity whose mathematical treatment is quite complex.

In order to facilitate the interpretation of the experimental results, to be able to model the material and make reliable predictions, studies have been centred around several elemental behaviours; **Hookean elastic, elastomeric,** and **linear viscoelastic.** It must be remembered that the conclusions derived from these studies are only valid within the bounds of the assumptions made previously.

In the third chapter, four examples of fibres are presented; one of vegetable origin (cotton) and three of animal origin (wool, silk and collagen). In all of these a brief description of the structure, mechanical properties and possible applications are given.

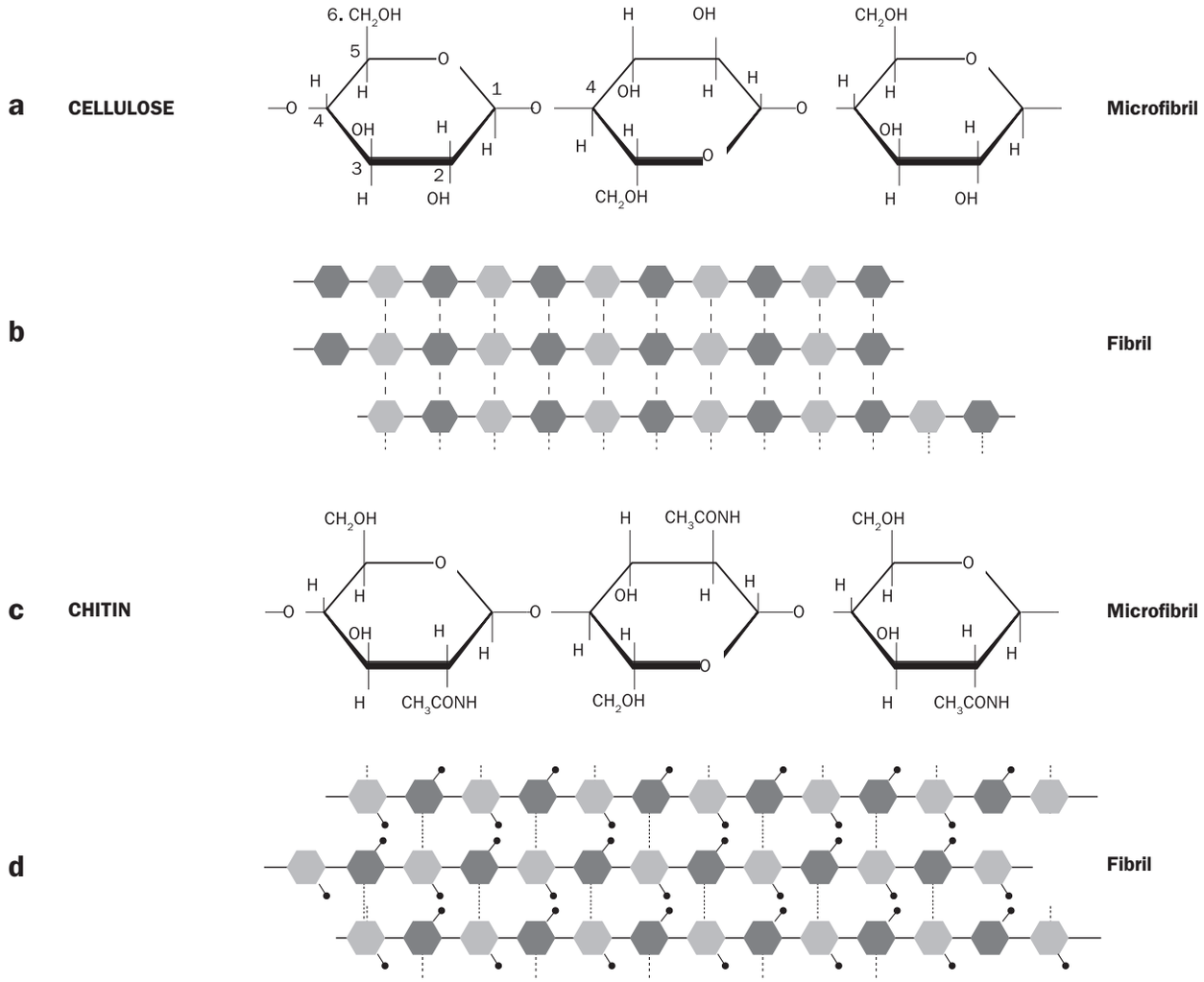

Fig. 2. *Structure of cellulose (a), and chitin (b) fibres.*

1.2. POLYSACCHARIDE FIBRES

Polysaccharides are natural polymers made up of a large number of monosaccharides (carbohydrates) connected by acetal links. The most common fibres are *cellulose* and *chitin,* both of which have similar primary structures, as shown in figure 2. Cellulose is formed of D- glucose monomers which condense through β (1→4) glycosidic bonds (the plane of the monomer rotates 1 8 0 °) between 1 and 4 carbons. Cellulose is present in the cell walls of plants, in most algae and some classes of mushroom. Chitin is formed of N-acetylglucosamine units and is found in the cell walls of fungi, yeast and arthopods, as well as in the exoskeletons of the last mentioned.

1.2.1. Cellulose fibres

Cellulose is the most abundant naturally occurring polymer and is the structural component in plant cell walls.

The most stable form of cellulose is shown in figure 2a, a configuration that allows the formation of long straight chains. In this structure, all the hydroxyl groups (-OH) can form hydrogen bonds, both within and between molecules. This promotes the creation of highly stable supramolecular fibres with excellent mechanical properties.

The fibril elements of cellulose have a diameter of 3.5 nm and are about 30 nm long, typically formed of 40 or so molecules [Vincent 1990]. When ordered into groups they form small monoclinic crystals, with parameters: a = 0.835 nm, b= 1.03 nm, c = 0.79 nm [Bledzki, Gassan 1999].

The fibrils are arranged in different forms around the axis of the fibre creating a hierarchical structure. In a mature cotton fibre six distinct levels can be observed. (figure 1a): the cuticle, the primary wall, outer layer S1, the secondary wall or middle layer S2, the lumen wall or inner layer S3 and the sixth level is the lumen itself, a channel that runs along the centre of the fibre.

Cellulose fibers in general are used as reinforcement for composite materials (Bledzki, Gassan, 1999, for instance).

Cotton fibre contains more than 90% cellulose. Generally, cellulose is associated with other amorphous polymers of lignin (polyphenol) and hemicelluloses (polysaccharides of glucose, galactose and fructose). For example wood contains between 40-55% cellulose, 15-35% lignin and 25-40% hemicellulose.

As a result of the variation in their specific components the differences between vegetable fibres lies more in the micro- and macrostructure of the fibres than in their chemical composition.

1.2.2. Chitin fibres

After cellulose, chitin is the most abundant naturally occurring polymer. It forms part of the cell walls of mushrooms and yeast, mollusc shells and the exoskeletons of arthopods and other invertebrates. Chitin takes its name from the Greek *chitón* (meaning tunic or or robe).

The microfibril elements of chitin have a diameter of about 3 nm and are typically formed of 20 or so molecules reaching a length of up to 300 nm [Vincent 1990]. The dominant acetic group (–CO-CH_3) promotes the formation of a large number of hydrogen bonds between the molecules which is difficult in cellulose, because if its size, and relative mobilty of the fibres. For these reasons the stiffness of chitin is greater than that of cellulose.

1.3. POLYPEPTIDE FIBRES

Polypeptides are amino acids (figure 3a). The joints between the amino acids are achieved through peptide links in which the nitrogen of an amino acid is connected to the carbonyl group (–CO–) of an amino acid and releasing water (figure 3b). Most natural polypeptides are a syntesis of the twenty naturally occurring amino acids, and which are given in the Appendix. The difference between them lies in the R (residue) group, linked to the central carbon of the amino acid, or carbon α (C^{α}) whose position is shown in figure 3a. A typical protein can contain about 500 amino acids although some can have as many as 6000.

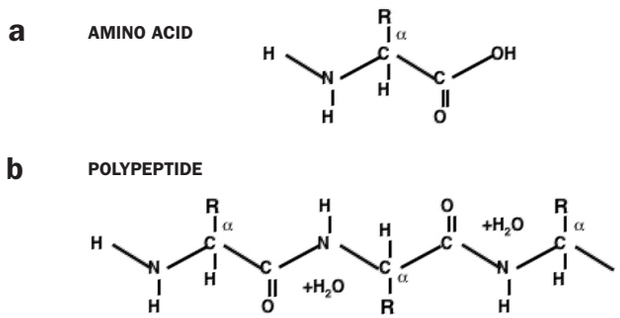

Fig. 3. *The basic structure of amino acid. R (the residue) represents the side group that characterises each amino acid.*
b. Polymerisation (by condensation) of three amino acids.

There are several families of protein fibres of significant structural relevance; *keratins*, proteins that contain sulphur and are the principal component of hair and wool, silks, produced by silkworms and spiders, *collagen* fibres, that constitute tissue in most animals, and *actin* and *myosin* fibres that form muscles. Other important protein fibres are; elastin, usually associated with collagen, *abductin*, that occurs in the ligament of the hinge of bivalves and *resilin*, that is found in some insects and arthopds.

1.3.1. Keratin fibres

There are many types of keratin fibres, all of which are characterised by their high cysteine content, amino acid containing sulphur (–SH) and capable of forming disulphide bridges (–S– S–) with other molcules. The sulphur present gives a characteristic odour in burnt fibres. One way of classifying them is in terms of the type of the animal in which they are found; keratin in mammals (hair, wool…), in birds (feathers) and in other animals (reptiles, among others). A wool fibre has an almost circular cross section with a diameter ranging from 20 to 40 microns and length between 5 and 50 cm (figure 1b). Human hair has a diameter of about 70 microns.

The structure of wool fibre is very complicated. The smallest unit is the α-*helix* that forms the dimer (figure 1b). The second hierarchical level is the *protofibril* or *protofilament*, formed by two double helices. The next level of complexity is the microfibril, formed of various protofibrils. The fibres are formed by the superposition of *microfibril*s, reinforced by hydrogen bonds and sulphur bridges, giving way to *macrofibril*s that, in turn, are grouped into the cortical cell.

The properties of the fibres depend upon the nature and number of crosslinks between fibres and are very sensitive to the ambient humidity. Indeed ancient weather sensors were based upon changes in the flexibilty of hair with humidity.

1.3.2.Silk fibres

Silk fibres are produced in particular glands of some creatures. They are of great interest owing to their biosynthesis, processing and functional properties. Silks have different compositions, structures and properties depending upon the animal and glands that produce them. The silks that have been most studied are those of the silkworm *(Bombix mori)* and some spiders *(Nephila, Araneus* and *Argiope).*

The silkworm cocoon thread –whose diameters range from 10 to 25 microns– contain structural proteins; the heavy fibroin chain (about 325 kDa) and lighter chain (about 25 kDa), more a sericin protein system (between 20 kDa and 310 kDa) that surrounds the fibroins and behaves like a glue between the different threads. The sericins are more hydrophilic than the fibroins, which is why they are more easily eliminated when the cucoon is boiled in an alkaline solution, a step known as degumming, and which allows later spinning of the fibroin filaments.

Orb-weaver spiders produce silk thread in diiferent glands in the their abdomens, according to its purpose; mooring and security threads, circular web threads, threads to wrap the prey, cocoons, etc. In general, the diameter of these fibres –between 2 and 5 microns– is less than that of silkworms. In particular, the security threads of spiders contain two proteins; one called MASp1 (for Major Ampullate Silk proteins, spidroin 1) with a molcular mass of 275 kDa, and the other, called MASp2, with a molcular mass and composition similar to the former.

The most common amino acids in webs are alanine (A) and glycine (G) that constitute 70% of the total, followed by tyrosine (Y), leucine (L), glutamine (Q), proline (P) and valine (V). These polypeptides are characterised by highly repetitive sequencing (AAA…, GGXGGX…) that makes them difficult to manipulate biochemically.

Despite being a material of great scientific and technological, interest, there is still little that is known about the structure and organisation of silk fibre.

1.3.3. Collagen fibres

Collagen is the most important protein fibre in the animal kingdom; it is the most common structural component in the extracellular matrix of vertebrates, invertebrates and sponges, and the principal component of tendons and ligaments (tendon connects the muscle to the bone and ligament joins one bone to another). Collagen is a generic term used to describe a variety of polypeptides composed essentially of glycine, proline and hydroxyproline, having the triple helix in common as an elementary component as shown in figure 1c). To date, more that 20 distinct families of collagen have been identified (with each type denoted by a roman numeral). Each family is distributed among particular tissues, having a specific function and characteristic structure with a different size of the triple helix domain.

Types of collagen I, II, III and IV are the most abundant (Kadler 1994). Type I collagen is found in a tendons, liagaments, bones and in the cornea, representing approximately 90% of the collagen in the body. Type II collagen forms the fibrils of cartilage and the notochord. Type III is present in the fibrils of blood vessels and skin. Type IV collagen appears in the basement membrane of the epithelium, forming a sort of molecular filter with protection and absorption functions.

The mechanical properties of collagen depend upon the diameter of the fibrils, the nature and number of crosslinks between molecules, the structural hierarchy of the fibrils and the interaction with other components of the matrix in which they are embedded. In tendon, the fibril diameter varies widely –between 50 and 500 nm– and are connected by numerous crosslinks and bundled to form fibres of diameter between 1 and 20 microns. The fibres, in turn, are bunded to form fascicles, as shown in figure 1c. This highly aligned structure is responsible for the excellent mechanical properties of tendons.

1.3.4. Actine and myosine fibres

Actine and myosine are the principal protein fibres in muscles. These stretch and contract thanks to a gliding and gripping mechanism between the actine and myosine fibres as shown schematically in figure 4. The thicker myosine possesses heads that join and unlock the thinner actine fibres as it moves, providing a relative displacement mechanism –similar to a rowing action– the origin of contraction and distension of muscle fibre.*

The structure of muscle is hierarchical, as shown in figure 4. Actine and myosine fibres form the basic unit called the *sarcomere*. These, in turn, are organised into microfibrils, and bundles of microfibrils to form muscle fibres (figure 4). Examination of the muscle, reveals characteristic striations, called Z-discs or Z-lines, that are the junctions between the sarcomeres. The actine filaments are fixed to the Z-discs, while the myosine can glide parallel to the actine thanks to the mechanism outlined above. The sarcomeres of vertebrates are about 1.5 microns long when fully contracted but can reach double that size when stretched.

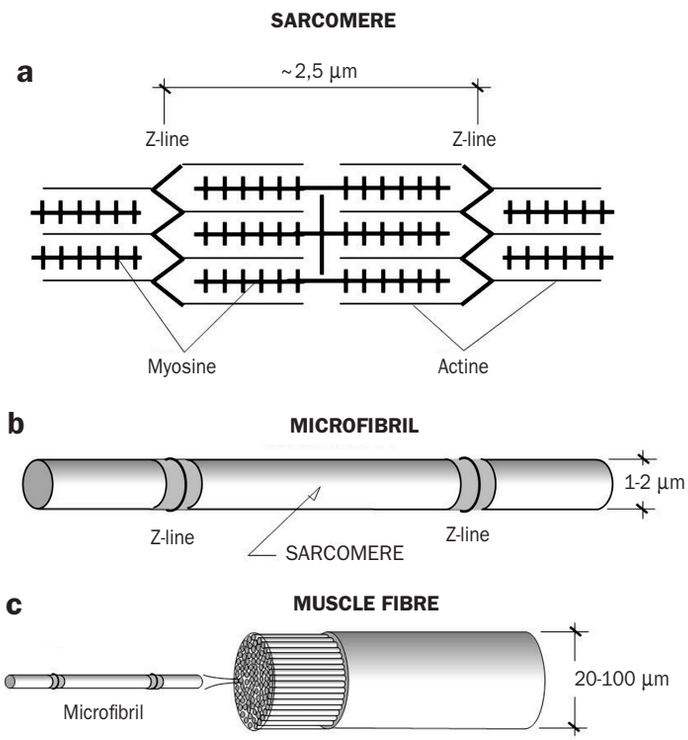

Fig. 4. *Structure of a muscle fibre.*
a. Sarcomere.
b. Microfibril.
c. Fibre.

* http://www.nature.com/nature/journal/v468/n7320/extref/nature 09450-s2.mov

1.3.5. Elastin, resilin and abductin

These fibres exhibit an elastomeric behaviour, similar to rubber and other elastic materials, (the *elastomeric* concept will be expanded upon later in the study of the mechanical properties of materials).

Elastin is a very stable insoluble protein rich in valine, glycine, alanine and proline with VPVGP being the most recurrent motif. It is present only in vertebrates, in elastic organs such as the walls of arteries and veins, in skin, and in the lungs. The ligament in the nape of ungulates is an organ rich in elastin; a kind of rope that runs along the upper part of the neck and which is always in tension, allowing the animals to keep their heads raised without the constant aid of their muscles.

Resilin is found in arthopods and is used to store and release elastic energy; insects use it in the elastic joints of their wings, and grasshoppers at the base of their hind legs, as a catapult when jumping. the reason for this is the recurrent GGRPSDSYGAPGGGN sequence.

Abductin occurs in the internal ligaments of the shells of bivalve molluscs, in which they act in opposition to the adductor muscles in the mollusc. The reason for this is the repeted FGGMGGGNAG sequence.

Abductin, like resilin, recovers elastic energy stored during deformation when the fibre is unloaded. Thanks to this phenomenon very little energy is dissipated, principally taking the form of heat in each unloading cycle. This permits not only great efficiency in flight, or in jumping, but it also avoids an overheating that could prove fatal.

1.4. CONCLUDING REMARKS

Following this brief introduction it might be thought that disentangling the relationships between the **microstructure** and **mechanical behaviour** of biological fibres is no easy task. The structure of natural fibres is complex because it is so hierarchical and when attempts are made to relate it to the mechanical response it is not easy to identify the most relevant aspects. On the other hand, the mechanical behaviour is also complex because these materials often sustain large deformations, which means that, in many cases, the theory of linear elasticity cannot be applied. Moreover, the deformations can depend upon time, temperature and humidity, among other parameters, making analysis even more difficult.

However, it is possible to add some order to these ideas and to propose simple, but realistic, models that allow an understanding of these materials and, in some cases, make predictions about their response to external mechanical stimuli. In general, for amorphous polymers, the most important variables that must be considered are the **duration of the stimulus** and the **temperature.**

When these materials are subjected to very fast actions, or tested at low temperatures, they demonstrate a rigid response, similar to a conventional solid. In this situation the molecular chains move with difficulty and the structure of the material remains essentially unchanged . The material deforms while maintaining the relative positions of their components and, as will be seen later, the change in internal energy due to the deformation governs its response. This situation is termed the glassy state and is usually studied –for small reversible deformations– applying models of **elastic behaviour.**

At high temperatures or when the tests are slow enough to allow molecular movement, the chains reorganise themselves during loading, producing a complex time-dependent response, which results in *hysteresis* phenomena (that is to say, the loading response is different from that which is observed during unloading), *creep* (the deformation increases with temperature although the load is held constant) and *relaxation* (material subjected to constant deformation sustains a gradually reducing force). When the deformations are not too great and can be considered reversible these phenomena can be approximated to **viscoelastic behaviour.**

If due to the temperature or other conditions (such as the presence of solvents that weaken the molecular interactions) the mobility of the chains is greatly facilitated or, also, if the load is applied in experiments over times much longer than that needed for molecular reorganisation, these materials demonstrate elastic behaviour (that is to say, there is always a one-to-one correspondence between the load and applied deformation, and the material recovers its original dimensions on unloading) although this may be non-linear on account of the large deformations sustained. In these circumstances the material is said to exhibit **elastomeric behaviour,** with a change in entropy (that is, its internal organisation) being principally responsible for this response.

The simplest representation of these concepts is shown in figure 5. The mechanical property of the material is represented on the vertical axis (in this case, the elastic modulus) and temperature or the duration of the test is on the horizontal axis. Note that the vertical scale is logarithmic, as is the time scale. T_g is the glass transition temperature and T_m is the melting point.

The three types of behaviour –*elastic, elastomeric* and *viscoelastic*– will be analysed in the next chapter.

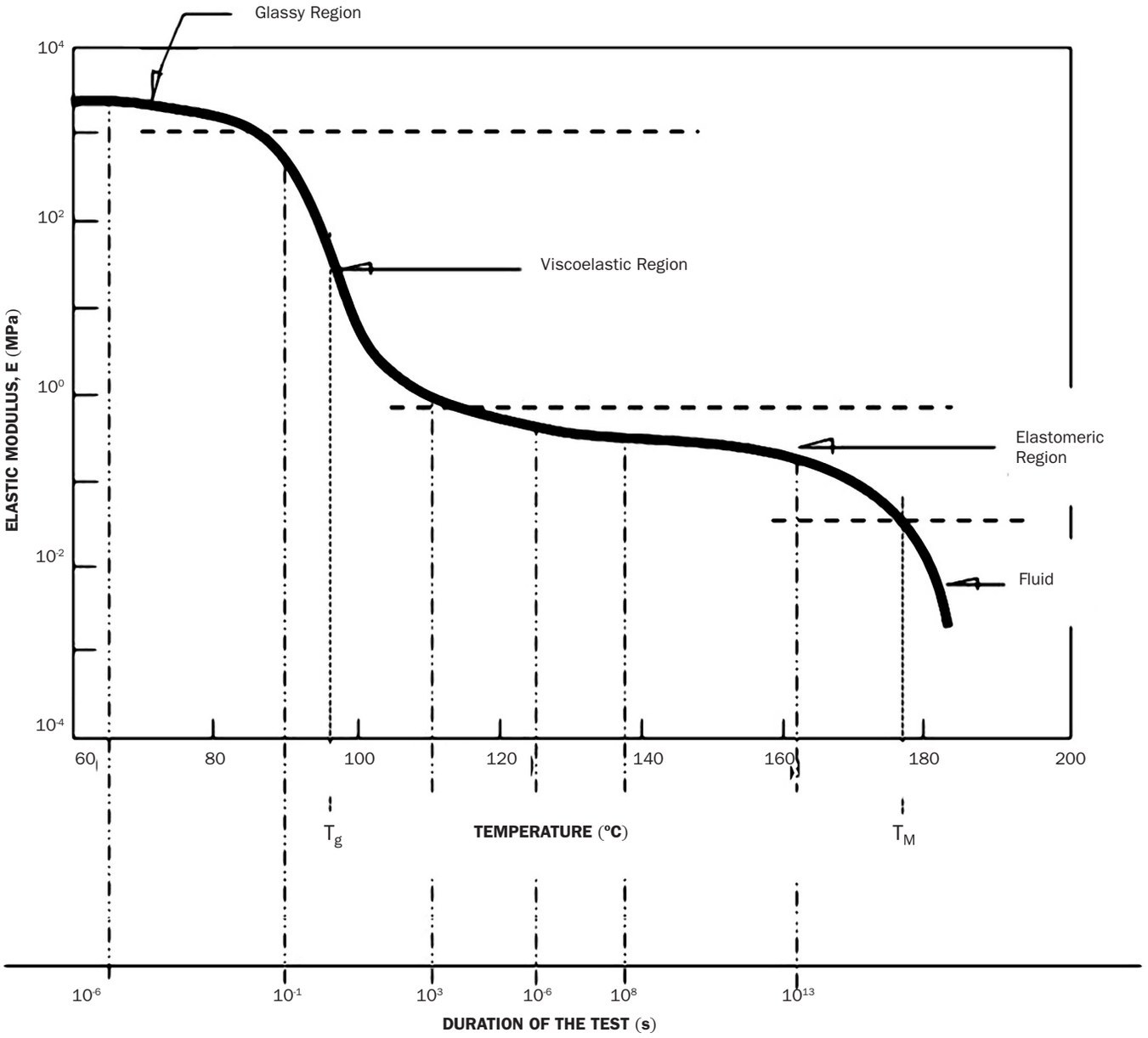

Fig. 5. *Schematic representation of the behaviour of the elastic modulus of a fibre as a function of temperature or time.*

As far as the microscruture is concerned, it is also difficult to give general guidelines, although at the most basic level all the materials have some common aspects: they are long polymer chains with sequences that are repeated many times (known as motifs), as shown in Table 1 . These chains can adopt particular configurations, depending upon the temperature, the external loading and particular composition (not only their monomers and their associated "motifs" –see the table– but, also, their side chains). Thanks to the repetition of the established sequences part of these long chains can organise themselves into small ordered structures (called crystallites, or microcrystals). In this case it is possible to model the behaviour of these polymers as composites of microcrystals embedded in an amorphous matrix; little crystalline tablets joined by fringes that come from their edges, as shown in figure 6. The simple model of a composite material –microcrystals embedded in an amorphous matrix– allows, as will be seen later, prediction of the mechanical behaviour of many biological materials.

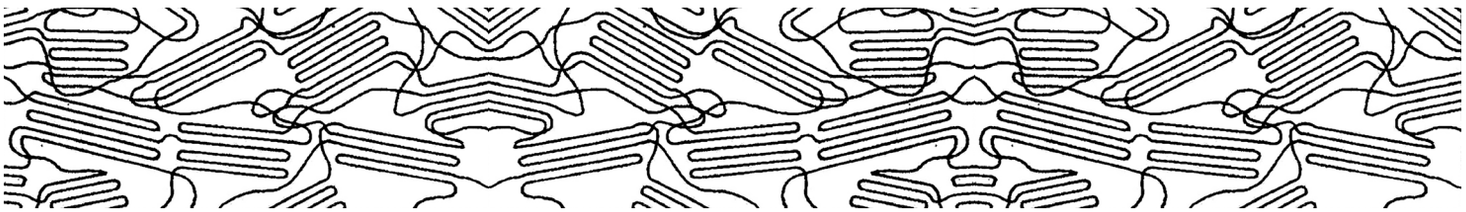

Fig. 6. *Model of fibre, idealised as a composited material of micro (or nano) crystals embedded in an amorphus matrix. Fiber crystalinity is related with the percentage of crystal zones.*

TABLE 1. MOTIFS AND SECONDARY STRUCTURES IN SOME POLYPEPTIDES

POLYPEPTIDE	MOTIF	SECONDARY STRUCTURE
Keratin	$(abbabbb)_n$*	β Sheets, Coils
Silkworm silk	$(GAGAGS)_n$	β Sheets
Spider silk	A_n	β Sheets
	$(GXG)_n$	Coils
Collagen	$(GXP)_n$	Coils
Elastin	$(VPGVG)_n$	–
Resilin	GGRPSDSYGAPGGGN	–
Abductin	FGGMGGGNAG	–

* a = non-polar residues, b = polar residues
A = alanine, G = glycine, S = serine, P = proline, V = valine, R = arginine, D= aspartic acid, Y = tyrosine, N = asparragine, M = methionine

1.5. APPENDIX

Abbreviations for the 20 most common amino acids

AMINO ACID	ABBREVIATION (3 letters)	ABBREVIATION (1 letter)
Alanine	Ala	A
Arginine	Arg	R
Asparragine	Asn	N
Aspartic acid	Asp	D
Cisteine	Cys	C
Glutamine	Gln	Q
Glutamic acid	Glu	E
Glycine	Gly	G
Histidine	His	H
Isoleucine	Ile	I
Leucine	Leu	L
Lisine	Lys	K
Methionine	Met	M
Phenylalanine	Phe	F
Proline	Pro	P
Serine	Ser	S
Treonine	Thr	T
Tryptofan	Trp	W
Tyrosine	Tyr	Y
Valine	Val	V

2 CHAPTER Mechanical Behaviour of Fibres

2.1. INTRODUCTION AND OBJECTIVES

In order to study the mechanical properties of a material experiments must be performed, in which predetermined forces and/or deformations are applied to a body and to measure the resulting deformation and/or forces. In the case of fibres, in which one of the geomertical dimensions –the length– is much greater than the other two –the cross section–, the most useful experiment is the *tensile* test, so the greater part of the following section will be dedicated to it.

The information obtained from a tensile test allows, in most cases, the determination of the one-dimensional constitutive equation for the material. Constitutive equations relate the applied forces on a material to the resulting deformations. In general, the information derived from a tensile test is macroscopic, that is; it allows for example prediction of the deformations if the forces are known, or vice versa, but it does not provide information about the microscopic menchanisms that give rise to the phenomenon, that are usually multiple and act simultaneously. For example a tensile test on a tendon yields a relationship between the applied force and the extension of the tendon. However, if the intimate deformation mechanisms in the collagen fibres, responsible for the tendon extension, are required, complementary experiments and hypotheses about the composition and structure are needed.

From tensile tests on materials it is apparent that there are three broad classes of behaviour, according to the type of deformation produced.

i) When the deformation produced is immediate, a function only of the applied force and not how it is applied, the material undergoes **elastic behaviour**. The relation between the force (F) and deformation (Δ) is one-to-one (see figure 1), and the constitutive equation of the material is represented by a function $F=f(\Delta)$, which can be inverted to yield $\Delta= f^{-1}(F)$.

Hookean[3] *elastic* or *linear elastc behaviour* is simplest type of elastic behaviour. In this case the relation between the force and deformation is linear: $F = k \cdot \Delta$, where k is a constant. The mechanical response is determined, to a great extent, by the internal energy stored or released when the material deforms.

If the relation between the force and deformation is not linear, the behaviour is termed *hyperelastic* or *nonlinear elastic*. A case of particular importance is that of *elastomeric behaviour* which is seen in some materias such as rubber. In these materials the mechanical response is principally due to a change in the configurational entropy of the molecules, associated with its conformation in chains, as will be discussed later.

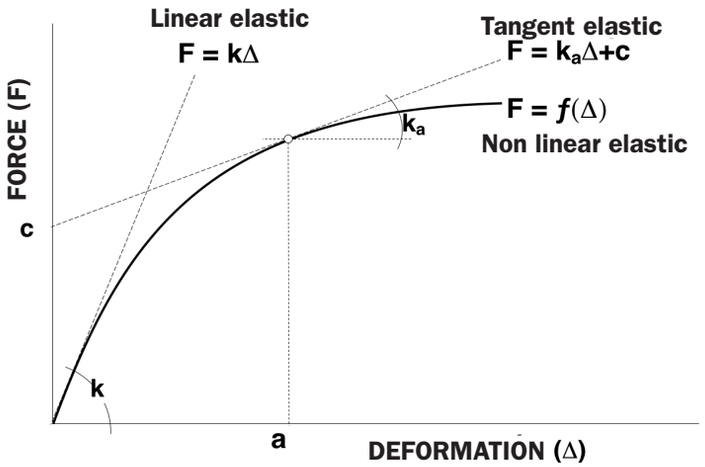

Fig. 1. *Non linear behaviour and linear approximations (tangents).*

Since any elastic constitutive equation $F=f(\Delta)$ can be approximated at the origin ($\Delta \approx 0$) by its tangent line, the initial behaviour (= for small deformations) of any elastic material can be taken as linear elastic. Equally, for small increments of deformation from a particular point Δ_a, the elastic constitutive equation can be approximated by the tangent at $F=f(\Delta)=k_a \cdot \Delta + C$ at this point, and once more the behaviour can be considered as locally linear elastic.

ii) When the deformation produced is instantaneous, but the value of which *depends on the loading sequence*, for example, because there are loading and unloading processes the *behaviour* is termed **plastic**. In this case there is no fixed relationship between the force and the deformation, it being necessary to know the complete loading history suffered by the material in order to determine the final deformation. The material generally displays permanent deformation (or plasticity) once the applied force is removed since the mechanical response is governed by internal irreversible dissipative processes.

iii) When the deformation of a material subjected to a constant force varies with time this is **time dependent** or *deferred mechanical* behaviour. This is, without doubt, the most complex situation and, unfortunately, the most frequently encountered in the study of biological materials.

One situation of great interest, and something simpler, is when under a constant applied force the deformation stabilses over a long period of time (theoretically an infinite time), and its final value Δ_∞ depends only upon the applied load, in a manner similar to the elastic case, through biunivocal relationship $F=f(\Delta_\infty)$. In this case the *behaviour* of the material is *viscoelastic* and the mechanical response is associated with changes in both internal energy and entropy.

The behaviours described in ii) and iii) are called *anelastic* or *inelastic*, in contrast to the elastic behvaviour shown in i) because there is no one-to-one relationship between forces and deformations. In this section the most important behaviours in the analysis of biological fibres such as **Hookean elastic, elastomeric** and **linear viscoelastic** will be considered.

In some experiments the fibre may fracture. The fracture process is complex and depends as much on the fibre as on the applied loading. It is ususal to distinguish between two types of fracture; *brittle*, characterised by the absence of permanent deformation after the specimen has broken, and *ductile*, when the fibre suffers large plastic deformation during the fracture process. However, the boundaries between both types of behaviour are not well-defined.

When the fibres are brittle, or slightly ductile, the fracture behaviour can be approximated by means of a probabilistic fracture model based on Weibull's theory of the weakest link. This model is helpful in accounting for the variation in strength values obtained experimentally.

In this section a brief introduction to Weibull's model is presented, but a more detailed study of the fracture of biological materials will be left until section III.

[3] Robert Hooke (1635-1703) was an English experimantal scientist who in 1660 first enunciated the law of proportionality between the extension of an elastic body and the force on it (Hooke's Law).

2.2. MECHANICAL TESTS

The simplest and most frequently performed tests on fibres are tensile tests (also called uniaxial tension or simple tension tests) and torsion tests.

2.2.1. The tensile test

This consists of a sample of material in the form of a cylinder or flat strip (in this second case the length is the predominant dimension) which is subjected to an increasing traction, causing force F and displacement, $\Delta L=L-L_0$, with respect to a base measurement L_0, as indicated in figure 2.

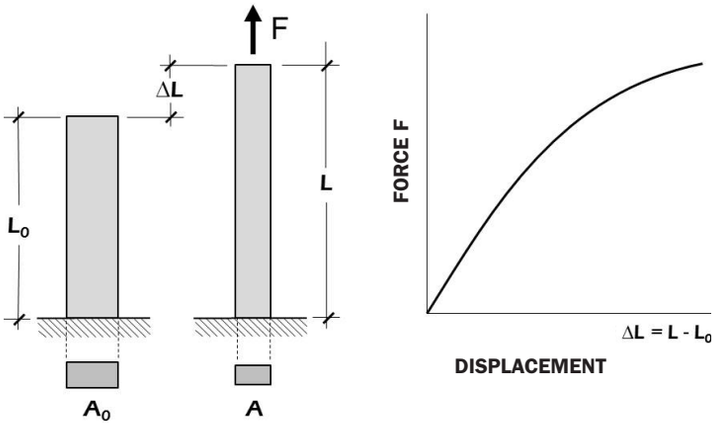

Fig. 2. *Specimen concept: L_0 and A_0, initial length and cross sectional area. Schematic of the result from a tensile test: Force-displacement curve.*

In general, the force F is measured as a function of the displacement Δ_L, this being the variable that controls the process. Occasionally the test is performed by varying the force and measuring the corresponding displacement. The test may be influenced by the rate of change of the displacement with time (or of the force, if it is that which is controlled) and by external factors such as temperature, pressure, relative humidity or the medium surrounding the sample.

Even though, in the region of the grips, there is a complex stress state, if the specimen is sufficiently long –for practical purposes a length which is greater than five times the diameter is sufficient– the effects of the teeth of the grips decay rapdily. As a result it is possible to assume that the loading is uniform across the transverse section and that the deformation is uniform through out the specimen (excluding the gripping regions). Furthermore, in what follows, it is assumed that the material is isotropic.

In order to study properties of materials which are independent of the geometry of the test-piece stresses and strains are used, which are values of the force and displacement normalised with respect to the specimen dimensions.

– Engineering or nominal stresses and strains

The **engineering stress** s is defined as:

$$s = \frac{F}{A_0} \tag{1}$$

where F is the force on the sample and A_0 is its initial cross sectional area.

The **engineering strain** e is defined as:

$$e = \frac{\Delta L}{L_0} = \lambda - 1 \tag{2}$$

where $\Delta L=L-L_0$ is the change in length with respect to the base measurement L_0 and λ is the elongation, defined as the ratio of lengths $\lambda = L/L_0$.

As a consequence of these definitions the force-displacement curves $(F\text{–}\Delta L)$ and engineering stress-engineering strain curves $(s\text{-}e)$ are similar, and differ only in scaling factors, which are the constants A_0 and L_0.

– True stresses and strains

It is common for biological materials to undergo large deformations before fracture, with significant changes in the length and cross section. At a given time, the initial values A_0 and L_0 can be quite different from the actual cross sectional area and length of the specimen, so that it is usually preferable to employ the true stress and strain instead of engineering ones.

The **true stress** σ is defined as:

$$\sigma = \frac{F}{A} \tag{3}$$

where A is now the cross sectional area of the specimen under the applied load F.

For an infinitesimal process in which length increases from L to $L+dL$ the **true strain** ε produced is defined as:

$$d\varepsilon = \frac{dL}{L} \tag{3bis}$$

When the base measurement L_0 has deformed as much as L, the total true strain will be, by integration of $d\varepsilon$:

$$\varepsilon = \int_{L_0}^{L} \frac{dL}{L} = \ln\frac{L}{L_0} = \ln\lambda \tag{4}$$

The relationship between the true and engineering strains is simple given that:

$$\varepsilon = \ln\frac{L}{L_0} = \ln\left(1+\frac{\Delta L}{L_0}\right) = \ln(1+e) \tag{6}$$

The relationship between the stresses can be readily deduced if *conservation of volume* of the specimen is assumed, that is, if:

$$A_0 L_0 = AL = \text{constant} \tag{5}$$

Although this assumption may appear limiting, it can be applied to almost all biological materials, since they may be considered incompressible for the levels of stress usually experienced by these materials given their high water content[4].

In these circumstances:

$$\sigma = \frac{F}{A} = \frac{F}{A_0}\frac{A_0}{A} = \frac{F}{A_0}\frac{L}{L_0} = s\lambda = s(1+e) \tag{7}$$

The sign convention for stresses and strains is the same; tension is considered as positive and compression negative.

The results of tensile tests on two different materials are shown in figure 3. The s-e curve represents engineering values which, as mentioned above, are proportional to the force F and displacement ΔL. The curve in figure 3a has a naximum that coincides with the beginning of an instability in the test (a phenomenon known as *necking* and which will be discussed below). The $\sigma - \varepsilon$ curve corresponds to values that are called true. When volume is conserved these values can be calculated from equations (6) and (7) up to the point of instability (maximum of the s-e curve). Beyond this point the true stress varies throughout the specimen, since the cross section is not uniform due to necking. The curve in figure 3b does not have the instability mentioned above and true values can be calulated for the entire experimental curve from equations (6) and (7), if volume is conserved during the test.

Interpretation of the curves shown in figure 3 is not trivial, in particular at large strains. For small deformations the behaviour is usually elastic; if the specimen is unloaded, the curve returns to zero and, moreover, it follows the same path as on loading.

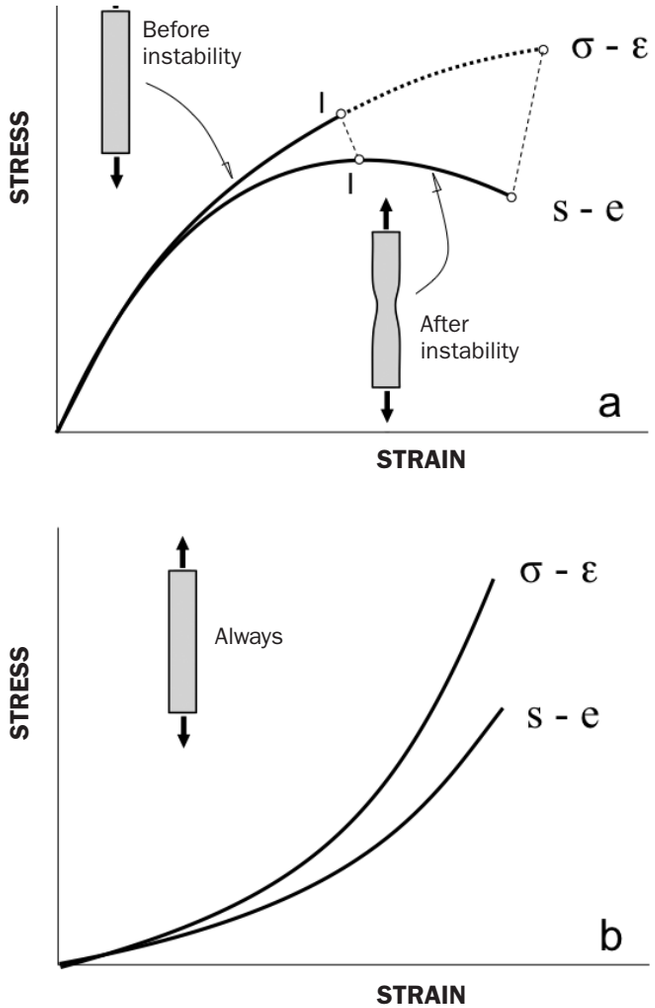

Fig. 3. *Stress strain curves (iengineering and true).*
a. Material with a response that exhibits necking (point I).
b. Material with a response that does not show necking.

When the strains are large –a common situation in biological materials– unloading does not usually follow the loading path and a new phenomenon, called hysteresis that, again, will be discussed later. It is also possible that the deformation is not totally recovered after the specimen is completely unloaded –including when the unloading takes place over a long period of time– in thses cases the deformation is called plastic. When time is a factor and there is plasticity, interpretation of the tensile test is much more complcated, as will be seen in the examples presented later in this chapter.

[4] The ratio of the pressure Δ_p applied to a body and ithe resulting change in volume $\Delta V/V$, with sign reversed, is called the bulk modulus. The bulk modulus of water (2GPa) is similar to that of polymeric materials (~2 a 4GPa), and much less than those of metals and ceramics (~30 a 200GPa). The water contained in soft biological materials such as the fibres –which can be treated as polymers– makes an important contribution to changes in rigidity under hydrostatic stresses, causing the change in deformation. This fact, together with the usually low values of these stresses (≈1/3 of the axial stress) supports the incompressible hypothesis.

EXERCISE

Calculate up to what point it is possible to consider the engineering and true strains as measured in a tensile test as equivalent, if the allowable error is 3%.

Solution:

From equation (6), that defines the relationship between the true strain (ε) and engineering strain (e) we obtain

$$e = \exp(\varepsilon) - 1$$

hence

$$\text{error relativo} = \frac{e-\varepsilon}{\varepsilon} = \frac{1}{\varepsilon}\left(\exp(\varepsilon) - 1 - \varepsilon\right) = \frac{1}{\varepsilon}\left(1 + \varepsilon + \frac{\varepsilon^2}{2} + \ldots - 1 - \varepsilon\right) \approx \frac{\varepsilon}{2}$$

The we see that the error will be less than 3% provided that (ε, e) < 0.06, or in other words they will be the same so long as the engineering (or true) strain does not exceed 6%.

EXERCISE

Demonstrate that when the strains are not small, only true strains are additive, but not the engineering ones. That is, if starting from L_0 the final length is L_2 with an intermediate value L_1 then $e_{02} \neq e_{01} + e_{12}$ and that $\varepsilon_{02} = \varepsilon_{01} + \varepsilon_{12}$

Solution:

From equation (4) we obtain

$$\varepsilon_{01} = \ln\left(\frac{L_1}{L_0}\right), \qquad \varepsilon_{12} = \ln\left(\frac{L_2}{L_1}\right), \qquad \varepsilon_{02} = \ln\left(\frac{L_2}{L_0}\right)$$

from which

$$\varepsilon_{01} + \varepsilon_{12} = \ln\left(\frac{L_1}{L_0}\right) + \ln\left(\frac{L_2}{L_1}\right) = \ln\left(\frac{L_2}{L_0}\right) = \varepsilon_{02}$$

Similarly, from equation (2)

$$e_{01} = \frac{L_1}{L_0} - 1, \qquad e_{12} = \frac{L_2}{L_1} - 1, \qquad e_{02} = \frac{L_2}{L_0} - 1$$

from which

$$e_{01} + e_{12} = \frac{L_1}{L_0} + \frac{L_2}{L_1} - 2 \neq \frac{L_2}{L_0} - 1 = e_{02}$$

- *Necking*

Necking is an instability that can occur in a tensile test before rupture. During a tensile test $F = \sigma A$; where F is the applied force, σ the true stress, and A the cross sectional area at that instant, and which is the same throughout the specimen. As the specimen deforms, σ increases and A decreases. If the specimen does not break, force F can reach a maximum value that can be determined from the condition $dF = 0$, or:

$$dF = \sigma\, dA + A\, d\sigma = 0$$

from which

$$\sigma = - A\, d\sigma/dA$$

If the volume of the specimen is constant, A_L is constant and

$$dA\, L + dL\, A = 0$$

which leads to

$$-\frac{A}{dA} = \frac{L}{dL} = 1/d\varepsilon$$

then the condition for the maximum can be espressed as

$$\sigma = d\sigma/d\varepsilon \qquad (8)$$

Equation (8) indicates that the maximum stress is achieved when the slope of the strain hardening, $d\sigma/d\varepsilon$, is numerically equal to the true stress, σ. Provided that $d\sigma/d\varepsilon > 0$, the strain will be uniform along the length of the specimen, but when $\sigma = d\sigma/d\varepsilon$ ($\equiv dF = 0$) he strain localises. A particular section deforms a little more than the others (due to some geometrical imperfection or some defect in the material) so it will have a lower load carrying capacity and the load will fall to this level. The other regions will not continue deforming and the defromation will be concentrated around the weakened section, creating a neck by striction (or simply *necking*).

When the constitutive equation of the material is known it is possible to calulate the maximum load that a specimen can support as well as the maximum uniform strain.

EXERCISE

In 1885 the French scientist A. Considère proposed a graphical construction for the maximum load that can be supported by the specimen in a tensile test. The maximum value is obtained by drawing the tangent from the origin (*0,0*) to the stress-elongation ($\sigma - \lambda$) curve.

Illustrate this graphical construction and show that the result coincides with the instability criterion of equation (8)

Solution:

From equation (8) we can write:

$$\sigma = \frac{d\sigma}{d\varepsilon} = \frac{d\sigma}{d\lambda}\frac{d\lambda}{d\varepsilon} = \frac{d\sigma}{d\lambda}\lambda$$

Since equation (4) yields $d\lambda/\lambda = d\varepsilon$.

The equation can be rewritten as

$$\frac{\sigma}{\lambda} = \frac{d\sigma}{d\lambda}$$

which means that in a diagram the tangent at the point of instability coincides with the value of the secant slope σ / λ. Therefore, at this point of instability a straight line from the origin is tangent to the curve, as shown in the figure.

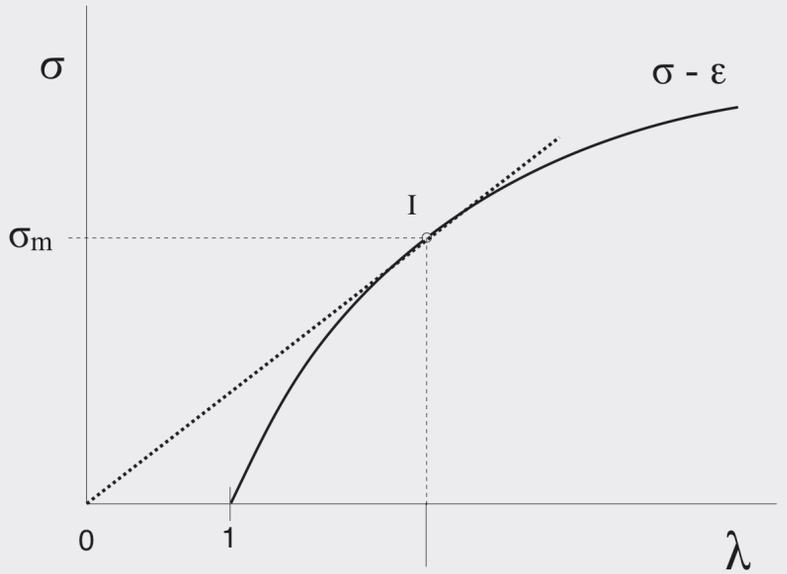

EXERCISE

A common model for a pair of blood vessels is based on Deimirai's constitutive equation, which in unidirectional form can be written as $\sigma = C_1(\lambda^2 - \lambda^{-1}) \exp [C_2 (\lambda^2 + 2/\lambda - 3)]$, where λ is the elongation of the sample L/L_0.

Calculate the values of $\sigma - \varepsilon$ at the instigation of necking if C_1= 50kPa and C_2=–0.1

What values must C_1 and C_2 have for necking to occur? Compare the results obtained with typical values for the ascending aorta C_1=64kPa and C_2=2. What conclusions can be drawn?

Solution:

Instability occurs when $\sigma = (d\sigma/d\lambda)\lambda$ (see the previous exercise). Therefore

$$\sigma = C_1\left(\lambda^2 - \frac{1}{\lambda}\right)\exp\left[C_2\left(\lambda^2 + \frac{2}{\lambda} - 3\right)\right] = \frac{d\sigma}{d\lambda}\lambda = \lambda C_1 \exp\left[C_2\left(\lambda^2 + \frac{2}{\lambda} - 3\right)\right]\left[2\lambda - \frac{1}{\lambda^2} + C_2\left(\lambda^2 - \frac{1}{\lambda}\right)\left(2\lambda - \frac{2}{\lambda^2}\right)\right]$$

from which

$$\left(\lambda^2 - \frac{1}{\lambda}\right) = \lambda\left[2\lambda - \frac{1}{\lambda^2} + C_2\left(\lambda^2 - \frac{1}{\lambda}\right)\left(2\lambda - \frac{2}{\lambda^2}\right)\right]$$

which reduces to

$$-\lambda - \frac{2}{\lambda^2} = C_2\left(\lambda^2 - \frac{1}{\lambda}\right)\left(2\lambda - \frac{2}{\lambda^2}\right)$$

since the values of the parentheses are always ≥0 for $\lambda \geq 1$, there is only a solution if C_2<0. In the case of the aorta C_2=2 so no instability is observed. This explains the absence of aneurisms.

For C_1= 50kPa and C_2=–0.1 we obtain

$$\lambda^3 - 5\lambda - 2 - \frac{10}{\lambda^2} + \frac{1}{\lambda^3} = 0$$

whose solutions are λ = 0.09975 (<1, compression; so this is ignored) and λ =2.5272 which leads to ε = 0.9271 and σ=197.3kPa. These results are shown in the figure. Note that when C_2=2 it is not possible to draw a tangent from the origin. However, for C_2=-0.1, a tangent can be constructed.

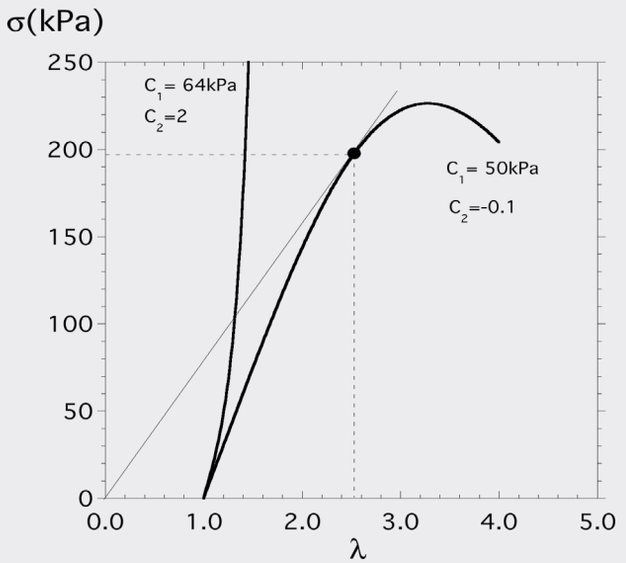

- Units used in the textile industry

Measurements of the cross sections of fibres employed in the textile industry create problems because of their small dimensions and shapes. It is common, then, to take as a reference some measurements based on the mass of a specific length of fibre. Initially, the *denier* (the mass in grammes of a 9 km length of fibre) was used. The selection of a 9 km length is not arbitrary, and is based on the fact that a thread of natural silk of that length usually ways about 1 gramme. Currently the *tex* is used, this is the mass in grammes, corresponding to a length of 1 km. Since this unit results in such a small quantity it is common to use the *decatex* (dtx) which is a value close to the denier.

If it is assumed that a fibre has a constant cross section, the value of the cross sectional area can be deduced from the tex (T) by means of the simple relationship

$$T = 10^6 \rho A \tag{9}$$

provided that the density ρ and cross sectional area A are expressed in SI units; that is, in kgm^{-3} and m^2, respectively.

Another unit used in the textile industry is the specific strength (also known as the *tenacity*, although this term can lead to confusion, because it is a term specific to Fracture Mechanics, as will be seen later). The specific strength (SR) is defined as the breaking force divided by the tex and is measured in the SI system in newton/tex (Ntex^{-1}). The relationship between the specific strength in Ntex^{-1} (SR) and the engineering fracture stress (ultimate tensile strength) s_R is:

$$\text{SR (Ntex}^{-1}\text{)} = 10^{-6}\, s_R\, \rho^{-1} \tag{10}$$

where s_R and ρ must be expressed, again in SI units, that is in Pa and kgm^{-3}, respectively.

The units used in the textile industry (in Europe the **tex** is preferred while in the USA it is the **denier**) are rarely used in other engineering fields, so for this reason the following summary is presented.

Tex = mass in grammes of 1,000 metres of fibre
denier = mass in grammes of 9,000 metres of fibre
specific strength = failure load in Newtons divided by tex
= grammes force/denier

The following equivalences may be useful (*A* cross sectional area)

1 gf/denier = 0.088 N/tex 1 tex = ρ(kg/m^3). *A*(m^2) 1 Pa = 1(N/tex).10$^6\rho$(kg/m^3)

EXERCISE

A polyester fibre has an average strength of 40cN/tex and an engineering failure strain of 20%. Given that the density of polyester is 1380 kg/m^3 caculate the true stress and strain at failure of the fibre.

Solution:

From equation (10) we obtain

$$s_R(\text{Pa}) = 10^6 \rho(\text{kgm}^{-3})\, SR(\text{Ntex}^{-1})$$

from which

$$s_R(\text{Pa}) = 10^6 \cdot 1380 \cdot 0.01 \cdot 40 = 552\ 10^6 \text{Pa} = 552\ \text{MPa}$$

Equations (6) and (7) then provide the true strain and stress

$$\varepsilon_R = \ln(1+e_R) = \ln(1+0.2) = 0.182$$
$$\sigma_R = s_R(1+e_R) = 662\text{MPa}$$

2.2.2. The torsion test

In the torsion test a *cylindrical* sample of material is subjected to an increasing torque (or torsional moment) T, while recording the angle of twist ϕ, as shown in figure 4a.

This test admits the possibility of large strains because it is not limited by the necking instability that occurs in a tensile test. As in the latter, the experiment is influenced, especially in biological fibres, by the loading rate and by external factors such as temperature, pressure, relative humidity or the type of medium surrounding the specimen.

Note that the torision test presents important differences from the tensile test since the forces are now parallel (tangential) to the cross section and not perpendicular, as in the tensile test. In the torsion test, moreover, the strain is not uniform (equal at every point, as happens in the tensile test) since it varies as a function of the distance from the axis of rotation (figure 4d).

Therefore, when the term $R\,\phi / L$ is **small,** it is possible to make hyptheses that simplify calculation of the stress state and to establish a linear relationship between the torsional moment T, and the angle of twist ϕ, a result that agrees with experiment when this requirement is satisfied.

In these conditions (small $R\,\phi / L$) every element of material deforms under a state of pure shear (as shown in figure 4b, and which will be detailed later in section 2.3.2). The Coulomb[5] hypothesis that sections perpendicular to the axis of the fibre remain plane and parallel to each other after deformation, keeping their shape, the motion of the section being a rotation relative to its centre is also satisfied.

The *shear strain* $\gamma\,(r)$, defined as the angular change of a right angle (see figure 4b), is the same at two points located at a distance r from the axis, does not depend upon z, and is given by

$$\gamma\,(r) = r\,\phi / L \tag{11}$$

The corresponding *tangential* or *shear stress* τ, is defined as the tangential (or shear) force divided by the area over which it acts. (Recall that it has been assumed that deformations are small, so that the area is essentially constant, so it is not necessary to distinguish between true and engineering stresses). The value of τ cannot be measured directly, or calculated from the external torsional moment T, because τ depends on $\gamma\,(r)$ and this relationship is unknown *a priori* because it depends on the material properties.

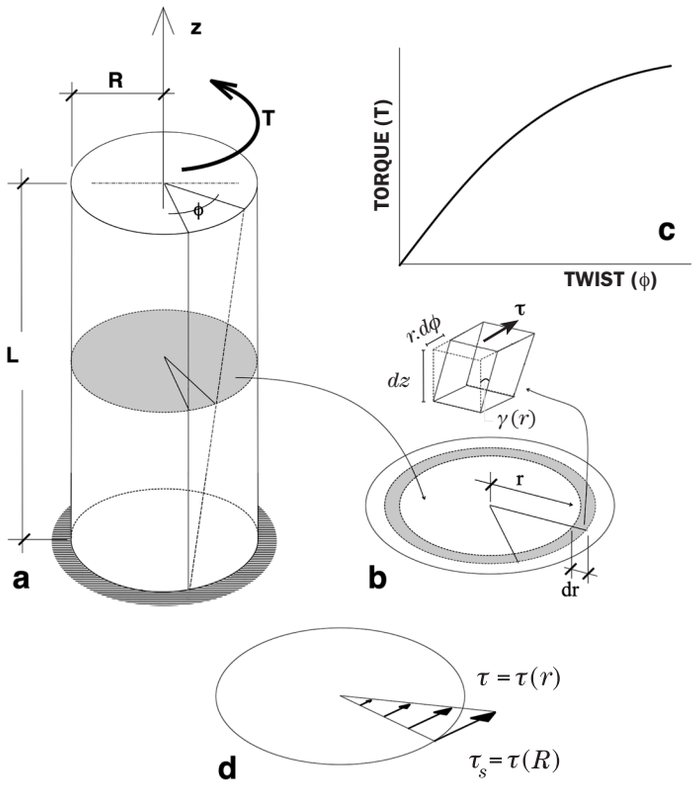

Fig. 4. *a. Torsion test. Notation used.*
b. Detail of an element of the specimen subjected to pure shear.
c. Example of the torsional moment curve as a function of the angle of twist.
d. Distribution ofthe stesses on a plane perpendiculat to the axis z.

The relationship between the torsional moment and the angle of twist can be calculated –provided $R\,\phi / L$ is small– as follows:

The shear stress acting on an annular element of radius r and width dr makes an infinitesimal contribution to the total torsional moment T equal to:

$$dT = \tau \text{ x area x radius} = \tau(2\pi r dr)r = 2\pi\tau r^2 dr$$

and, as a result

$$T = 2\pi\int_0^R \tau r^2\,dr \tag{12}$$

[5] Charles-Augustin de Coulomb (1736 - 1806) was a French engineer most famous for his law of attraction between two electric charges (the S.I. unit of charge is named after him). He also made many contributions to physics and the mechanics of solids. He is credited with the theory of simple torsion and the definition of the coefficient of friction.

This equation cannot be integrated directly because τ depends on r through γ and this relationship is unknown.

The way to solve it is to assume *a priori* some relationship between τ and γ, this being the simplest, a linear relationship between stress and strain, that is, $\tau = G\,\gamma$. This approximation is equivalent to assuming that the material is Hookean elastic. The constant G is measured in Pascals (Pa = Nm^{-2}) and is usually called the *shear modulus, stiffness modulus* or *transverse modulus* of elasticity. With this hypothesis:

$$T = \frac{\pi R^4}{2}\frac{G}{L}\phi = \frac{IG}{L}\phi \tag{13}$$

where $I=\pi\,R^4/2$; the polar moment of area of the circular section of the cylindrical specimen under consideration.

Clearly, the relationship between T and ϕ is linear in these circumstances and the slope of the straight line can be used to estimate the value of G.

The result obtained in equation (13) can also be expressed as a function of the shear stress on the boundary with the lateral surface $\tau_S = \tau(R)$, in the following

$$T = \frac{\pi R^4}{2}\frac{G}{L}\phi = \frac{\pi R^3}{2}\tau_S \tag{14}$$

When the curve departs slightly from a straight line, the value of G determined from the slope at the origin is normally used, obtained from

$$G = (L/I)\,(dT/d\phi)_{\phi=0}$$

As already noted, one of the advantages of this test is the possibility of achieving larger deformations than in the tensile test without instability problems. (In any case, the deformation must be **sufficiently small** so that the shear stress and strain can be defined as indicated and that equations (11) and (12) remain valid). The danger in this advantage is that for deformations the material can become nonlinear, so that equations (13) and (14) cease to be valid.

EXERCISE

Derive a relationship between τ and γ from two experiments with values R and $R + \Delta R$.
From this relationship determine the curve $T = T(\phi)$ for a torsion test.

Solution:

For a particular value of the angle of twist ϕ the torque on a fibre of radius R will be (equation (12))

$$T_R(\phi) = 2\pi\int_0^R \tau r^2\,dr$$

while for a fibre of radius $R+\Delta R$, for the same twist ϕ, the value of the torque will be

$$T_{R+\Delta R}(\phi) = 2\pi\int_0^{R+\Delta R} \tau r^2\,dr$$

splitting the integral in this last equation we can write

$$T_{R+\Delta R}(\phi) = T_R(\phi) + 2\pi\int_R^{R+\Delta R} \tau r^2\,dr \approx T_R(\phi) + 2\pi\ \tau(R)\int_R^{R+\Delta R} r^2\,dr \approx T_R(\phi) + 2\pi\ \tau(R)R^2\,\Delta R$$

in which we have approximated τ in the interval $(R, R+\Delta R)$ by its value at $r=R$, and neglecting second order and higher terms in ΔR. Rearranging, $\tau(R)$ becomes

$$\tau(R) = \frac{T_{R+\Delta R}(\phi) - T_R(\phi)}{2\pi R^2\,\Delta R} \tag{a}$$

this equation, together with (11) when $r=R$

$$\gamma(R) = \frac{R\phi}{L} \tag{b}$$

provides the parametric equation for the curve τ–γ in terms of T and ϕ.

If the function $\tau = \tau(\gamma)$ is known, it is possible to obtain the relation $T = T(\phi)$ without use of equation (12)

$$T(\phi) = 2\pi\int_0^R \tau(\gamma) r^2\,dr = 2\pi\int_0^R \tau\left[\gamma(r\phi/L)\right] r^2\,dr$$

in which we used equation (11)

EXERCISE

Deduce a general relationship similar to equation (14) for elements of arbitrary cross section, assuming that τ and γ are linearly related. Is it necessary that the section has a centre of symmetry in order to satisfy the conditions for the torsion test

Solution:

Figure a) shows an arbitrary section subjected to a torque. If we assume that Coulomb's hypothesis is valid (sections perpendicular to the axis remain plane and parallel to one another after deformation, keeping their shape) the motion of the section will be simply a rotation with respect to some point O in the section.

The shear stress at a point A acts parallel to the section and perpendicular to the segment OA, as shown in the figure. The torsional moment about point O will be,

$$T = \int_{\Omega} \tau r \, d\Omega$$

where Ω is the area of the section and $d\Omega$ is an infinitesimal element of area centred around point A. Imposing a linear relationship between τ and γ we can write

$$\tau = G\gamma = G\frac{\phi}{L}r$$

in which we have also used equation (11), substituting this in the previous expression, the integration for T gives us

$$T = G\frac{\phi}{L}\int_{\Omega} r^2 \, d\Omega = G\frac{\phi}{L} I_O$$

where the integral is none other than the polar moment of area of the section I_O about point O. This is a general form of equation (14).

Point O cannot be arbitrary since equilibrium requires that the resultant force in the plane of the section must be zero (see figure b))

$$0 = \int_{\Omega} \tau_y \, d\Omega = \int_{\Omega} \tau_x \, d\Omega$$

and since

$$\tau_y = \tau \cos\beta = G\frac{\phi}{L} r \cos\beta = G\frac{\phi}{L} x$$

then

$$0 = \int_{\Omega} G\frac{\phi}{L} x \, d\Omega = G\frac{\phi}{L}\int_{\Omega} x \, d\Omega$$

and similarly for coordinate y. Hence point O must be the centroid of the section. If the section has a centre of symmetry then it must coincide with the centroid.

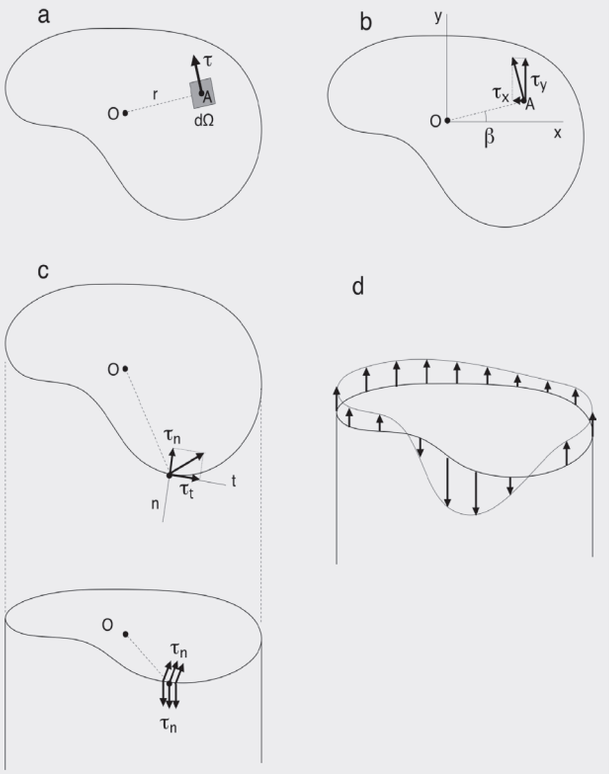

Note that for non-circular sections, Coulomb's hypothesis is never strictly satisfied. The reason is that points on the contour in which the edge is not perpendicular to r (see figure c)) have a normal component of shear stress (τ_n) that requires a shear stress component in the direction parallel to the axis of the fibre, as shown in figure c), which is impossible if the surface is stress free. The inability to satisfy the equilibrium condition means that the section warps, and there will be non-uniform deformation in the axial direction of the fibre (figure d)).

In analysing torsion tests on biological fibres it is usually assumed that the cross section of the fibre is circular. A more detailed examination shows that this is not always so; the cross section of silk from the silkworm is triangular and that of cotton is kidney-shaped, as mentioned previously.

2.3. ELASTIC BEHAVIOUR

2.3.1. Introduction

As mentioned above, the experiment most frequently performed on fibres is the tensile test. In order to interpret its results it is necessary to make certain assumptions about the relationships between true stresses and strains, relationships that are known as *constitutive equations*.

The simplest constitutive equation is that for the behaviour of an elastic material, for which the value of the stress is only a function of the strain at that instant; it does not depend upon the loading history, nor time and other variables. Figure 5 shows two types of stress-strain curve for elastic materials following a tensile test. The (approximately) linear curves in figure 5a are characteristic of many metallic and ceramic fibres, as well as some biological fibres such as linen and cotton. Linear-elastic behaviour is only possible if the deformation is small, and in this case it is not usual to distinguish between true and engineering stresses and strains ($e \approx \varepsilon$; $s \approx \sigma$).

The curve in figure 5b is typical of elastomeric fibres, such as rubber, in which the stress is no longer proportional to the strain. However, the strain returns to zero –and along the same load path– when the stress is removed. A common mistake is to assume that elastic behaviour is always linear. The behaviour of rubber fibres shows that ther are notable exceptions.

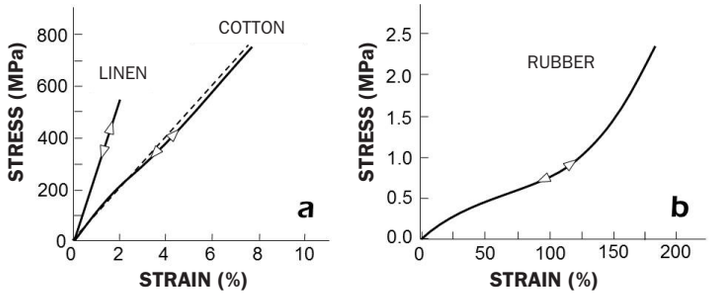

Fig. 5. *Exampes of stress-strain curves showing elastic behaviour.*
a. Linear elastic (linen and cotton).
b. Nonlinear elastic (rubber) (Treloar L., 1975).

2.3.2. Linear Elasticity

Linear elastic behaviour of a fibre and, also, the initial part of nonlinear behaviour (that part of the curve that can be represented by the tangent at the origin, which is usually in the region of small deformations) can be characterised using two parametrs: the *elastic modulus* E or Young's[6] modulus and *Poisson*'s[7] ratio v. Under these conditions it is said that the response of the fibre is **Hookean,** or **linear elastic.**

The *elastic modulus* E is measured in Pascals (Nm^{-2}) and is the slope of the stress-strain line (σ-ε) recorded in a tensile test (figure 6a)

$$E = \sigma / \varepsilon \tag{15}$$

The *initial elastic modulus* for a fibre of a nonlinear elastic material, such as that shown in figure 6b, is given by

$$E_0 = (d\sigma/d\epsilon)_{\epsilon=0}$$

As noted above, it is always possible to represent the response of a nonlinear elastic material in the region of a point ε_0 by its local tangent. In this way it is possible to talk about a *tangent elastic* modulus (figure 6b)

$$E' = (d\sigma/d\epsilon)_{\epsilon_0}$$

The *Poisson*'s *ratio* ν, is a nondimensional quantity, and is defined as the ratio between the transverse and longitudinal strains in the fibre (see figure 7).

$$\nu = - \epsilon_x/\epsilon_z \tag{16}$$

where ε_z is the strain in the direction of the applied load (longitudinal) and ε_x is the strain in the transverse direction (ε_x=ε_y, since it is assumed that the material is isotropic).

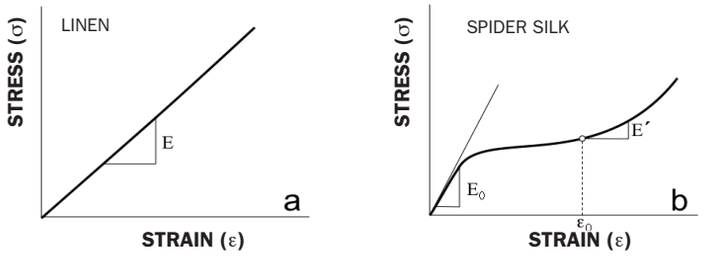

Fig. 6. *Concept of the elasic modulus of a fibre.*
a. Linear elastic.
b. Nonlinear elastic E_0 (Initial modulus), E' (Tangent modulus).

[6] Although it was the Swiss mathematican Leonhard Euler (1707 - 1783) who introduced this parameter, it was the English scientist Thomas Young (1773-1829) who popularised it in a work published in 1807.

[7] Siméon Denis Poisson (1781 - 1840), was a French physicist and mathematician who obtained the relationship (16)

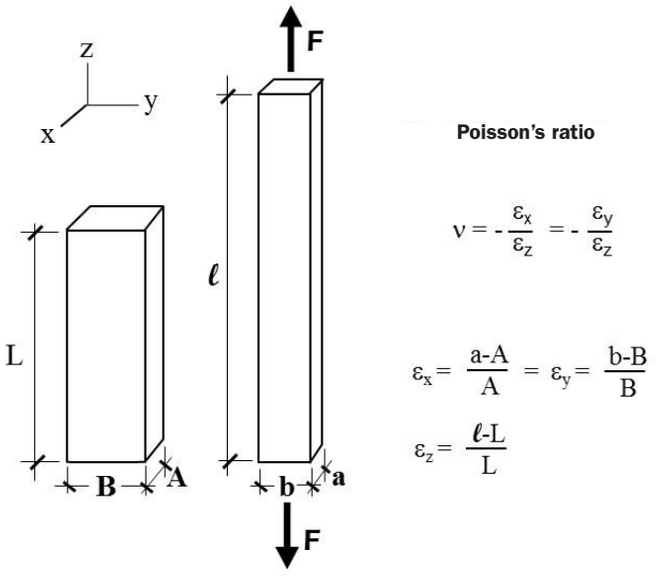

Fig. 7. *Definition of Poisson's ratio.*
Homogeneous isotrpic material, and small deformations ($e \approx \varepsilon$; $s \approx \sigma$)

A specimen usually contracts transversely under tensile loading. Since ε_x and ε_y will be negative then the Poisson's ratio will be positive (although for some very rare materials, called *auxetic*s, the opposite is true (Kolken et al. 2020)). Possible values of ν lie in the range –1 to +0.5 and are usually about 0.3 for metals, 0.2 for ceramics and approximately 0.5 for polymers and biological materials. When ν = 0.5 volume of the material remains constant during deformation.

Expressions relating the stresses and strains for a fibre subjected to tension σ in the axial direction, assuming Hookean elastic behaviour, are summarised in figure 8. The relationships will be generalised later for materials with two and predominantly three-dimensions.

For a cylindrical fibre loaded in torsion (as described in 2.2.2) an elemental volume of material will be in a state of pure shear and, if the behaviour is Hookean elastic, the stresses and strains will be as shown in figure 8b. Note that all of the components are zero except for the shear stress $\tau_{z\theta}$, which depends upon the distance, r, from the centre of the specimen. (The subindices "$z\theta$" indicate that shears act on a section perpendicular to the axis "z" pointing in the direction of increasing "θ". Likewise, subindex "zr" means that the forces lie in a plane parallel to "z=constant" acting in the radial direction "r", and in the case of "$r\theta$" they are applied to a surface with constant "r" and direction defined by "θ"). The relationship between stress and strain is given (according to 2.2.2) by

$$\tau_{z\theta} = G\,\gamma_{z\theta} = G\,r\,(d\phi/dz)_{\phi=0} \tag{17}$$

The shear modulus G, is a function of E and ν, and is given by

$$G = E/2\,(1+\nu) \tag{18}$$

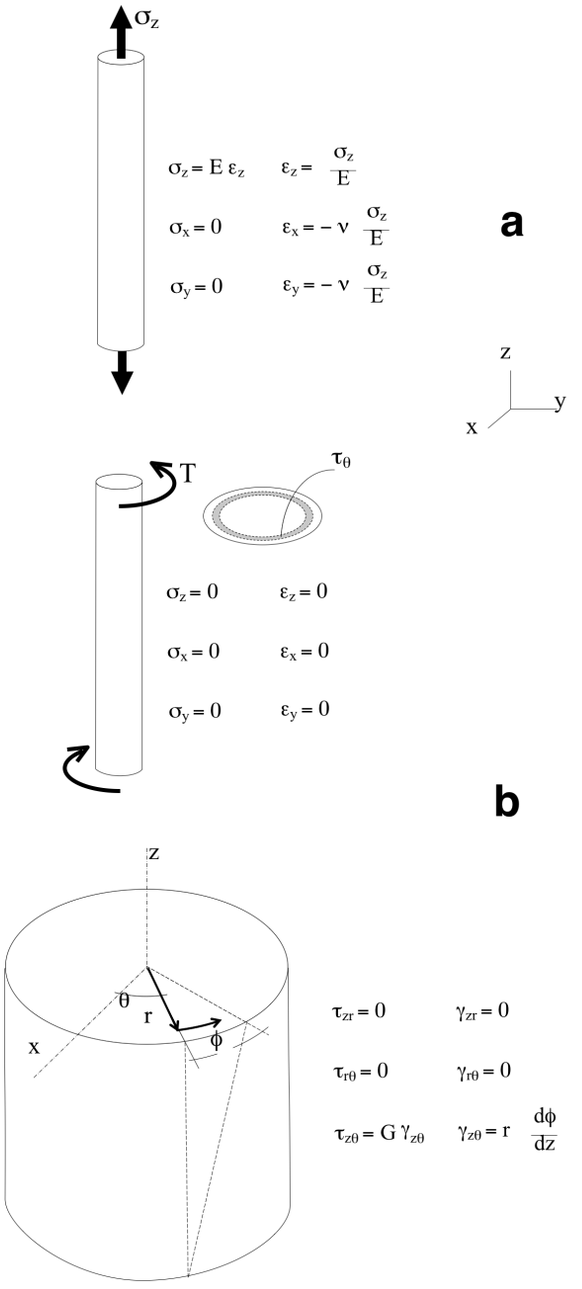

Fig. 8. *Summary of the stress state for a fibre in linear elatic regime .*
a. Tensile test.
b. Torsion test.

EXERCISE

Derive equation (18) $G=E/2(1+\nu)$ for a Hookean elastic material.

Solution:

Consider a cubic element of side L subjected to shear stresses $\tau_{zy}=\tau_{yx}=\tau$ as shown in figure a. At all times we consider small deformations and, in consequence, that the geometry remains unaltered because changes are small. However, in the figures the movements are axaggerated to provide greater clarity.

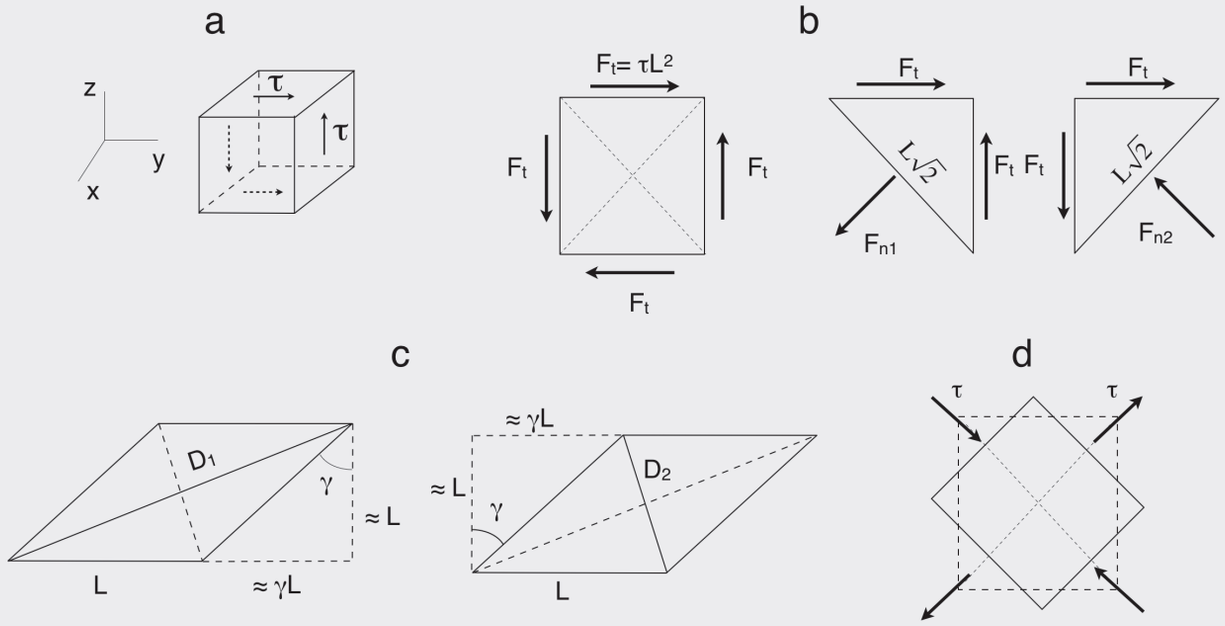

The effect produced by shear forces $F_t = \tau\, L^2$ is equivalent to two forces in the diagonal directions (figura b)),

$$F_{n1} = F_{n2} = \sqrt{2}\, F_t = \sqrt{2}\ \tau L^2$$

that give rise to a tensile stress along the diagonal that is stretched (direction 1), of value

$$\sigma_1 = \frac{F_{n1}}{L^2\sqrt{2}} = \ \tau$$

and a compressive stress along the diagonal that is shortened (direction 2)

$$\sigma_2 = \frac{-F_{n2}}{L^2\sqrt{2}} = \ -\tau$$

The length of the stretched diagonal is (figure c))

$$D_1 = \sqrt{L^2 + (L + L\gamma)^2} \approx L\sqrt{2}(1+\gamma/2)$$

with a corresponding strain

$$\varepsilon_1 = \frac{D_1 - L\sqrt{2}}{L\sqrt{2}} \approx \gamma/2$$

and the diagonal that is shortened sees its length reduced to

$$D_2 = \sqrt{L^2 + (L - L\gamma)^2} \approx L\sqrt{2}(1 - \gamma/2)$$

with a strain

$$\varepsilon_2 = \frac{D_2 - L\sqrt{2}}{L\sqrt{2}} \approx -\gamma/2$$

Considering the stress state in the diagonal directions (1) and (2) (figure d), we see that it is possible to represent them as a superposition of two states of simple traction

$$\sigma_1 = \tau\ ; \qquad \sigma_2 = 0\ ; \qquad \sigma_z = 0$$

and

$$\sigma_1 = 0; \qquad \sigma_2 = -\tau\ ; \qquad \sigma_z = 0$$

whose strains, represented in figure 8 a),are respectively

$$\varepsilon_1 = \tau/E\ ; \qquad \varepsilon_2 = -\nu\,\tau/E\ ; \qquad \varepsilon_z = -\nu\,\tau/E$$

and

$$\varepsilon_1 = \nu\,\tau/E\ ; \qquad \varepsilon_2 = -\tau/E\ ; \qquad \varepsilon_z = \nu\,\tau/E$$

and therefore the total strain seen by an element will be their sum

$$\varepsilon_1 = \tau(1+\nu)/E\ ; \qquad \varepsilon_2 = -\tau(1+\nu)/E; \qquad \varepsilon_z = 0$$

Since $\varepsilon_1 = \gamma/2$ we obtain

$$\varepsilon_1 = \gamma/2 = \tau(1+\nu)/E$$

from which, with the aid of the expression $\gamma = \tau/G$, we determine G

$$G = \frac{E}{2(1+\nu)}$$

EXERCISE

Justify that when $\nu = 0{,}5$ a material deforms while maintaining a constant volume.

Solution:

The change in volume produced during the deformation represented in figure 7 is

$$abl - ABL = A(1+\varepsilon_x)\,B(1+\varepsilon_y)\,L(1+\varepsilon_z) - ABL \approx ABL(\varepsilon_x + \varepsilon_y + \varepsilon_z)$$

in which we have neglected products of the deformations, since they are very small.

Substituting the value of the Poisson's ratio (following figure 7) we obtain

$$abl - ABL \approx ABL(\varepsilon_x + \varepsilon_y + \varepsilon_z) = ABL(-\nu\varepsilon_z - \nu\varepsilon_z + \varepsilon_z) = ABL\ \varepsilon_z(1-2\nu)$$

an expression in which we can verify that when ν=0.5 the change in volume is zero.

EXERCISE
Show that $-1 < \nu < +0.5$

Solution:
The shear modulus G is given by equation (18)

$$G = \frac{E}{2(1+\nu)}$$

which must be always positive, as must the Young's modulus E, so these conditions require that $\nu > -1$.

The bulk moduls K, defined as the relationship between the unifrom pressure applied to a body and the resulting change in volume, must also be positive. The value of K can be deduced from an experiment in which stresses $\sigma_x = \sigma_y = \sigma_z = -p$ are applied to a body.

This problem can be solved as a sum of the cases:

$$\sigma_x = -p \; ; \; \sigma_y = \sigma_z = 0$$
$$\sigma_y = -p \; ; \; \sigma_x = \sigma_z = 0$$

and

$$\sigma_z = -p \; ; \; \sigma_x = \sigma_y = 0$$

whose solution can be deduced from figure 8a, yielding for each case

$$\varepsilon_x = -p/E \; ; \; \varepsilon_y = \varepsilon_z = -\nu p/E$$
$$\varepsilon_y = -p/E \; ; \; \varepsilon_x = \varepsilon_z = -\nu p/E$$

and

$$\varepsilon_z = -p/E \; ; \; \varepsilon_x = \varepsilon_y = -\nu p/E$$

The total strain is the sum of each case, being equal to

$$\varepsilon_x = \varepsilon_y = \varepsilon_z = -p(1-2\nu)/E$$

The change in volume produced will be (see the previous exercise)

$$\Delta V = V(\varepsilon_x + \varepsilon_y + \varepsilon_z) = -Vp3(1-2\nu)/E$$

where V is the initial volume and ΔV its change, that will be negative. The value of K is, by definition

$$K = -\frac{p}{\Delta V/V} = \frac{E}{3(1-2\nu)}$$

In order to have $K > 0$ we see that $\nu < +0.5$.

2.3.3. Concluding remarks

Hookean, or linear, elastic behaviour is the simplest approximation to the response of a material. Figure 8 summarises the relationships between stresses and strains for a fibre that behaves in a Hookean manner.

At the microscopic level, this behaviour can be interpreted as the result of tiny reversible dispalacements of particles (atoms, molecules, etc.) from their eqilibrium positions. Consequently, the internal structure of the material does not change and the variations in the internal energy can be calulated with respect to the equilibrium positions, through a linear approach in which only the first two terms are considered; the constatnt equilibrium value and a linear term with the displacements of the particles. This implies that the force –as the energtically conjugate of the displacement– appears as the first derivative of the internal energy with respect to the dispacement.

As will be seen in the next section, when the deformation iimplies changes in the arrangement of the particles of the material the analysis is complicated, the *linear approximation* to the internal energy is not valid, and quantities such as entropy, related to the degree of disorder, come into play.

In general, in biological materials the deformation tends not to be proportional to the load. Fibres that exhibit *nonlinear elastic* behaviour in a tensile test cannot be characterised in such a simple way nor is it possible to obtain such a simple constitutive equation.

2.4. ELASTOMERIC BEHAVIOUR

2.4.1. INTRODUCTION

There is a family of polymers, capable of standing large reversible deformations, called elastomers; these are polymers whose chains are cross-linked. The classical example of an elastomer is vulcanised rubber. Natural rubber (cis-polyisoprene) is not properly an elastomer, because during deformation of the polymer chains slide over each other and the orginal length is not recovered on unloading; the deformation is not reversible and the material cannot be considered as elastic. Only when cross-links between the polymer chains are created –for example, by means of sulphur bonds, a process known as vulcanisation– is a polymer produced that recovers its original shape.

For this type of material it is possible to assume that under the action of a force the arrangement of its molecules change immediately, so that it is possible to apply the laws of thermodynamics and to relate the stress state to changes in the internal energy and entropy. For this approach to provide information about the physical nature of the parameters used it is essential, in a second step, to know how to relate the internal energy and the entropy of the materials to the movement of the molecular chains.

Typical curves obtained from a tensile test on an elastomer are shown in figure 9. Note that true strains approaching 170 per cent are achieved, and that this is reversible (the rise of the curve is conicident with the descent), and nonlinear. Only for small strains, of the order of 1 per cent, can it be assumed that the relationship between stress and strain is linear, that is to say Hookean. This behaviour indicates that the fundamental mechanism of the deformation of elastomers must be very different from metallic materials, ceramics and other types of solids. The nonlinearity that is exhibited for large deformations must be, as will be seen later, due more to changes in entropy than to variations in internal energy.

The entropy of an elastomer is reduced during deformation because the material is more ordered –the chains align themselves– and only recover their initial shape if they are unloaded, since the entropy of an isolated system tends to increase. The entropy of a completely extended polymer chain is zero because it is the only conguration possible. On the other hand, in the initial equilibrium position the chain is curled up, there are many possible configuration that produce the same contraction, and the entropy is large. However, the internal energy of a long chain is practically the same whatever the configuration, since its origin is mainly in the stretching of its "links" and not in their relative curling. For this reason, in the absence of external forces, a strectched chain will tend to return to its equilibrium position basically due to the effect of entropy.

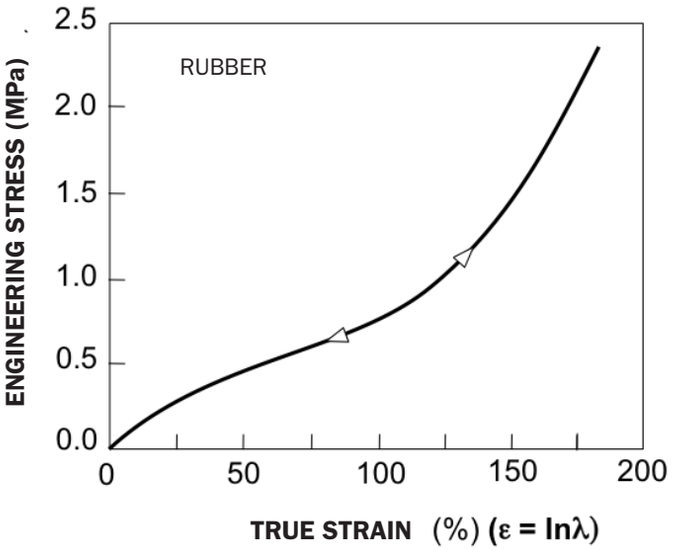

Fig. 9. *True stress-true strain curve for natural rubber vulcanised 8% sulphur. Up to strains of 200% the behaviour is elastomeric. (Data from Treloar, 1944).*

2.4.2. Thermodynamics of elastomeric deformation

The objective of this section is to find an expression that relates the force acting on a fibre to the change in entropy during deformation.

The First Law of Thermodynamics –conservation of energy– implies that:

$$dU = dQ + dW \tag{19}$$

where dU is the change in internal energy of the system, dQ is the heat energy contribution which, in a reversible process, is given by TdS (where T is the absolute temperature and S is the entropy), and dW is the contribution from the work done by the external forces.

Considering a tensile test, the work done by the external forces, dW will have two components, one due to the applied force F and the other resulting from the external pressure p, (which also exerts forces on the surface of the specimen) - see figure 10.

$$dW = F\,dl - p\,dV$$

where dl is the displacement of the applied force F and dV the change in volume during the deformation. Therefore, equation (19), for a tensile test, can be written as:

$$dU = TdS + Fdl - p\,dV \tag{20}$$

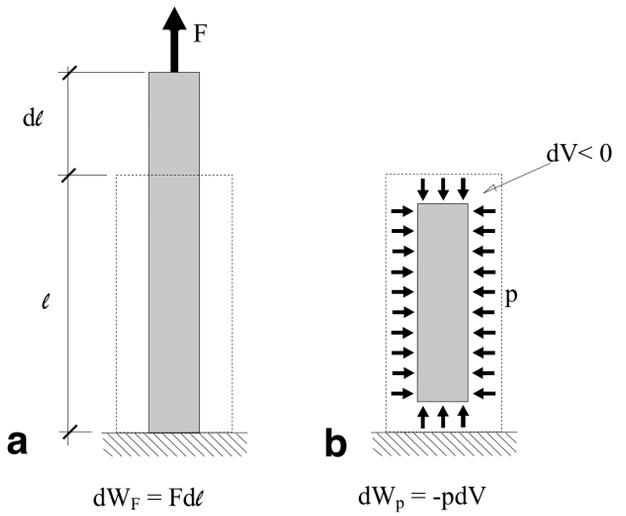

Fig.10. *Work done by the external forces on a fibre (the initial position is shown dotted).*
a. External tensile force.
b. Contraction due to the effects of the external pressure.

As observed above, most biological materials deform under constant volume and dV=0. In the case of elastomers this assumption can be justified for small deformations but, in general, it is not obvious. For small deformations the bulk modulus[8], K, is about 10,000 times greater than the shear modulus, G. The relationship between both moduli and the Poisson's ratio ν, is (see, for example, Landau 1986):

$$\nu = \frac{3K-2G}{2\,(3K+G)}$$

Therefore, when $K>>G$ is $\nu \simeq 0.5$, and the deformation occurs essentially at constant volume. In any case, for typical values of pressure (about 1 atm.) and solids or liquids (which unlike gases undergo little change in volume), the term pdV is negligible compared to Fdl.

It is possible then to ignore the effects of a change in volume and to consider only the thermodynamic variables of the problem which are the applied force, F, specimen length l, and temperature T.

$$dU = TdS + Fdl \tag{21}$$

It is interesting to note that, in this thermodynamic description of the deformation process, the equation of state of the thermodynamic system (for the problem considered) coincides with the constitutive relationship that exists between the applied force and the length, and, also, depends upon the temperature

$$F=f(l,T)$$

thus only three variables (F, l, T) are truely independent. Or, in other words, it is not possible to arbitrarily set values to the three variables at the same time, since the third is determined by the other two.

In 1935, Meyer and Ferri showed that, for some *elastomers*, if the specimen length l was kept constant, the force F would be proportional to the temperature T, that is:

$$F = a\,T \tag{22}$$

where a is a positive constant. Similar results have been obtained for biological materials which behave elastomerically, such as resilin (Weis-Fogh, 1961) and abductin (Alexander, 1966). Note that elastomers tend to shrink when heated, since according to equation (22) they develop tractions that increase with temperature for constant length. For this reason, if the length is held fixed, the specimen will tighten with increased temperature, as can be observed in figure 11.

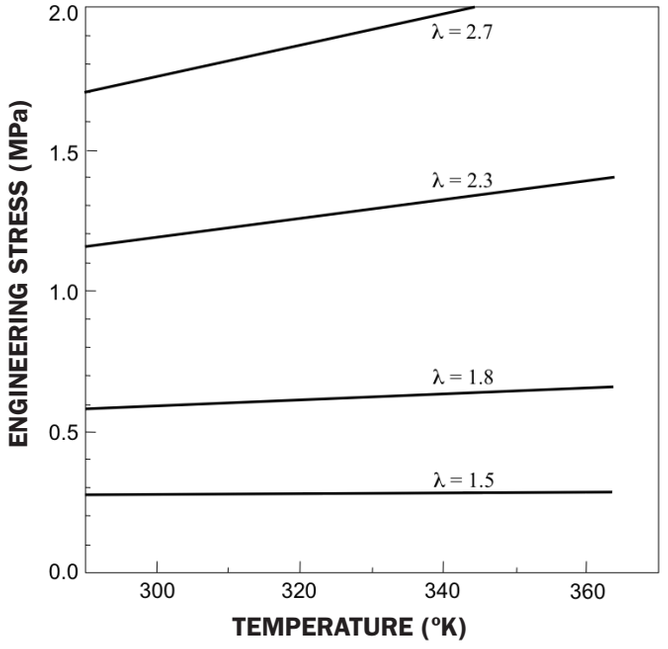

Fig. 11. *Variation of the engineering stress as a function of temperature for a resilin fibre in which the length L is held constant (for different elongations λ ($\lambda = L/L_0$), where L_0 is the initial length in each case, of dry fibre). The data are for the resilin in the libelula tendon Aeshna grandis (based on Weis-Fogh, 1961).*

[8] The bulk modulus is defined as the ratio of the infinitesimal pressure increase to the resulting relative decrease of the volume. (see vol.III, 2.3.2).

This behaviour (where it is assumed that $F = a\ T$, when l is constant) justifies the role of entropy in the calulation of force F.

From equation (20), and bearing in mind what was said above, the force F (see the exercise below) is given by:

$$F = \left(\frac{\partial U}{\partial l}\right)_T - T\left(\frac{\partial S}{\partial l}\right)_T \tag{23}$$

but the first term of equation (23) is zero, since (see the exercise that follows):

$$\left(\frac{\partial U}{\partial l}\right)_T = F - T\left(\frac{\partial F}{\partial T}\right)_l = F - T\frac{F}{T} = 0 \tag{24}$$

because $(\partial F/\partial T)_l = a = F / T$ according to the experimental results expressed by equation (22).

This shows that the sole contribution to the force F (under the assumptions made) is the entropy given, according to equation (23), by:

$$F = -T\left(\frac{\partial S}{\partial l}\right)_T \tag{25}$$

In order to proceed to the determination of the constitutive equation $F = f(l\ ,\ T)$ it is necessary to obtain information about $S(l)$, the entropy of the fibre.

EXERCISE

Derive equations (23) and (24).

Note: the use of the thermodynamic function $A = U - TS$, known as the Helmholtz free energy, helps the derivation.

Solution:

Differentiating A and observing that $dU = TdS + Fdl$

$$dA = dU - TdS - SdT = Fdl - SdT \tag{a}$$

from this result, and noting that A is a function of the variables and T,

$$dA = \left(\frac{\partial A}{\partial l}\right)_T dl + \left(\frac{\partial A}{\partial T}\right)_l dT \tag{b}$$

it is deduced, comparing (a) and (b), that

$$F = \left(\frac{\partial A}{\partial l}\right)_T = \left(\frac{\partial U}{\partial l}\right)_T - T\left(\frac{\partial S}{\partial l}\right)_T \quad \text{y} \quad -S = \left(\frac{\partial A}{\partial T}\right)_l$$

which yields equation (23).

Using Schwartz's theorem it is possible to write

$$\frac{\partial}{\partial T}\left(\frac{\partial A}{\partial l}\right)_T = \frac{\partial}{\partial l}\left(\frac{\partial A}{\partial T}\right)_l$$

in which

$$\left(\frac{\partial F}{\partial T}\right)_l = -\left(\frac{\partial S}{\partial l}\right)_T \tag{c}$$

then, taking into account equations (23) and (c)

$$\left(\frac{\partial U}{\partial l}\right)_T = F + T\left(\frac{\partial S}{\partial l}\right)_T = F - T\left(\frac{\partial F}{\partial T}\right)_l$$

resulting in equation (24).

2.4.3. Molecular theory of elastomeric deformation

The mechanical behaviour of elastomers can be modelled by assuming that they are composed of long molecular chains, capable of adopting a large number of configurations as a result of the thermal vibrations of their atoms. Although the molecular chains are linked together, it is assumed that the number of links is sufficiently small and that they do not significantly impede the movement of the chains so that, in the absence of external forces, the chains adopt positions corresponding to the state of maximum entropy. When a force is applied, the chains will tend to deform in the direction of the force, and entropy will be reduced, causing a state of tension.

Therefore, in order to obtain a relationship between stress and strain from equation (25) it will be necessary to calculate the entropy of a network of chains as a function of the length of the network. This calculation can be performed in two stages; first determining the entropy of an isolated chain and, then, calculating the variation of the entropy of the network as a function of its length.

The purpose of this section is to show the reader the route to an expression for the entropy as a function of the length of the polymer chain. The objective of this book is not to develop the detail of each step, the interested reader will find the fine detail of these calculations in the cited references. However, some steps in the process have been included in the Appendix as exercises.

Entropy of an isolated chain

a. Gaussian model

In order to facilitate the calculations, in a first approximation, the chain molecule is replaced by a series of links which can rotate freely between themselves, in this way some restrictions imposed by the stiffness of a molecular chain are eliminated.

It is assumed that the chain is formed of n links of each of length l_0. One end of the chain is located at the origin of coordinates, O, (as shown in figure 12). It is assumed that, as a result of thermal agitation, the molecular chain changes its configuration randomly with time. In order to obtain the value of any parameter of the chain (its length, for example) we must obtain a time average value. This is done using the function $p(\mathbf{r})$, which provides information about the probability of the various configurations of the chain over a sufficiently long period.

The Gaussian model states that the probability $p(\mathbf{r})\ dV$ of finding an end Q in a volume element, $dV = dx\ dy\ dz$, about point $\mathbf{r}$ is given by (see, for example, Flory 1989 and the posed exercise).

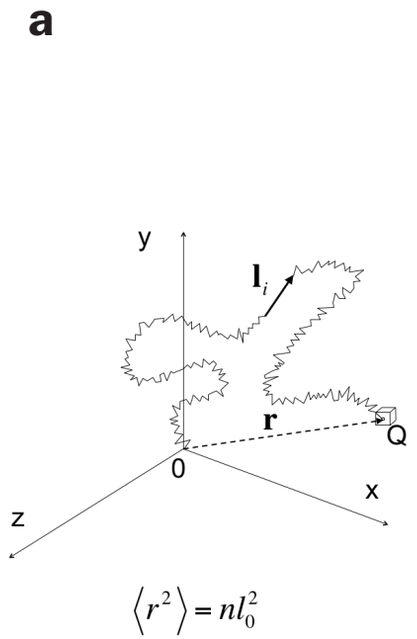

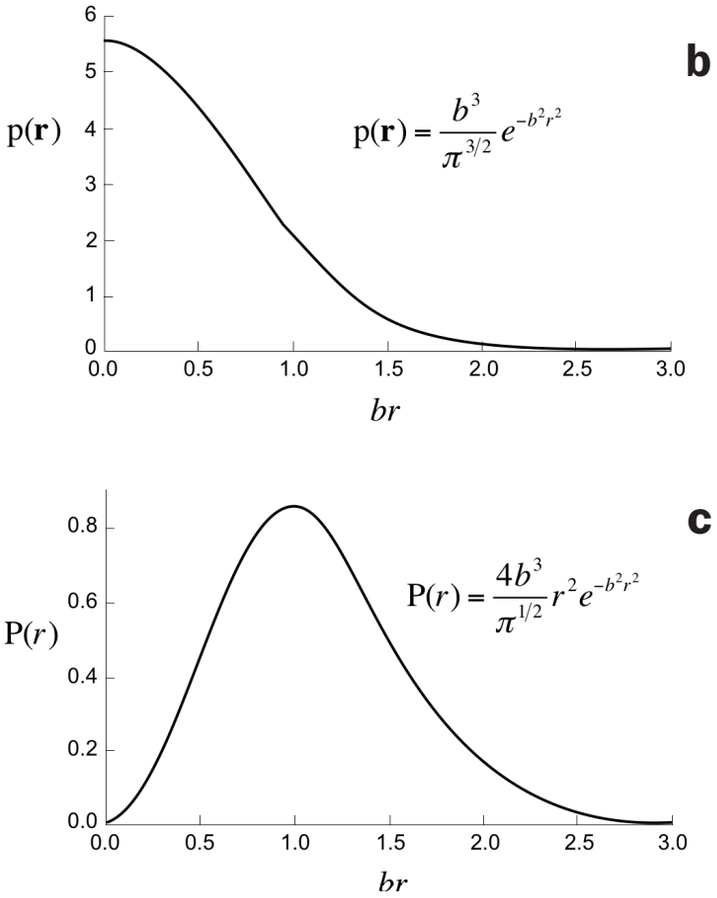

Fig. 12. *a. Idealised configuration of a polymer (Gaussian chain), together with functions $p(\mathbf{r})$ and $P(r)$.*
b. $p(\mathbf{r})$ – Probability of finding end Q inside dV, located at $\mathbf{r}$.
c. $P(r)$ – Probability of finding end Q inside a volume located between r and $r + dr$.

$$p(\boldsymbol{r})dV = \frac{b^3}{\pi^{3/2}} \exp(-b^2 r^2)\, dV \qquad (26a)$$

where $b^2 = 3/(2nl_0^2)$. Function $p(\boldsymbol{r})$ takes the form of a Gaussian probabilty distribution[9], symmetric about the origin, $\boldsymbol{r} = \boldsymbol{0}$, at which the function is a maximum (see figure. 12). Function $p(\boldsymbol{r})$ is normalised (its integral across space is 1) and it is only zero at infinity, which is contrary to the fact that the maximum chain length is nl_0, and the probability of exceeding that value must be zero. From a practical point of view, since the function $p(\boldsymbol{r})$ is practically zero for sufficiently large values of the exponent, it is sufficient to restrict its application to situations when $r << nl_0$.

In order for $p(\boldsymbol{r})$ to be symmetric about the origin, the most likely value –and also the average of the radius vector $\boldsymbol{r}$– is $\boldsymbol{0}$, and the average position of Q is point O. However, the mean value of the distance to the origin, r, is not zero. The probability $P(r)dr$ that Q falls within a volume located within a spherical shell between r and $r + dr$, independent of the direction of r, is the product of $p(\boldsymbol{r})$ and the volumen $4\pi\, r^2 dr$. That is, the probability is given by:

$$P(r)dr = 4\pi\, r^2\, dr\, p(\boldsymbol{r}) = \frac{4b^3}{\pi^{1/2}}\, r^2 \exp(-b^2 r^2)\, dr \qquad (27)$$

Function P(r) is shown in figure 12 and it can be seen that it has a maximum when $r = b^{-1}$, a value that depends upon the number of links n and the length of each one of them, l_0. The mean distance between the ends of the chain $< r >$, is obtained (see the exercise) as

$$< r > = \int_0^\infty r\, P(r)dr = \left(2/\sqrt{\pi}\right) b^{-1} = \sqrt{\frac{8}{3\pi}}\, n^{\frac{1}{2}}\, l_0 \simeq 1.13\, b^{-1} \qquad (28)$$

and the mean of the distance squared between the ends of the chain, $< r^2 >$, (which will be used in later calculations) is (see the exercise)

$$< r^2 > = \int_0^\infty r^2\, P(r)dr = 3/(2\, b^2) = nl_0{}^2 \qquad (29)$$

Note that $< r^2 > \neq < r >^2$.

The entropy S of the chain in a particular configuration can be calculated using Boltzmann[10], statistics, which yields a value that is proportional to the logarithm of the number of possible configurations (microstates), Z, compatible with that macroscopic configuration (macrostate). Its value is given by:

$$S = k \ln Z \qquad (30)$$

where k is the Boltzmann constant, equal to 1.3806488(13)×10^{-23} Joules/K. Then the number of possible configurations compatible with a value $\overline{OQ} = \boldsymbol{r}$ of the chain must be proportional to the probability density $p(\boldsymbol{r})$ of that macroscopic configuration, given by equation (26), and the entropy of the chain becomes

$$S = c - k\, b^2\, r^2 \qquad (31a)$$

where c is a constant.

b. FJC Model

The freely articulated chain model (FJC, Freely Jointed Chain) avoids the limitation of the Gaussian model which considered an infinite chain length (and led to the restriction that it could only be applied to cases where $r << nl_0$).

In this model, the probability density function $p(\boldsymbol{r})$ is the result of a random path of n steps each of length l_0 Function $p(\boldsymbol{r})$ turns out to be (Ward, Sweeney, 2004)

$$p(\boldsymbol{r}) = C \exp\left[-n\left\{\frac{r\beta}{nl_0} + \ln\left(\frac{\beta}{sinh(\beta)}\right)\right\}\right] \qquad (26b)$$

where C is a constant and parameter β is given by the Langevin[11] '$\mathcal{L}(\beta)$

$$\mathcal{L}(\beta) = \coth(\beta) - \frac{1}{\beta} = \frac{r}{nl_0}$$

in which $\beta = \mathcal{L}^{-1}(r/(nl_0))$

The development of equation (26b) for large values of , yields the Gaussian chain model (26) (see exercise and figure 13).

Applying equation (30), the entropy of the chain becomes

$$S = c - kn\left[\frac{r\beta}{nl_0} + \ln\left(\frac{\beta}{sinh(\beta)}\right)\right] \qquad (31b)$$

where c is a constant.

[9] Johann Carl Friedrich Gauss (1777 - 1855), was a German mathematician and physicist, who used Equation (26a) widely in the analysis of astronomical data, as did Abraham de Moivre, the French mathematician, who first derived it in 1733.

[10] Ludwig Edward Boltzmann (1844 - 1906), was an Austrian physicist and pioneer of statistics, who proposed Equation (30) for the calculation of entropy. That equation can be found engraved on his tomb in the central cemetery in Vienna.

[11] Paul Langevin (1872 - 1946), was a French physicist who derived the function $\mathcal{L}(\beta)$ during a study of the agnetisation of paramagnetic materials.

c. WLC Model

In order to obtain a better fit to the experimental data, more complex models have been developed.

One of these is the worm chain model (WLC, Worm-Like Chain model), which provides a good representation of chains that have some degree of bending stiffness. The model assumes that the average angle formed between two links of the chains is not zero –as in the FJC model– but its cosine decreases as $\exp(-s/l_p)$, where s is the distance between two links and l_p a distance particular to the model, known as the persistence length. The response of the model when the length of the chain nl_0 is much greater than l_p is

$$F = \frac{kT}{l_p}\left[\frac{1}{4(1-r/nl_0)^2} - \frac{1}{4} + \frac{r}{nl_0}\right]$$

which, as can be seen in figure 13 (Bustamante et al. 2000), is in good agreement with experimental results.

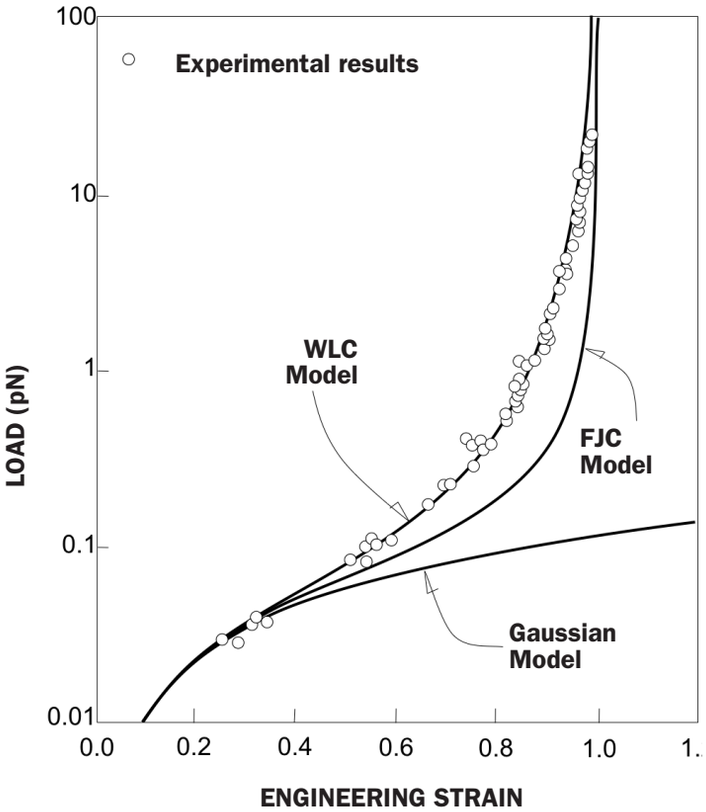

Fig.13. *Load versus engineering strain curves for dsDNA (48,502 bp) of phage λ obtained by traction with magnetic microspheres. Comparison with the worm chain model WLC, which was obtained with an lp f 53 nm. The FJC model assumes a chain length l_0 of 106 nm. (Bustamante et al. 2000).*

Commentary on experiments with DNA molecules:
When tensile tests are performed on DNA molecules using optical tweezers[12]– or AFM[13], for example, the data shown in figure 13 are obtained. In this figure it is apparent that the Gaussian model (Hooke' law) only fits for small deformations, while the FJC model is good at the two asymptotic extremes: for small deformations and at very large ones. This suggests that the molcular chains (of DNA, in this case) do not behave as rigid links which rotate freely

[12] Optical tweezers use the confinement effect produced near the focal point of a spatially inhomogeneous beam of light on very small objects (microns). If the object is just outside the focus, the resulting refractive and dispersive forces of the light rays (of the order of pN) create a resultant that attracts the object to the focal point.

[13] Atomic Force Microscopy. An atomic force microscope (AFM) allows a very sharp pointer (~nm) to closely track a surface with very high precision, while measuring the force (~nN) between the surface and the tip of the pointer. It is also possible to attach the end of a molecule to the tip of the AFM and to pull it with great precision, performing a micro-tensile test.

EXERCISE

Using equations (25) and (26b), calculate the force on a chain as a function of its length r. Determine, also, the limits for large and small displacements.

Solution:

The force comes from equation (25) and the entropy from equation (31b). Thesefore:

$$F = -T\left(\frac{\partial S}{\partial r}\right)_T = kTn\left[\frac{\beta}{nl_0} + \left(\frac{r}{nl_0} + \frac{1}{\beta} - \coth(\beta)\right)\frac{d\beta}{dr}\right]$$

and, bearing in mind that

$$\mathcal{L}(\beta) = \coth(\beta) - \frac{1}{\beta} = \frac{r}{nl_0}$$

we obtain

$$F = kTn\left[\frac{\beta}{nl_0}\right] = \frac{kT\beta}{l_0}$$

or

$$\mathcal{L}\left(\frac{Fl_0}{kT}\right) = \frac{r}{nl_0}$$

For small values of the argument (F and β, smalls), $\mathcal{L}(x) \approx x/3$, recovering the result for a Gaussian chain, which is no more than the linear relationship between force and displacement of Hooke's law

$$F = \frac{3kT}{nl_0^2}\, r$$

When the chain is highly stretched (F and β, large), F increases rapidly. For large values of the argument $\mathcal{L}(x) \approx 1 - 1/x$, giving

$$F = \frac{kT/l_0}{1 - r/nl_0}$$

In Figure 13, both results agree with experimental results.

Entropy of a molecular network

In this section an approximate form of the entropy of a network of polymer chains connected by crosslinks will be calculted. To facilitate the calculations the following assumptions are made.

Each chain between two anchor points behaves as a *Gaussian chain* with n links each of length l_0.

The chains are randomly distributed and in their initial state (at rest and unloaded) their mean values can be approximated as a free chain.

When the material deforms, the network of anchor points undergoes an *affine deformation*[14], as shown in figure 14. This type of deformation is usually considered, and occurs whenever the element remains homogeneous (same composition at all points) and isotropic (with the same properties in all directions) during the deformation.

Consider, in the first instance, the entropy of one of the chains in the initial state, without load, which is, according to equation (31a),

$$S_{b0} = c - kb^2\left(x_0^2 + y_0^2 + z_0^2\right) \tag{32}$$

where it has been assumed, for simplicity, that one end of the chain is at the origin of coordinates and the other is at point $\boldsymbol{r}_0\ (x_0, y_0, z_0)$.

After deformation of the material, the new contribution of this chain will be

$$S_b = c - k\,b^2\left(\lambda_1^2 x_0^2 + \lambda_2^2 y_0^2 + \lambda_3^2 z_0^2\right) \tag{33}$$

in which, again, we have eliminated the position of the origin of the chain–which has no relevance– in order to write the coordinates of the deformed end $(\lambda_1 x, \lambda_2 y, \lambda_3 z)$, see figure 14. The coefficients $(\lambda_1, \lambda_2, \lambda_3)$ are the elongations (ratios of the final and initial lengths) which produce the affine deformation in each of the three coordinate directions (x, y, z).

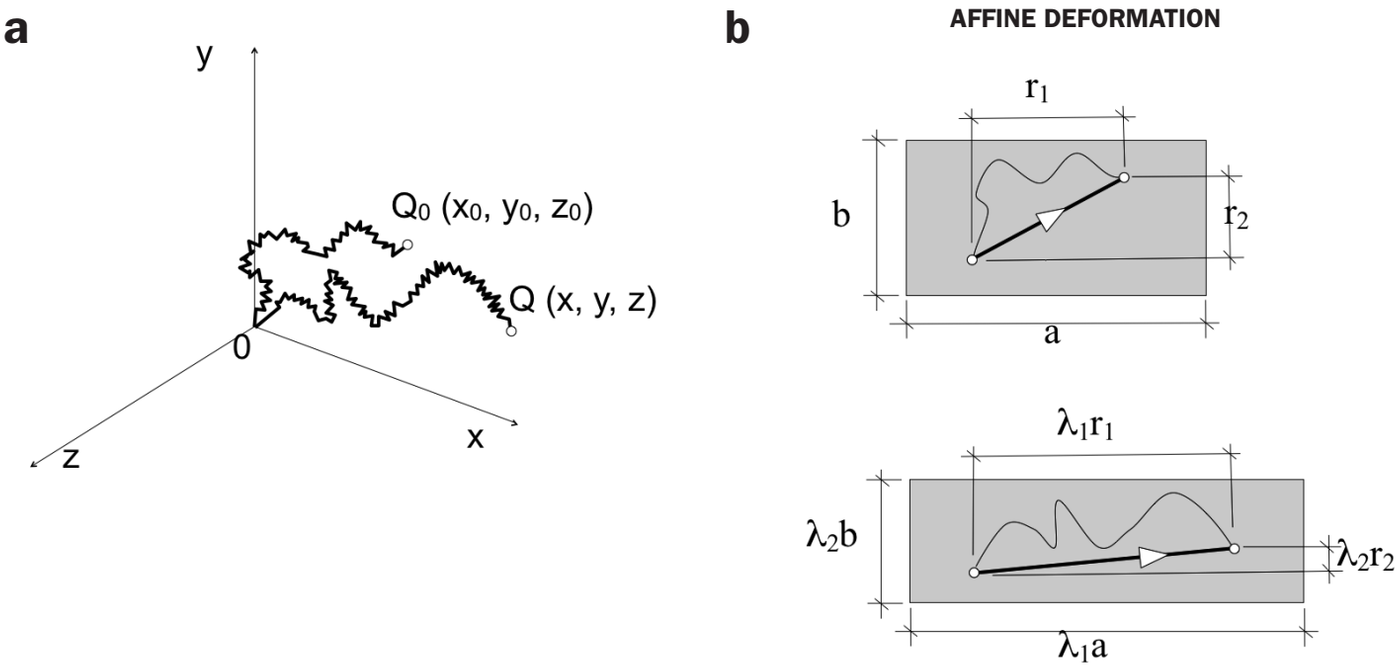

Fig. 14. *a. Idealised configuration of a polymer chain before and after deformation.*
b. The concept of an affine deformation. *The components in direction (1) change in the ratio λ_1 while those in direction (2) with λ_2.*

[14] In an affine deformation, the components of a vector that join two points in a material change in the same proportion as the corresponding components of the macroscopic strains. It is a linear transformation in which points initially situated on a straight line, or in a plane, remain in a straight line or forming a plane after deformation, although the lines and planes are usually different. Similarly, the transformation preserves parallelism between the lines, although not, generally, the angles or distances.

If N_b is the number of chains, the entropy due to all of them will be

$$S = \sum_{N_b} S_b$$

In more detail

$$S = cte - kb^2 \sum_{N_b} \left(\lambda_1^2 x_0^2 + \lambda_2^2 y_0^2 + \lambda_3^2 z_0^2 \right) =$$

$$= cte - kb^2 \left(\lambda_1^2 \sum_{N_b} x_0^2 + \lambda_2^2 \sum_{N_b} y_0^2 + \lambda_3^2 \sum_{N_b} x_0^2 \right) =$$

$$= cte - kN_b b^2 \left(\lambda_1^2 \overline{x_0^2} + \lambda_2^2 \overline{y_0^2} + \lambda_3^2 \overline{z_0^2} \right) \qquad (34)$$

where use has been made of the fact that the deformation is the same in all of the chains and the mean values of x_0^2, y_0^2 and z_0^2 have been introduced. In the calculation it is assumed that the change in entropy due to the interaction between chains is negligible so that its only source is that due to the form of the chains (configurational entropy).

If it is assumed that the spatial average of the rest state coincides with that over the space of the free chains and that this, in turn, coincides with the time average[15], it is possible to substitute the mean values over all the chains at a given time with that over one of them, represented by the symbol < >, calculated in equation (29).

Since the chains are distributed randomly, the mean values must be equal in all directions:

$$\sum_{N_b} r_0^2 = N_b \left\langle r_0^2 \right\rangle = \sum_{N_b} \left(x_0^2 + y_0^2 + z_0^2 \right) = 3 \sum_{N_b} x^2 = 3N_b \left\langle x_0^2 \right\rangle$$

and

$$\left\langle x_0^2 \right\rangle = \left\langle y_0^2 \right\rangle = \left\langle z_0^2 \right\rangle = \frac{\left\langle r_0^2 \right\rangle}{3} = \frac{1}{2b^2} \qquad (35)$$

Therefore

$$S = cte - \frac{kN_b}{2} \left(\lambda_1^2 + \lambda_2^2 + \lambda_3^2 \right) \qquad (36)$$

This equation indicates that, although S_{tb} is proportional to N_b (as would be expected) it does not depend explicity on b and, therefore, the change in entropy per unit volume s, is given by

$$s = cte - \frac{kN}{2} \left(\lambda_1^2 + \lambda_2^2 + \lambda_3^2 \right) \qquad (37)$$

where N is now the total number of chains per unit volume of the network.

The *constitutive equation,* that is the relationship between stress and strain, can be deduced from equation (25), since the total entropy of the network is obtained by adding a constant, independent of the strain, to equation (37).

For a tensile test in direction x, where $\lambda_1 = \lambda$, and $\lambda_2 = \lambda_3 = \lambda^{-1/2}$ (assuming the material is incompressible $\lambda_1 \lambda_2 \lambda_3 = 1$), the following result is obtained for the applied force F (see the exercise)

$$F = NkT \left(\lambda - \lambda^{-2} \right) \cdot A_0 \qquad (38)$$

where A_0 is the initial cross section of the specimen. Recalling that the true stress is given by $\sigma = F/A$, equation (7), and $A = A_0/\lambda$, due to concentration of volume, then:

$$\sigma = NkT \left(\lambda^2 - \lambda^{-1} \right) \qquad (39a)$$

or, since $\sigma = s\,\lambda$

$$s = NkT \left(\lambda - \lambda^{-2} \right) \qquad (39b)$$

This result provides reasonable values for moderate and medium strains (upto about 200% , corresponding to λ=3) as can be seen in the example in figure 15, despite the simplifications that have been made.

Perhaps, the most satisfactory result is that equation (39) gives a physical meaning to the parameters of the equation, something that does not occur with empirical constitutive equations. In this case it can be seen that the initial elastic modulus is directly proportional to the absolute temperature T and, also, the number of cross links, characterised by N. (For an ideal network, N is equal to double the density of cross links).

[15] Systems in which the temporal average of certain quantities can be obtained as averages over the state space are termed ergodic, and are of great importance in statistical physics.

A similar development of the entropy in equation (31b) for the FJC model for a spatial network of three families of chains, leads to a value of the true stress in a tensile test equal to

$$\sigma = \frac{NkT}{3}\,\lambda\sqrt{n}\left[\mathcal{L}^{-1}\left(\frac{\lambda}{\sqrt{n}}\right) - \lambda^{-\frac{3}{2}}\mathcal{L}^{-1}\left(\frac{1}{\sqrt{\lambda}\sqrt{n}}\right)\right] \qquad (40)$$

which is shown in figure 15, where the engineering stress $s = \sigma/\lambda$ is depicted. The agreement is excellent even for large strains. In this case, the stress depends explicitly on the number of cross links in the chains, n. It can be readily shown (see the exercise) that for small elongations λ equation (40) converges –as would be expected– to equation (39) and the dependence upon n disappears.

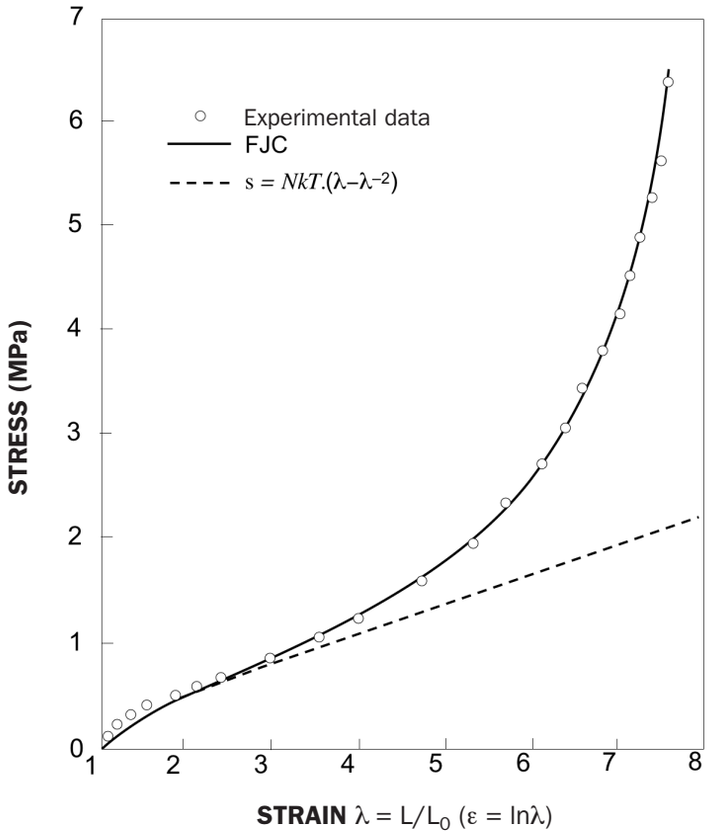

Fig. 15. *Engineering stress-strain curve for vulcanised rubber. Symbols – Experimental data (Treloar 1944). Solid curve –FJC model, after James and Guth (1943). Dashed curve – Gaussian chain model, from equation (38).*

2.4.4. Final remarks

Biological materials are, in general, quite complex as has been mentioned repeatedly. The arguments above –the thermodynamic approach and the molecular chain model– are only a first approximation in order to understand them when they exhibit elastomeric behaviour. It is, therefore, not surprising that the results obtained with this hypthesis have a limited value, which is usually confined to a regime of small deformations.

These concepts were developed in the middle of the last century and the interested reader will find a good summary in Treloar's book (Treloar, 1975). Since then there have been many attempts to refine this model: attempts to generalise the concept of cross links, removing the restriction that they should be fixed and with some able to slide or even disappear (if they are caused by the entanglement of chains). Gaussian statistics has been generalised by taking into account the structure and mobility of real chains. And the contibution of the internal energy has also been incorporated.

In particular, the influence of different types of cross links and the modelling of more realistic molecular chains have given rise to more sophisticated constitutive equations, whose results can be found in (Ball et al. 1981) and (Edwards and Vilgis, 1986), and which better reflect the stress-strain curves for large deformations. Generalisations of the non-Gaussian models have been produced for molecular chains perpendicular to each other (models with three, four, eight or more) (Arruda et al. 1993 and Wu and Giessen 1993) which can also reproduce the behaviour of the material for large deformations.

The objective of this section was to obtain a constitutive equation for fibres which exhibit elastomeric behaviour, that is to say, an expression which relates the force to the length of the fibre and the temperature, $F = f(l\ ,\ T)$. he effects of humidity and other external factors have not been considered. The weak influence of the variation of internal energy has been justified, and it has been concluded that the constitutive equation can be obtained from the variation of entropy of the fibre with length, that is:

$$F = -T\left(\frac{\partial S}{\partial l}\right)_T \qquad (25)$$

The problem has been reduced to calculation of the entropy for various models of the fibre stucture.

EXERCISE

Show that a material subjected to tension and whose constitutive equation is given by equation (39) does not neck before fracture.

Solution:

In a tensile test, the true strain ε, is related to the elongation λ through equation (4)

$$\varepsilon = \ln\frac{L}{L_0} = \ln\lambda$$

which can be inverted to give

$$\lambda = e^{\varepsilon}$$

Equation (8) gives the necking condition:

$$\sigma = \frac{d\sigma}{d\varepsilon}$$

introducing the constitutive equation of the material equation (39)

$$\frac{d\sigma}{d\varepsilon} = \frac{d\sigma}{d\lambda}\frac{d\lambda}{d\varepsilon} = NkT\left(2\lambda + \frac{1}{\lambda^2}\right)e^{\varepsilon} = NkT\left(2\lambda + \frac{1}{\lambda^2}\right)\lambda = \sigma = NkT\left(\lambda^2 - \frac{1}{\lambda}\right)$$

which leads to

$$\lambda^3 + 2 = 0$$

this has a solution $\lambda = -1.26$, which has no physical meaning.

The absence of necking can be confirmed graphically with Considère's construction:

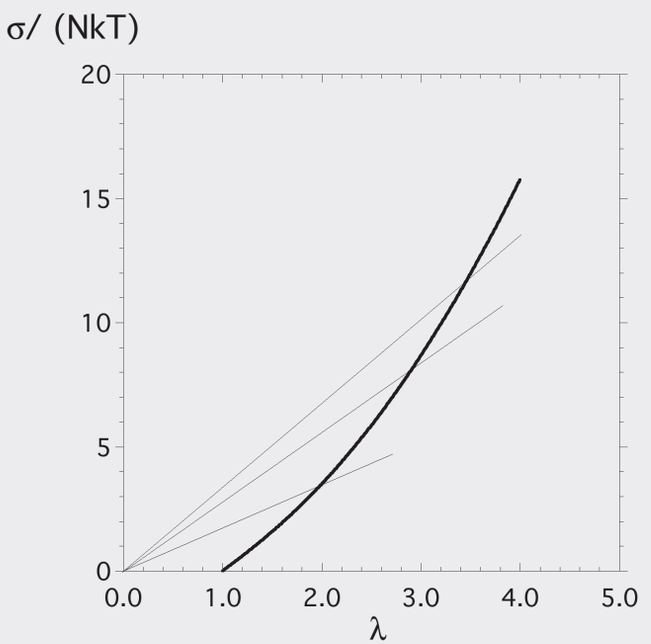

EXERCISE

Show that throughout the deformation of an incompressible material $\lambda_1\lambda_2\lambda_3 = 1$ and deduce equations (38) and (39).

Solution:

Consider an infinitesimal element $dV_0 = dx\ dy\ dz$ before deformation, and whose edges are orientated along directions (1), (2) y (3). After deformation, its dimensions become $dV = \lambda_1 dx\ \lambda_2 dy\ \lambda_3 dz = \lambda_1\lambda_2\lambda_3\ dV_0$

From a simple inspection of the above equation, we see the incompressibility condition (= constant volume, $dV=dV_0$) requires $\lambda_1\lambda_2\lambda_3 = 1$.

Suppose that the element is incompressible, homogeneous and isotropic, and subjected to tensile loading, with initial lengths and cross sectional area L_0 and A_0 , respectively. If the material is stretched to length L it will suffer an elongation

$$\lambda_1 = \lambda = \frac{L}{L_0}$$

The elongations in the other two orthogonal directions (those of the cross section A_0) confirm that $\lambda_1\lambda_2\lambda_3 = 1 = \lambda\,\lambda_2\lambda_2$ then the material is incompressible, and $\lambda_2 = \lambda_3$ by symmetry. From this last equation we see that $\lambda_2 = \lambda_3 = \lambda^{-1/2}$

The value of the initial cross sectional area A_0 changes under deformation depending on the values λ_2 y λ_3, giving

$$A = \lambda_2\lambda_3\, A_0 = \lambda^{-1}\, A_0$$

So that the true stress will be equal to (see equations (3) y (7))

$$\sigma = \frac{F}{A} = \lambda\frac{F}{A_0}$$

where F is the applied force. In order to calculate its value, we use equation (25): $F = -T\left(\frac{\partial S}{\partial L}\right)_T$ with $S = s\,A_0L_0$

noting that s is given by equation (37) and $V_0 = A_0\,L_0$ the volume of the specimen. Derivation yields

$$F = -TA_0L_0\left(\frac{\partial s}{\partial L}\right)_T = -TA_0L_0\sum_{i=1}^{3}\left(\frac{\partial s}{\partial \lambda_i}\right)_T\frac{\partial \lambda_i}{\partial L}$$

The derivatives of the elongations are $\frac{\partial\lambda_1}{\partial L} = \frac{\partial\lambda}{\partial L} = \frac{\partial}{\partial L}\left(\frac{L}{L_0}\right) = \frac{1}{L_0}$ and $\frac{\partial\lambda_2}{\partial L} = \frac{\partial\lambda_3}{\partial L} = \frac{\partial\lambda^{-1/2}}{\partial L} = -\frac{1}{2}\lambda^{-3/2}\frac{\partial\lambda}{\partial L} = -\frac{1}{2}\lambda^{-3/2}\frac{1}{L_0}$

resulting in

$$F = -TA_0L_0\left[Nk\lambda_1\frac{1}{L_0} + Nk\lambda_2\left(-\frac{1}{2}\lambda^{-3/2}\frac{1}{L_0}\right) + Nk\lambda_3\left(-\frac{1}{2}\lambda^{-3/2}\frac{1}{L_0}\right)\right] = NkTA_0\left[\lambda - \lambda^{-2}\right]$$

And the true stress is

$$\sigma = \lambda\frac{F}{A_0} = NkT\left[\lambda^2 - \frac{1}{\lambda}\right]$$

Which are equations (38) and (39).

The engineering stress s (not to be confused with the entropy per unit volume!) is simply

$$\mathrm{s} = \frac{F}{A_0} = NkT\left[\lambda - \lambda^{-2}\right]$$

and which is represented in figure 15.

2.5. VISCOELASTIC BEHAVIOUR

2.5.1. Introduction

Figure 16 shows the results from three tensile tests on a natural rubber fibre, vulcanised with 8% sulphur (Treloar, 1944).

For small strains, up to ε of about 0.40 (λ = 1.5), **Hookean elastic** behaviour can be assumed (Figure 16a).

Even as the maximum strain approaches ε = 1.7 (λ = 5.5) the response is still reversible –the loading line coincides, more or less, with that of unloading. The behaviour is nonlinear elastic and the material considered as **elastomeric** (Figure 16b).

For larger deformations the unloading curve no longer coincides with that on loading, as apparent in the figure 16c. This effect, known as *hysteresis*, complicates the analysis of the tensile test since, for example, for a particular value of strain there are two values of stress. This result means that a new variable, time, must be introduced in order to characterise this behaviour which, in what follows, will be called **viscoelastic;** *visco*, to emphasise the influence of time and *elastic* because it will be assumed that the deformation will be recovered when the specimen is unloaded.

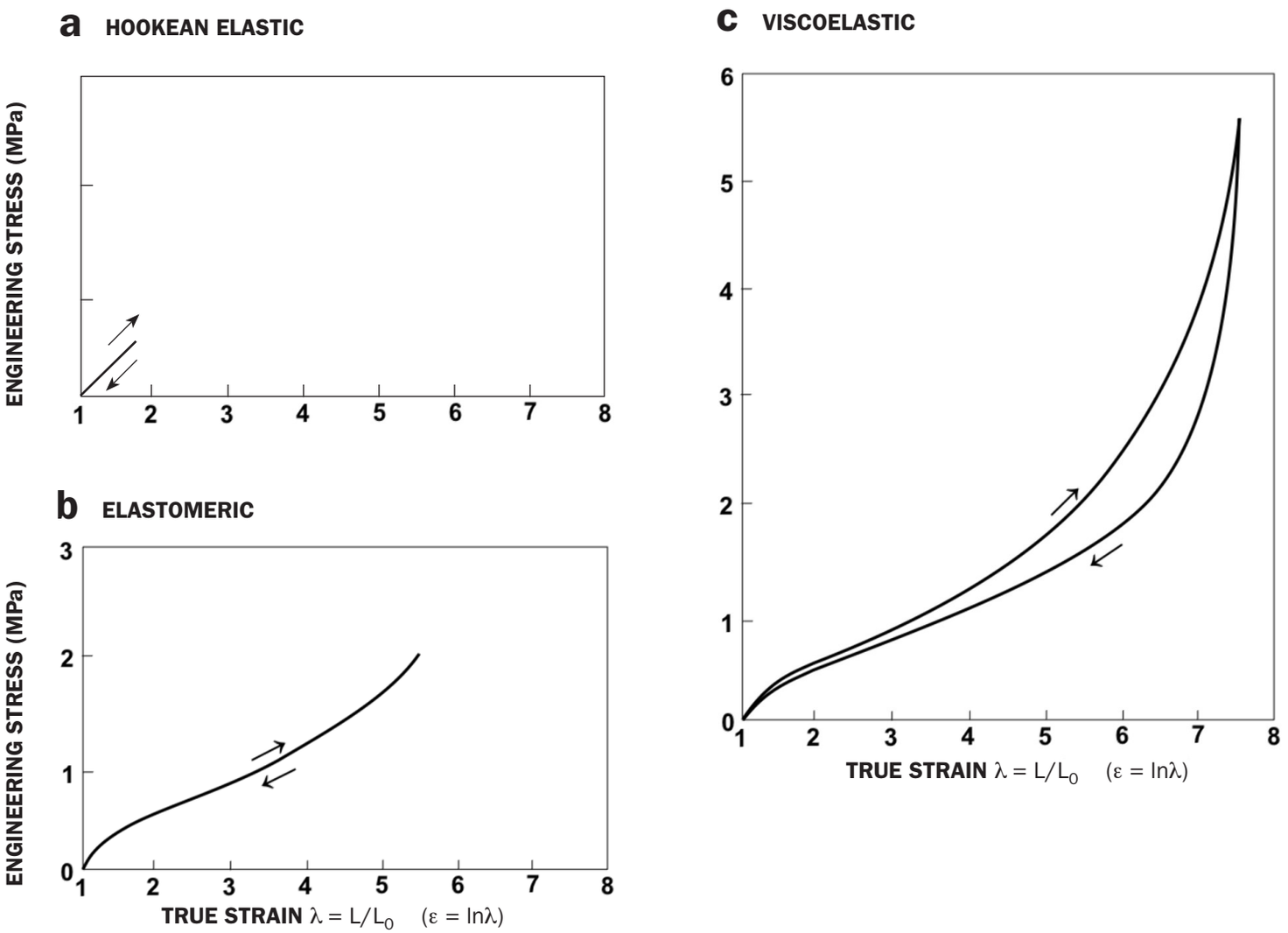

Fig. 16. *Engineering stress-elongation curves for a vulcanised rubber fibre (Treloar 1944).*
a. Hookean eleastic up to λ = 1.5
b. Elastomeric behaviour up to λ = 5.5.
c. Viscoelastic behaviour when λ_{max} *= 7.5.*

2.5.2. Mechanical tests

Various forms of tensile test allow characterisation of the viscoelastic behaviour of a material. The simplest are; the *creep* test, that of *relaxation*, and *cyclic* tests.

The **creep** test consists of subjecting the specimen to a constant stress and recording its deformation as a function of time.

Creep results for the mesoglea jellyfish *Cyanea capillata* (Alexander, 1964) are shown in figure 17a. The stress has been kept constant at 125 Pa and the deformation increases with time (note the difference in the two curves when the same phenomenon is represented using a natural scale and a logarithmic one).

When the specimen deforms a lot, such as happens with the example cited, the cross section may change significantly, compared to the initial value, so it is necessary to change the applied load in order to achieve a constant (true) stress experiment. When there is no information available about the variation of cross section, the specimen constant volume assumption is usually made for the purpose of calculations. This assumption is not always accurate for biological materials and it must be confirmed on a case by case basis.

In a creep test the *flexibility* of the specimen, J, is proportional to the strain ε because the stress is kept constant; $J(t) = \varepsilon(t)/\sigma_0$.

The variation of the flexibility that occurs in creep tests has the characteristics shown in figure 17b, in a very general schematic form. The viscoelastic response is only shown for the duration of the experiment. For very short times, or after a long time, the material does not flow but has glassy and elastomeric behaviours, respectively. The creep test helps characterise a section of this curve.

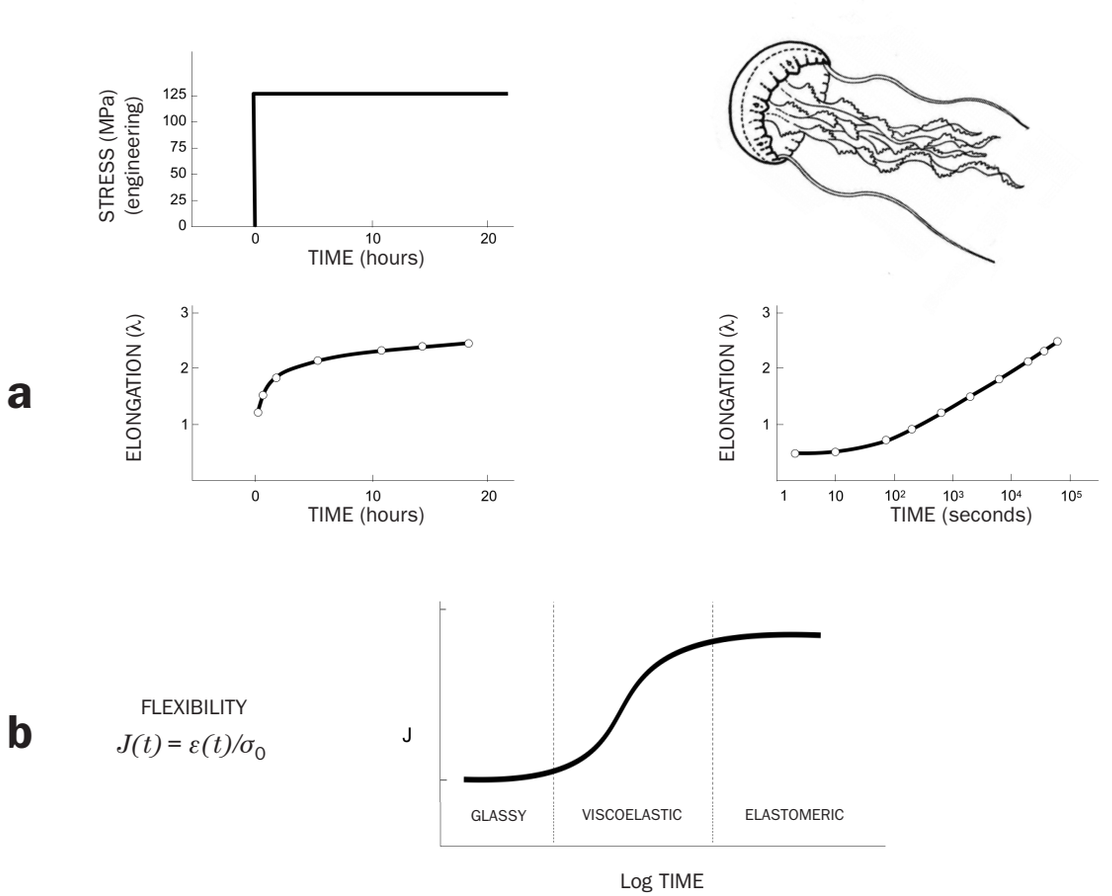

Fig. 17. *a. Creep test on a fibre of the mesoglea jellyfish* Cyanea capillata *(Alexander, 1964). The creep curves are quite different when drawn with natural and logarithmic scales.*
b. Variation of flexibility in a creep test as a function of time. In the figure all possible states have been represented, the experiment takes place over a particular time interval.

The **relaxation** test consists of subjecting the specimen to a constant deformation and recording the stress as a function of time.

Results for elastin are shown in figure 18a. The specimen is a ring taken from the porcine aortic wall from which everything except the elastin has been removed (Dorrington 1975). The initial strain –about 30%– was kept constant throughout the duration of the experiment and the load relaxation monitored (due to difficulties in estimating the cross section at any time, only the reduction in force is represented).

In a relaxation test the *rigidity* of the specimen, G, is proportional to the stress, σ, since the strain is kept constant; $G(t) = \sigma(t)/\varepsilon_0$.

The evolution of the rigidity in relaxation experiments, figure 18b, exhibits similar stages to those reported above for creep. Viscoelastic relaxation is shown only for the duration of the test. For very short times the material does not relax and behaves like a glassy solid. For very long times the behaviour is elastomeric.

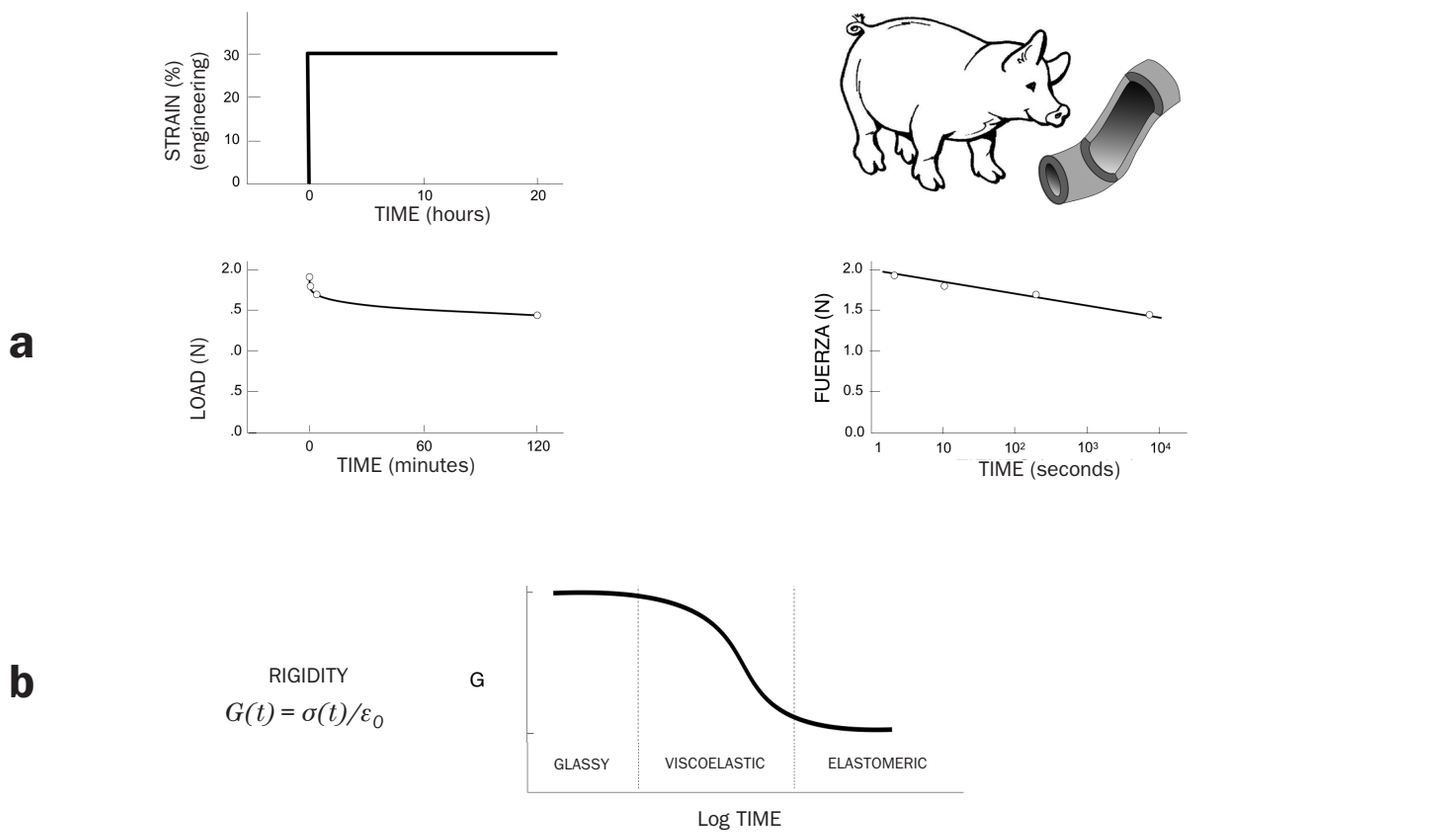

Fig. 18. *a.- Relaxation test on a ring of aorta (Dorrington, 1975). The relaxation curves are shown with natural and logarithmic time scales.*
b.- Variation of the rigidity in a relaxation test as a function of time. In the figure all possible stages have been represented, the experiment only runs for a fixed duration.

The **cyclic strain** test (also called dynamic, or forced vibration) consists of loading the specimen to an initial strain, $\varepsilon_{inicial}$, and then deforming it cyclically, with an amplitude ε_0, which is generally small, so:

$$\varepsilon = \varepsilon_{inicial} + \varepsilon_0 \sin \omega t$$

where ω is the frequency of oscillation, and t time.

Only when the material is *linear viscoelastic* (a concept introduced later) the stress response –after a transitory time of material accommodation– is of the same form although out of phase, as shown in figure 19, that is

$$\sigma = \sigma_{inicial} + \sigma_0 \sin\left(\omega t + \delta\right)$$

where δ is the phase angle, and $\sigma_{inicial}$ and σ_0 are constants..

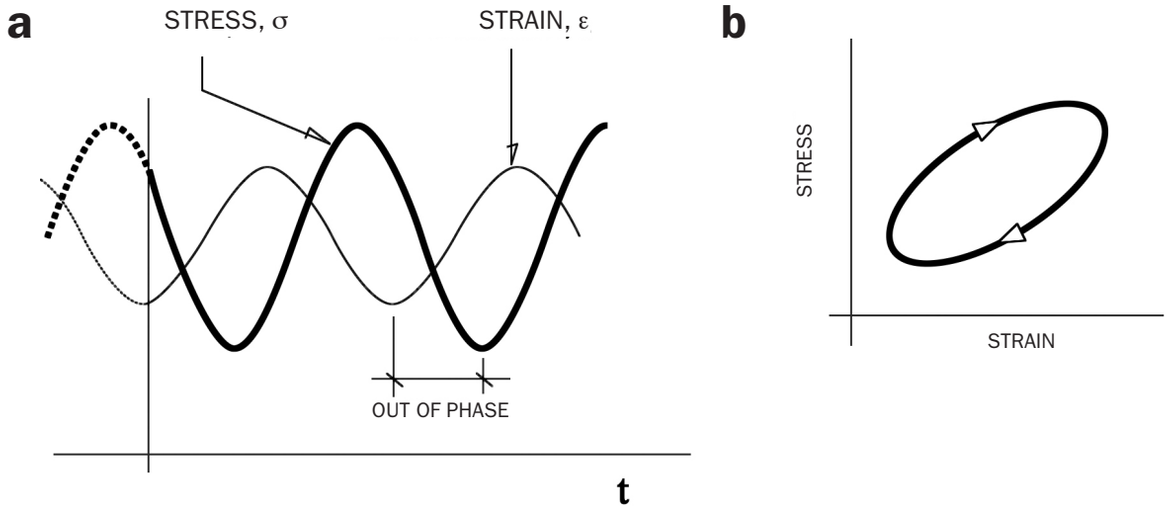

Fig. 19. *a. Cyclic test for a fibre with a linear viscoelastic behaviour. b. Hysteresis loop*

BIOLOGICAL MATERIALS AND VISCOELASTIC MODELS

Time is an essential factor in understanding the mechanical behaviour of biological materials and must be taken into account when formulating models of these materials. When subjected to a constant load, the materials deform with the passage of time –a phenomenon known as *creep*– if, on the other hand, they are subjected to a constant strain, the stresses relax with time –a phenomenon known as *relaxation*–. In a process of loading and unloading the paths, in a force-displacement diagram, are not coincident and form a loop, known as *hysteresis*. Time also influences the restructuring of biological materials, because they age, but they can be *rejuvenated* and reorganise themselves with time, under the appropriate conditions. The tool used for studying these phenomena –at the macroscopic level– is viscoelasticity, an essential chapter in the study of the mechanics of continuous media

In animal tissue, for example, knowing how the response to mechanical loading can play a major role in understanding their functioning –under both normal and pathological conditions– and the influence of time must be considered in interpreting its behaviour: Synchronised contractions of the cardiovascular system allow the circulation of blood. Contractions of the diaphragm and the intercostal muscles facilitate breathing. Peristalsis of the intestines helps the passage of food through the digestive tract. Muscles and tendons contract and stretch during physiological activities. Examples which, while only from animal tissue, would alone justify these studies. Other reasons for outlining the role played by time in the relationship between structure and biological properties are the advantages that this knowledge can bring to the design of new intelligent materials.

The mathematical formulation of viscoelastic models (or better, perhaps, *visco-elasto-plastic,* because plastic phenomena also occur) is more complex than that of purely elastic or elastomeric materials and, in general, viscoelastic models require much more experimental data in order to make reliable predictions. However, in certain circumstances and for small deformations, it is possible to use simplified models –based on linear viscoelasticity– which are useful, as a first step, on the way to the study of more complex situations. In this book only linear models are considered and the interested reader must consult specialist books, some of which are mentioned in this text.

In order to characterise the viscoelastic behaviour of biological materials several techniques are used: The simplest are based upon *tensile and torsion tests.* (For this reason, the section on viscoelasticity has been placed in this volume in which these tests are discussed in some detail. Another reason is that the results of these experiments are sufficient to create a *one-dimensional formulation* of linear viscoelasticity, which is the commonly used approach). The above procedures allow the performance of *creep, relaxation* and *fatigue* experiments, with the ability to vary, in all of these, the rate of loading, the temperature and other ambient parameters.

Other more specialist techniques, not discussed here, are based upon rheometers for studying how time intervenes in the relationships between forces and shear deformations. Measurements based on indentation techniques (see Volume III) provide information on the microscopic scale. For example, for animal tissue, and at the nanoscale, they provide information on the viscoelastic behaviour between cells and the extra-cellular matrix. More recent techniques, based on magnetic resonance (MRE) (Magnetic Resonance Elastography) or on ultrasonics (SDUV) (Shearwave Dispersion Ultrasound Vibrometry), have the advantage of not being invasive but the disadvantage, currently, of a low signal to noise ratio.

2.5.3. Linear viscoelasticity

1. Assumptions upon which linear viscoelasticity is based

The simplest description of viscoelastic behaviour is that of linear viscoelasticity, based two hypotheses (Boltzmann 1876). In order to define the concepts reference is made to a *relaxation* experiment but the same steps could be taken for a *creep* test.

Linearity hypothesis

Figure 20 illustrates the concept. Two identical specimens are used in two **relaxation** experiments; one with a strain value of ε_A (figure 20a) and the other with a strain ε_B (figure 20b). If the corresponding stresses are measured at the same time t_1 in both tests, σ_A and σ_B, the quotient of the stresses and strains must be the same (figure 20c), that is, $\sigma_A / \varepsilon_A = \sigma_B / \varepsilon_B = G(t_1)$. As a result, in a general form, for a relaxation test with strain ε_0:

$$\sigma(t) = \varepsilon_0 G(t) \tag{40}$$

where $G(t)$, is called the **modulus of relaxation.** Evidently, $G(t)$ is a function of time, depending only upon the material, but neither the test nor the specimen used. This function should not be confused with the Hookean elastic shear modulus, defined in linear elasticity.

Superposition hypothesis

It is now supposed that equation (40) is not only applicable the total values of stress and strain, but also to their increments, that is:

$$\Delta\sigma(t) = G(t\text{-}t')\ \Delta\varepsilon(t') \tag{41}$$

which gives the stress increment in time, t, due to a strain increment suffered in t'.

Figure 21 illustrates the hypothesis. In this figure, a relaxation experiment in which the strain is applied in the form of a series of steps is shown. The deformation is decomposed into steps $\Delta\varepsilon_i$ which give rise, according to equation (40), to stress increments $\Delta\sigma_i$, as shown (figure 21b). The stress response of the material at some time t is given by:

$$\sigma(t) = \sum G(t - t_i)\ \Delta\epsilon_i \tag{42}$$

The result can be generalised for each applied strain history, $\varepsilon(t)$, as far as the limit of infinitesimal strain increments, as illustrated in figure 21c. The stress can then be evaluated from the following integral expression:

$$\sigma(t) = \int_0^{\varepsilon} G(t-\tau)\,d\varepsilon = \int_0^{t} G(t-\tau)\frac{d\varepsilon(\tau)}{d\tau}\,d\tau \tag{43}$$

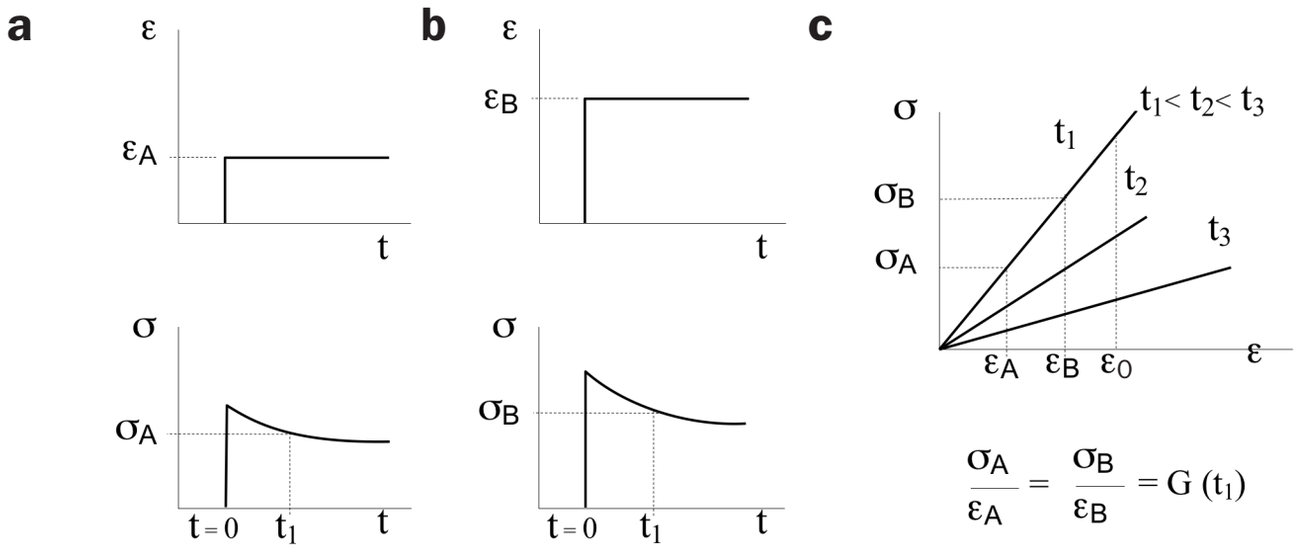

Fig. 20. *Linearity hypothesis.*
a. Relaxation with ε_A. Variation of strains and stresses with time
b. Relaxation with ε_B. Variation of strains and stresses with time
c. Isochronic stress-strain curves. For a particular time, the relaxation stress-strain is always linear and independent of the test

Therefore, the stress response to general strain loading $\varepsilon(t)$, can be determined if relaxation modulus function of the material, $G(t)$, is known.

In the case that the initial strain, ε_0, is not zero it is necessary to take into account the jump in strain that is produced at $t=0$. Equation (43) then becomes (Winemann 2000):

$$\sigma(t) = \varepsilon_0 G(t) + \int_{0^+}^{t} G(t-\tau)\frac{d\varepsilon(\tau)}{d\tau}d\tau \qquad (43b)$$

in which the integral is evaluated from the positive side of 0 (that is, 0^+) without including the jump ε_0.

Creep tests can be handled in an analogous manner, producing the following result: the strain response to an applied stress, given by $\sigma(t)$, can be determined, if the material **creep modulus** $J(t)$ is known, from the expression

$$\varepsilon(t) = \int_0^{\varepsilon} J(t-\tau)d\sigma = \int_0^{t} J(t-\tau)\frac{d\sigma(\tau)}{d\tau}d\tau \qquad (44)$$

In the same way, as with equation (43), when the initial stress, σ_0, is not zero the jump produced at $t=0$ must be considered. Equation (44) then becomes (Winemann 2000):

$$\varepsilon(t) = \sigma_0 J(t) + \int_{0^+}^{t} J(t-\tau)\frac{d\sigma(\tau)}{d\tau}d\tau \qquad (44b)$$

in which the integral is evaluated from 0^+, without including the jump σ_0.

Note that both $G(t)$ and $J(t)$ on their own completely characterise the linear viscoelastic response of the material and are not, therefore, independent, so that each one can be deduced from the other. The equations relating them can be found in Winemann (2000).

The restrictions imposed by linear viscoelasticity are so severe, that practically no material, biological or otherwise, complies with them. It is sufficient to calculate the ratio $\sigma(t)/\varepsilon_0=G(t)$ in a relaxation test and to check that it is not independent of the imposed strain level, as would be expected. The same happens if $J(t)=\varepsilon(t)/\sigma_0$ s calculated in a creep test, which turns out to be dependent upon σ_0. However, the linear viscoelastic model is frequently used with all types of material, restricting it to a very limited range of stresses and strains so that its predictions are not to inaccurate.

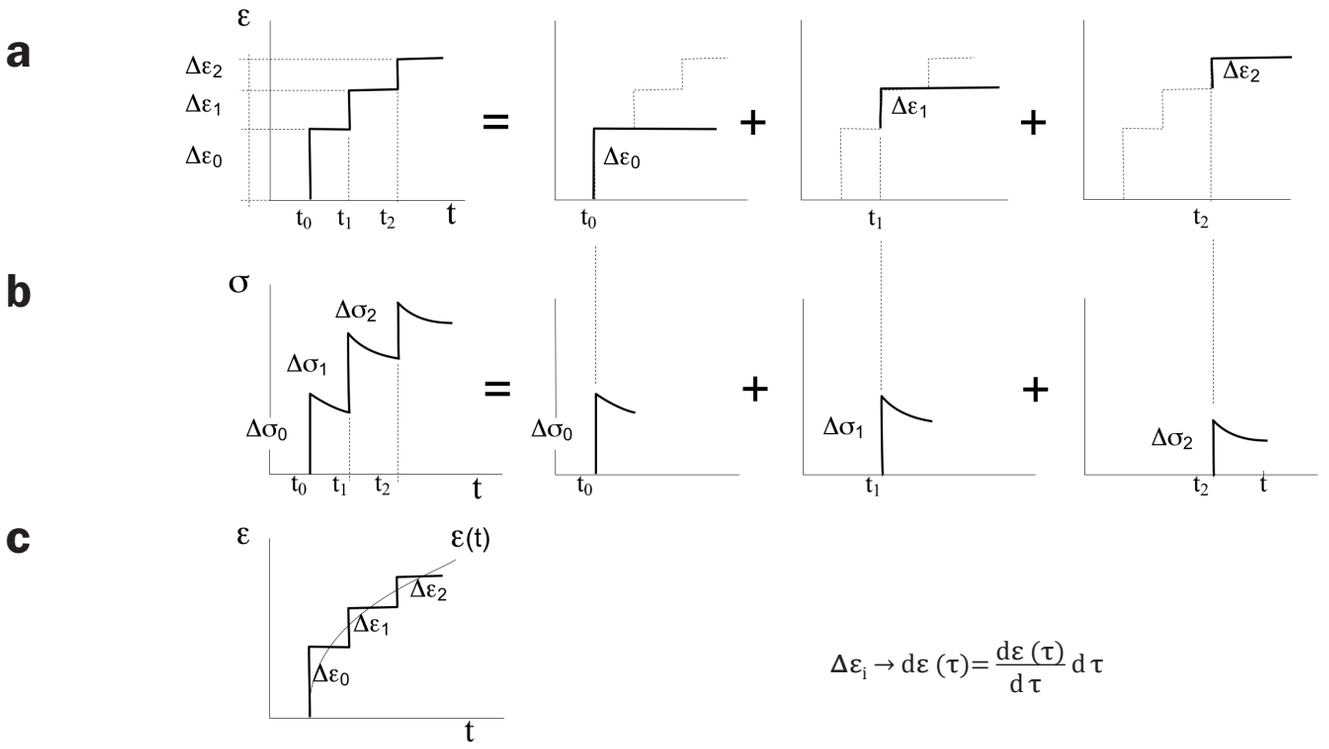

Fig. 21. *Superposition hypothesis.*
a. Stepped relaxation test and decomposition of the strain into steps
b. Obtaining stresses as a sum of the responses to each strain step
c. Decomposition of general loading $\varepsilon(t)$ into strain steps

LINEAR VISCOELASTICITY

The experiments performed by Smart and Williams (1972) with polypropylene fibres serve to illustrate the concepts above, although not strictly based on natural fibres.

In figure **a** isochronic curves corresponding to *relaxation* tests are presented for several values of strain (curves analogous to those shown in figure 20c)

For small strains (less than 0.5%) it can be seen that a set of straight lines are obtained. This indicates that the **linear** hypothesis is valid in this range of strains. In an experiment of loading and unloading –within the cited interval– a straight line is obtained, as shown in figure **a**.

For large strains, the isochronic curves are no longer straight lines and the *linearity* assumption is not valid. If a loading and unloading test were performed the phenomenon of hysteresis would occur, as shown in figure **c**, for a strain of 4%.

(Stress is in thousands lbf/in^2. 1Pa= 1,450x10^{-4} lbf/in^2)

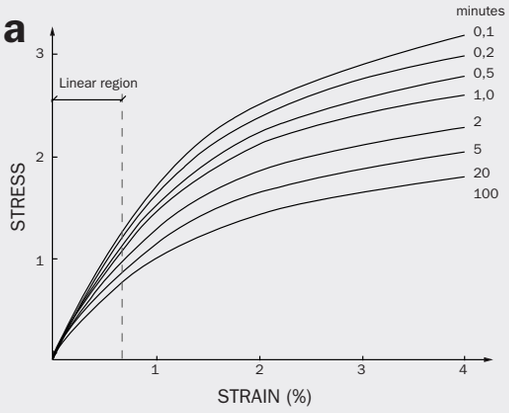

Isochronous relaxation curves

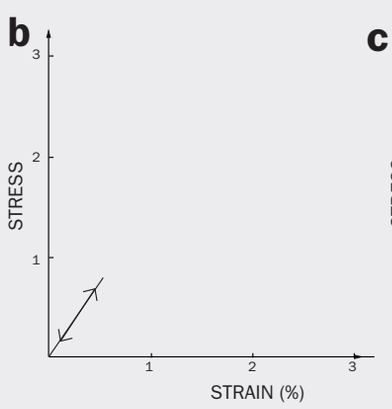

Loading/unloading curve until 0,7% strain

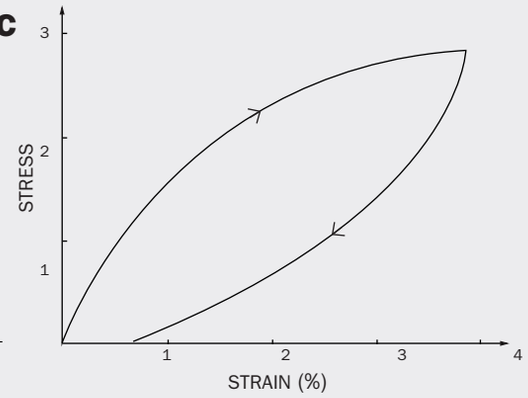

Loading/unloading curve until 4% strain

The properties of *linearity* and *superposition* are independent. It is possible that the experimental results satisfy the conditions of linearity but not those of superposition, and the contrary. Only, when a viscoelastic material obeys both hypotheses, for different loadings, can the material be considered as *linear viscoelastic.*

In general, viscoelastic biological materials only show *linear viscoelastic* behaviour for small strains (less than 1%) and in certain temperature ranges.

When characterising the large strain behaviour of a viscoelastic material behaviour, the experimentation is more complicated and the mathematical treatment more arduous. See, for example, R Lakes (2009) or A Wineman and K Rajagopal (2000).

2. Mechanical models

The search for constitutive equations within the framework of linear viscoelastity is reduced, as mentioned above, to the determination of expressions for the relaxation or creep modulus. Ideally these expressions must come from a knowledge of the microstructure of the material and its response to mechanical stimuli, a complex task because biological materials are, in general, composite materials and very hierarchical, and it is difficult to unravel the role that each component plays in this process.

An attempt to simplify viscoelastic behaviour can be made by means of phenomenological models based on ideal springs and dampers (dashpots). These elemental components are represented in figures 22a and 22b.

The simplest model for a solid, capable of reproducing creep and relaxation phenomena, is called the *standard linear solid* (Zener, 1948), shown in figure 22c and is composed of a Hookean spring (of modulus E_H) in parallel with a Maxwell fluid model (figure 22d), which is an element formed of a Hookean spring, E_V, in series with Newtonian damper of viscosity η.

The corresponding constitutive equation for this model is obtained by noting that the stress is equal in the damper and spring collocated in series, and the total stress σ is the sum of the stresses in the isolated spring of the assembled damper+spring element, with both devices having the same strain ε since they are in parallel. The resulting equation is:

$$\sigma + \tau_R \frac{d\sigma}{dt} = E_H \epsilon + (E_H + E_V) \tau_R \frac{d\epsilon}{dt} \qquad (45)$$

where the time $\tau_R = \eta / E_V$ is usually called the *relaxation time*.

The responses of the model to different basic loadings; relaxation, creep, or cyclic are presented below, leaving to their deduction to the reader (see, for example, Winemann and Ragagopal 2000).

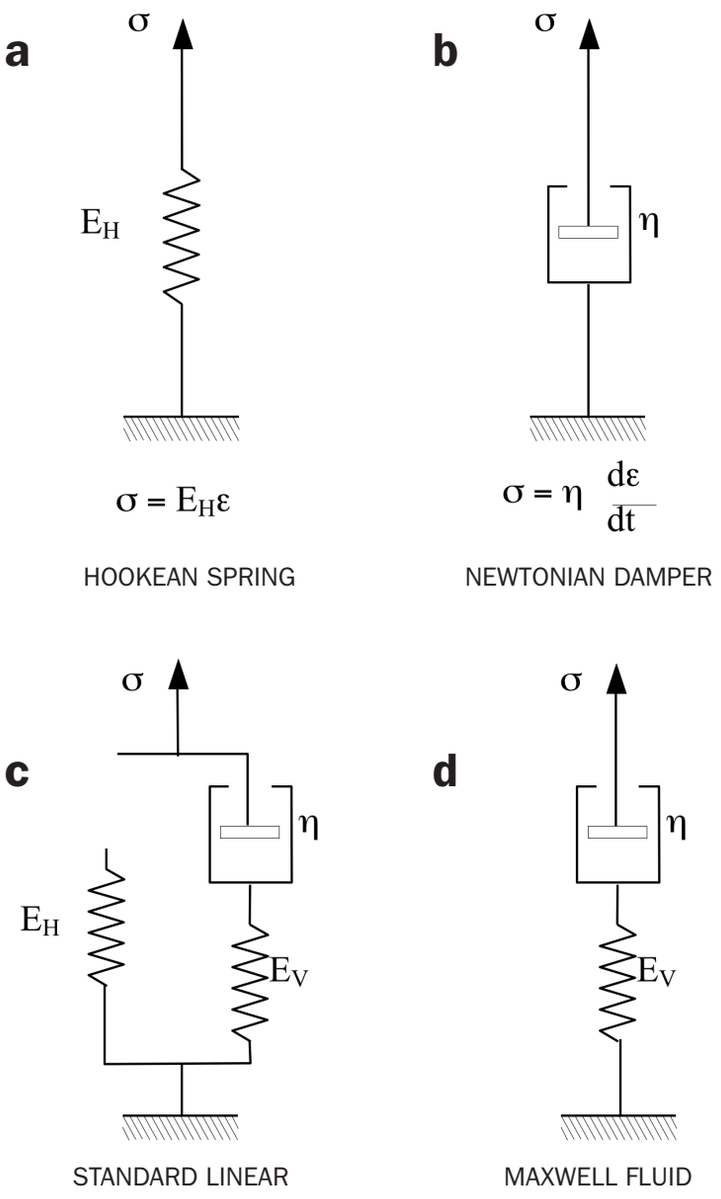

Fig. 22. *a. Hookean spring; characterised by elastic modulus E_H.*
b. Newtonian damper; characterised by viscosity η.
c. Standard linear model; characterised by elastic moduli E_H, E_V and viscosity η.
d. Maxwell fluid; characterised by elastic modulus E_V and viscosity η.

EXERCISE
Derive equation (45).

Solution:
Consider the solid in figure 22c, subjected to a stress σ *and strain* ε. Let the strain in the Hookean spring be ε_H=ε, that in the spring of the Maxwell element ε_V and that in the damper ε_η. Compatibility of strains leads to ε=<ε_V+ε_η

The stress in spring E_H is σ_H. In the Maxwell element the stress in the damper is σ_η and in the spring, σ_V.

Equilibrium of forces means that: σ=σ_H + σ_V y σ_η=σ_V, since the damper and spring of the Maxwell element act in series. The constitutive equations of the elements requires that

$$\sigma_H = \varepsilon_H E_H = \varepsilon E_H; \quad \sigma_V = \varepsilon_V E_V = \sigma_\eta = \dot{\varepsilon}_\eta \eta$$

In order to obtain the constitutive equation of the solid we combine the above equations from the equilibrium of forces. Differentiating with respect to time gives:

$$\dot{\sigma} = \dot{\sigma}_H + \dot{\sigma}_V = E_H \dot{\varepsilon} + E_V \dot{\varepsilon}_V = E_H \dot{\varepsilon} + E_V (\dot{\varepsilon} - \dot{\varepsilon}_\eta) = \left(E_H + E_V\right)\dot{\varepsilon} - E_V \frac{\sigma_\eta}{\eta}$$

since ε_V=ε −ε_η. Susbstituting σ_η=σ_V=σ −σ_H

$$\dot{\sigma} = \left(E_H + E_V\right)\dot{\varepsilon} - \frac{E_V}{\eta}\left(\sigma - \sigma_H\right) = \left(E_H + E_V\right)\dot{\varepsilon} - \frac{E_V}{\eta}\left(\sigma - \varepsilon E_H\right)$$

and rearranging the terms

$$\dot{\sigma} + \frac{E_V}{\eta}\sigma = \left(E_H + E_V\right)\dot{\varepsilon} + \varepsilon \frac{E_V E_H}{\eta}$$

which is equation (45).

Use of mechanical analogue models is relatively widespread not only because their equations are easy to handle, but also because the results are particularly helpful in idealising and better understanding linear viscoelastic behaviour and its peculiarities. Thus, in a relaxation test it is apparent that the initial response is only due to the springs E_H and E_V, because, with the infinite loading rate (the initial step from 0 to ε_0) the viscoelastic damper works like a rigid solid (just as if a load is suddenly applied to a real damper). Therefore, the initial stiffness must be E_H + E_V. Similarly, for an infinite time the strain rate in the damper is extremely slow –theoretically zero– it can be seen that the damper provides no resistance to motion (as in applying a very slow load to a real damper) and the stress is borne only by the spring E_H, whose stiffness determines the behaviour.

On the other hand, it is often useful to associate the different strain micromechanisms of a material to the mechanical analogue models characterised by their relaxation time. For example Johnson *et al*. (2010), modelled the viscoelastic behaviour of cortical bone using spring-damper elements with a relaxation times of 30ms and 10μs, corresponding to two very different mechanisms: the sliding between lamellae and tissue fluid flow in the haversian canals, respectively. In this way, mechanical analogue models help to isolate the different resistance mechanisms of each material and allow separate consideration of their effects.

Relaxation test *(standard model)*
The loading and the response are shown schematically in figure 23a. The values of strain and stress are given by (see the exercise):

$$\epsilon\,(t) = \epsilon_0$$
$$\sigma\,(t) = \epsilon_0\left(E_H + E_V\, e^{-t/\tau_R}\right) = \epsilon_0\, G(t) \qquad (46)$$

where τ_R, the characteristic relaxation time, is given by

$$\tau_R = \eta/E_V \qquad (47)$$

From this result which determines $G(t)$, it is possible to calculate the variation of the stress $\sigma(t)$ as a function of any strain history $\varepsilon(t)$, using equation (43b).

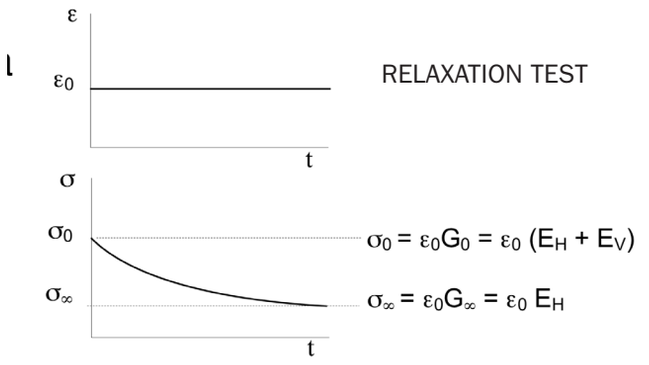

Fig. 23a. *Standard linear solid. Relaxation test.*

EXERCISE
Derive equation (46).

Solution:
Since $\varepsilon = \varepsilon_0$, a constant, then $d\varepsilon/dt = 0$ at all times, which when substituted into equation (45) gives

$$\dot{\sigma} + \frac{E_V}{\eta}\sigma = \varepsilon_0 \frac{E_V E_H}{\eta}$$

This a differential equation which can be integrated with the initial condition $\sigma(0) = (E_H + E_V)\,\varepsilon_0$, since right at the beginning, and for an infinitely rapid loading, the damper behaves like a perfectly rigid material, and the solid behaves like two springs in parallel, with stiffnesses E_H and E_V.

The homogenous equation is

$$\frac{d\sigma}{dt} = -\frac{E_V}{\eta}\sigma$$

which has the solution

$$\sigma = Ce^{-\frac{E_V}{\eta}t}$$

where C is a constant. The particular integral i $\sigma = E_H\,\varepsilon_0$, which when combined with the solution to homogeneous equation gives the general solution

$$\sigma = Ce^{-\frac{E_V}{\eta}t} + E_H\varepsilon_0$$

Imposing the boundary condition $\sigma(0) = (E_H + E_V)\,\varepsilon_0$ yields

$$C = E_V\varepsilon_0$$

and

$$\sigma = E_v\varepsilon_0 e^{-\frac{E_V}{\eta}t} + E_H\varepsilon_0 = \varepsilon_0\left(E_H + E_v e^{-\frac{E_V}{\eta}t}\right)$$

Creep test *(standard model)*
The loading and response are shown in shown in figure 23b, in a simplified form. The values of stress and strain are given by:

$$\sigma(t) = \sigma_0$$
$$\epsilon(t) = \sigma_0 \left[\frac{1}{E_H} + \left(\frac{1}{E_H + E_V} - \frac{1}{E_H}\right) e^{-t/\tau_C}\right] = \sigma_0 J(t) \quad (48)$$

where τ_C, the creep time characteristic, is defined by

$$\tau_C = \frac{E_H + E_V}{E_H E_V}\,\eta \quad (49)$$

With this result, knowing $J(t)$ from equation (48) it is possible to calculate the evolution of strain $\varepsilon(t)$ as a function of any stress history $\sigma(t)$ using equation (44b)

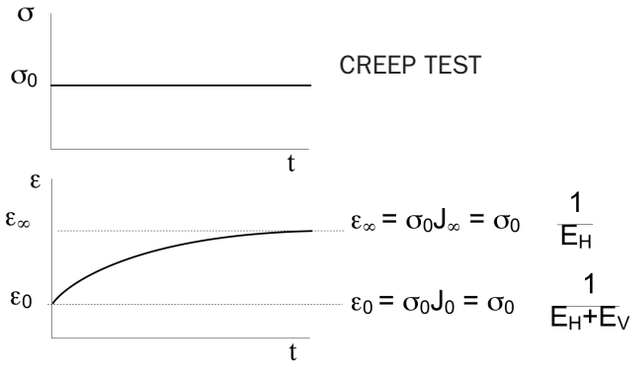

Fig. 23b. *Standard linear solid. Creep test.*

EXERCISE
Derive equation (48). Justify the values of the flexibility obtained at times t=0 and t=∞ in a creep test for a standard linear solid.

Solution:
In the case we have $\sigma = \sigma_0$, a constant, and $d\sigma/dt = 0$ at all times. These conditions, substituted in equation (45) yield

$$\left(E_H + E_V\right)\dot{\varepsilon} + \varepsilon\frac{E_V E_H}{\eta} = \frac{E_V}{\eta}\sigma_0$$

which is again a first order differential equation that can be integrated with the initial condition $\varepsilon(0) = \sigma_0/(E_H + E_V)$, since, initially, and for an infinitely rapid loading, the damper behaves like a perfectly rigid body, and the standard solid behaves like two springs in parallel, with stiffnesses E_H and E_V.

The homogeneous equation is

$$\frac{d\varepsilon}{dt} = -\frac{E_H E_V}{\eta\left(E_H + E_V\right)}\varepsilon$$

whose solution is

$$\varepsilon = Ce^{-\frac{E_H E_V}{\eta(E_H + E_V)}t}$$

where C *is a constant. The particular integral of the complete equation is* $\varepsilon = \sigma_0/E_H$, which when combined with the solution to the homogeneous equation gives the general solution

$$\varepsilon = Ce^{-\frac{E_H E_V}{\eta(E_H + E_V)}t} + \frac{\sigma_0}{E_H}$$

Imposing the initial condition $\varepsilon(0) = \sigma_0/(E_H + E_V)$ gives C

$$C = \frac{-\sigma_0 E_V}{\left(E_H + E_V\right)E_H}$$

and

$$\varepsilon = \frac{\sigma_0}{E_H}\left(1 - \frac{E_V}{E_H + E_V}e^{-\frac{E_H E_V}{\eta(E_H + E_V)}t}\right)$$

Cyclic tests

Using the notation defined above and assuming a sinusoidal loading (see figure 19) with a small amplitude ε_0, the strain is:

$$\epsilon\,(t) = \epsilon_i + \epsilon_0 \,\text{sen}\,\omega t$$

the response, after reaching **stable test,** will be (see the exercise):

$$\sigma\,(t) = \sigma_i + \sigma_0\,\text{sen}\,(\omega t + \delta) =$$

$$= \epsilon_i\, G_\infty + \epsilon_0\, G_1\,\text{sen}\,\omega t + \epsilon_0\, G_2 \cos\omega t \qquad (51)$$

where G_1 and G_2 are known as *storage* and *loss* moduli respectively, and G_∞ is the value of $G(t)$ at $t=\infty$.

From the two previous results it can also be deduced that

$$\text{tg}\,\delta = G_2/G_1 \qquad (52)$$

If the energy dissipated in one cycle is calculated, then

$$\Delta E = \int_{t=T+0}^{t=T+2\pi/\omega} \sigma\,(t)\,d\epsilon\,(t) = \pi\,\sigma_0\,\epsilon_0\,\text{sen}\,\delta = \pi\,G_2\,\epsilon_0^2 \qquad (53)$$

which is the area under the curve $\sigma-\varepsilon$ and which accounts for the name of loss modulus for G_2.

For the standard *linear solid*, G_1 and G_2 are given by

$$G_1 = \frac{G_\infty + G_0\,(\omega\,\tau_R)^2}{1+(\omega\,\tau_R)^2} \qquad (54)$$

and

$$G_2 = \frac{\omega\,\tau_R\,(G_0 - G_\infty)}{1+(\omega\,\tau_R)^2} \qquad (55)$$

where the values of G_0 and G_∞ are obtained from equation (46) for $t=0$ and $t=\infty$, respectively. Both limiting values are shown in figure 24.

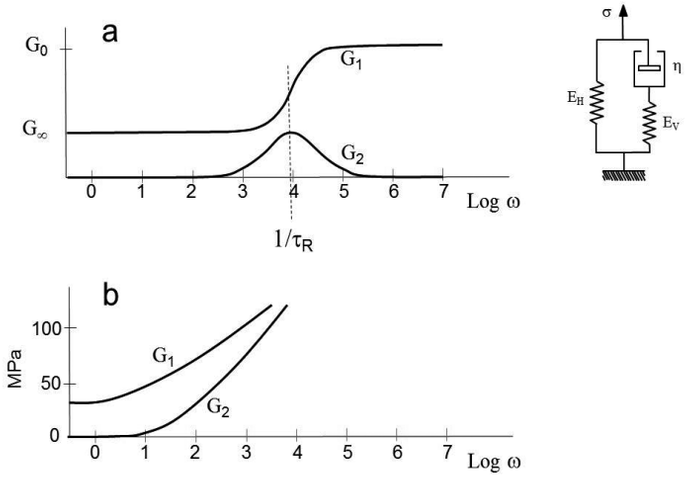

Fig. 24. *Standard linear solid.*
a. Response to forced vibrations of frequency ω; moduli G_1 and G_2.
b. Experimental results for elastin fibres (after Gosline and French, 1979).

Equations (54), (55), (46) and (48) provide, for the special case of the standard linear solid, a set of relationships which yield the moduli G_1 and G_2 from $G(t)$ or $J(t)$. This is always possible, no matter what linear viscoelastic model is used, since the values of $G(t)$, $J(t)$ and the pair $G_1(\omega)$ and $G_2(\omega)$ are uniquely related (see Winemann, 2000).

Figure 24a contains a schematic representation of the values of moduli G_1 and G_2 as a function of the frequency, ω. For very high frequencies the material behaves as a purely elastic solid since the damper acts like a rigid solid, and there is hardly any dissipation of energy (G_2 is practically zero). For very low frequencies (very long deformation times) the damper offers no resistance and the material also responds elastically, exhibiting hardly any hysteresis and the energy dissipation is practically zero. The material only exhibits a viscoelastic behaviour in an intermediate range of frequencies in which G_2 reached a maximum.

Experimental results for cyclic tests on elastin are shown in figure 24b (Gosline, French 1979). In that figure it can be seen that G_1 and G_2 follow the expected trends in the achievable range of frequencies.

In general, a model as simple as the standard linear solid is not capable of reproducing the behaviour of complex biological materials (see, for example, figure 25), but it does serve as a starting point other more satisfactory models.

When the loss modulus G_2 is measured a bell-shaped curve centred around the relaxation time τ_R is not always obtained. On the contrary, the measurements often produce curves with a rather flat maximum, or *plateau*, in the central region, as shown in figure 25b, corresponding to the test on the vascular wall of sheep. That figure also contains data for the differing viscoelastic responses of veins and arteries.

In order to try to replicate this relatively frequency-insensitive behaviour the mechanical model is enhanced by inserting in parallel various Maxwell modules and a Hookean spring (generalised Maxwell model). Each Maxwell module gives rise to its own relaxation time τ_i with the objective of summing the bell-shaped curves resulting in a curve with a plateau. The relaxation function $G(t)$ is given, in this case, by an expression of the type

$$G\,(t) = E_0 + \sum E_i\, e^{-t/\tau_i} \qquad (56)$$

which is known as a Prony series. E_i are the discrete values of the relaxation time spectrum. These ideas can be generalised by introducing a continuous distribution $E(t)$ of relaxation times (or creep) giving rise to

$$G\,(t) = E_0 + \int_0^\infty E\,(\tau) e^{-t/\tau}\,d\tau \qquad (57)$$

EXERCISE
Derive equation (51).

Solution:
Let $\varepsilon = \varepsilon_{inicial} + \varepsilon_0 \sin(\omega t)$ be strain applied to a material whose relaxation is described by $G(t) = G(\infty) - \Delta G(t)$. Note that the function $\Delta G(t)$ *decreases monotonically* and that for sufficiently long times $\Delta G(t) \approx 0$.

Since that loading occurs rapidly at t=0, we calculate $\sigma(t)$ using equation (43b)

$$\sigma(t) = \varepsilon_{inicial} G(t) + \int_{0^+}^{t} G(t-\tau)\frac{d\varepsilon(\tau)}{d\tau} d\tau = \varepsilon_{inicial} G(t) + \omega\varepsilon_0 \int_{0^+}^{t} G(t-\tau)\cos(\omega\tau)\, d\tau$$

Making the substitution $u = t-\tau$, the equation becomes

$$\sigma(t) = \varepsilon_{inicial} G(t) - \omega\varepsilon_0 \int_0^{t^-} G(u)\cos\left[\omega(t-u)\right] du$$

and applying $G(t)$

$$\sigma(t) = \varepsilon_{inicial} G(t) - \omega\varepsilon_0 G(\infty)\int_0^{t^-} \cos\left[\omega(t-u)\right] du + \omega\varepsilon_0 \int_0^{t^-} \Delta G(u)\cos\left[\omega(t-u)\right] du = \varepsilon_{inicial} G(t) + \varepsilon_0 G(\infty)\sin\omega t + \omega\varepsilon_0 \int_0^{t^-} \Delta G(u)\cos\left[\omega(t-u)\right] du$$

since

$$\cos\left[\omega(t-u)\right] = \cos\omega t\cos u + \sin\omega t\sin u$$

$$\sigma(t) = \varepsilon_{inicial} G(t) + \varepsilon_0 G(\infty)\sin\omega t + \omega\varepsilon_0 \cos\omega t \int_0^{t^-} \Delta G(u)\cos(\omega u)\, du + \omega\varepsilon_0 \sin\omega t \int_0^{t^-} \Delta G(u)\sin(\omega u)\, du$$

which can be rearranged as

$$\sigma(t) = \varepsilon_{inicial} G(t) + \varepsilon_0\left[G(\infty) + \omega\int_0^{t^-} \Delta G(u)\sin(\omega u)\, du\right]\sin\omega t + \varepsilon_0\left[\omega\int_0^{t^-} \Delta G(u)\cos(\omega u)\, du\right]\cos\omega t$$

If the integral of ΔG is bounded, that is to say

$$\int_0^{\infty} \Delta G(u)\, du \le M$$

since both since and cosine functions are less than or equal to one, the integrals in the expression for $\sigma(t)$, for times tending to infinity, approach certain limiting values which allow definition of the storage modulus (G_1), and loss modulus (G_2).

$$G_1 = G(\infty) + \omega\int_0^{\infty} \Delta G(u)\sin(\omega u)\, du$$

$$G_2 = \omega\int_0^{t^-} \Delta G(u)\cos(\omega u)\, du$$

With these values we have

$$\sigma(t \to \infty) = \varepsilon_{inicial} G(\infty) + \varepsilon_0 G_1 \sin\omega t + \varepsilon_0 G_2 \cos\omega t$$

which corresponds to the steady state solution, equation (51). From a practical point of view, convergence is always rapid, achieving a stable behaviour after a few cycles, generally less than 10.

In these cases the relaxation functions, or creep, can no longer be derived from mechanical models with a finite number of modules. Expressions (56) and (57) and their analogues for creep are a particularisation of the integrands which appear in equations (42) and (43).

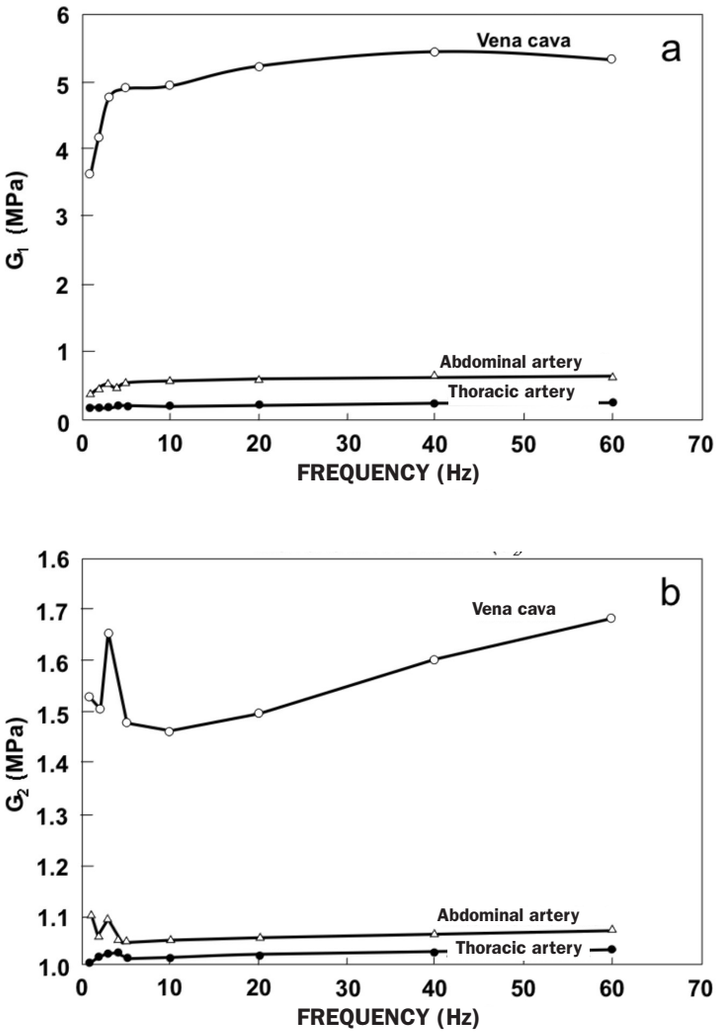

Fig. 25. *Storage modulus, G_1, (a) and loss modulus, G_2 (b), for different sheep vessels. Note the different viscoelastic behaviour of veins and arteries. Observe also the relative insensitivity of the moduli to frequency.*

2.5.4. Final remarks

The *linear viscoelastic* model is well-founded and has an elegant well-developed mathematical foundation. For example, starting from tensile loading –load history– it is possible to calculate the strain response –the corresponding strain history– if the creep modulus is known. Likewise, knowing the relaxation modulus it is possible to calculate the tensile stress response to an applied strain. The model allows calculation of one modulus from a knowledge of the other, providing predictions of the energy dissipated in cyclic processes and many other things.

However, the linear viscoelastic model has its limitations when attempts are made to apply it to biological materials which are capable of withstanding large deformations, because the assumptions on which it is based are, in general, only good for small deformations.

Experimental measurement of the moduli (creep, relaxation, loss, *etc*.) is not always easy and often requires several complementary processes. In figure 26 the time scales of different experimental techniques are shown (note that the time scale is logarithmic).

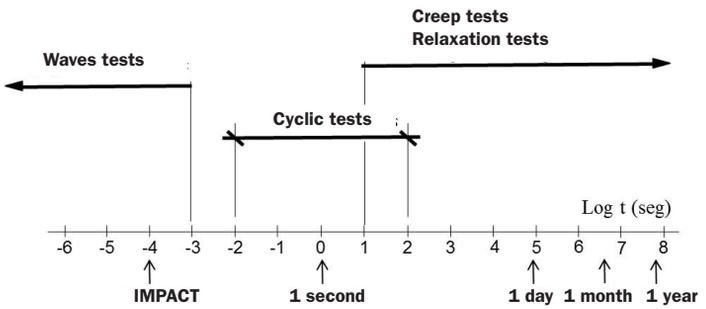

Fig. 26. *Approximate domains of various experiments for the determination of viscoelastic model parameters.*

Having obtained the curves for creep, relaxation or the dynamic moduli, the next step is to try to fit them to a model. In general, a model with a single relaxation time will not be sufficient and it will be necessary to use models with a spectrum of relaxation (or creep) times reflecting the specific deformation micromechanisms of each material. If successful, the material tested can be described by the model and predictions made about the mechanical behaviour. Furthermore, as already indicated, viscoelastic models assume that the deformation is recoverable (can be cancelled) when the applied load is removed, a situation that does not occur in real materials, which can be classified more precisely as *visco-elasto-plastic*.

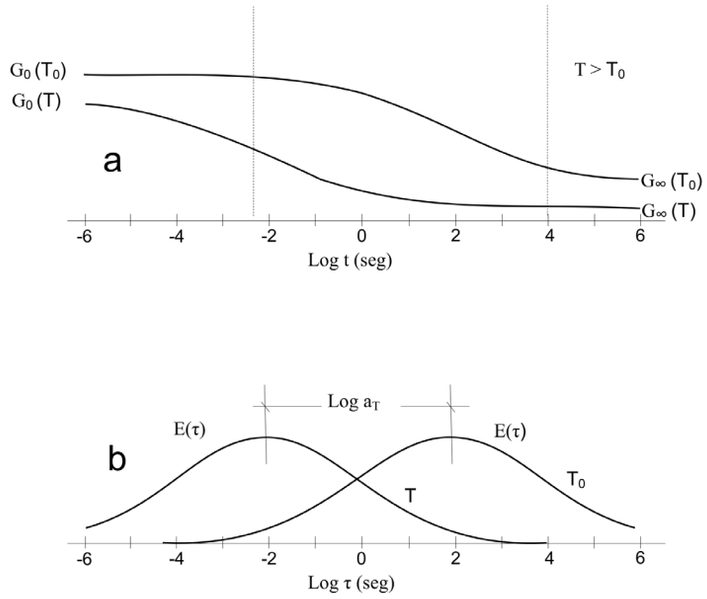

Fig. 27. *Effect of temperature on*
a. the relaxation modulus,
b. the distribution function of relaxation times.

Temperature is another variable which influences the viscoelastic behaviour of biological materials. For example, if the temperature is increased in a relaxation test, the relaxation will accelerate and the modulus of relaxation curve will move to the left, when the horizontal scale represents time (figure 27a). If the test temperature is decreased, the opposite occurs.

In many cases this displacement of the curves is associated with a shift in relaxation time function $E(\tau)$ (figure 27b). The temperature also influences the extreme values of the moduli (G_0 and G_∞, in the current example), as shown in figure 27a. It is usually assumed that the temperature has an equal effect upon the two moduli, that is to say; for two temperatures T and T_0:

$$\frac{G_0\,(T)}{G_0\,(T_0)} = \frac{G_\infty\,(T)}{G_\infty\,(T_0)} \tag{58}$$

In these circumstances it is possible to make the curves, obtained for temperatures T and T_0, coincide and represent them on a logarithmic scale, by means of a horizontal translation, $log\ a_T$, and a vertical displacement $log\ b_T$, that is to say, $G(t,\ T)\cdot b_T = G(t\cdot a_T, T_0)$. In general, $log\ a_T >> log\ b_T$ and the vertical displacement is usually ignored. The same considerations can be made for the creep modulus and the dynamic moduli G_1 and G_2 (51), and $tan\ \delta$ ((equation 52).

In 1955, Williams, Landel and Ferry proposed an empirical expression for the calculation of a_T, applicable to many amorphous polymers, and known as the WLF equation. This relation is:

$$\log a_T = -\frac{C_1\left(T - T_g\right)}{C_2 + \left(T - T_g\right)}$$

where C_1 and C_2 are positive constants and T_g is the glass transition temperature. The displacement obtained with this expression is relative to the curve corresponding to the glass transition temperature. This empirical recipe must be applied with care.

The existence of a relationship such as $G(t, T)\cdot b_T = G(t\cdot a_T, T_0)$ allows an easy expansion of the measurement interval in the time scale –always difficult experimentally– without performing experiments at different temperatures.

The complexity of the mechanical behaviour of biological materials does not end with the inclusion of time and temperature in their constitutive equations, other variables also have influence; the water content of the material or the relative humidity during the test are parameters that must be taken into account.

For example, the glass transition temperature of dry elastin is about 200˚C. If 10% by weight of water is added, that temperature reduces to 70˚C and if the amount of water is increased to 38% the glass transition temperature reaches 0˚C (Kakivaya and Hoeve 1975).

The shapes of the moduli curves as a function of time for different water contents are similar to those at different temperatures and, attempts have also been made to correlate them using appropriate translations (shifts).

The effect of humidity, temperature and time on mechanical tests are factors to take into account when interpreting experimental results. It has already been noted that, according to the values of these parameters, it is possible to obtain a behaviour which is elastic, viscoelastic or elastomeric. What is more, with a certain combination of these values it is possible to return the specimen to its original state and to erase the memory of its mechanical history. So, for example, with wool fibres, if strained less than 30% and tested for less than 1 hour, it is possible to recover the initial state if they are submerged in water, at 52˚C, for 1 hour (Feughleman, 1997).

2.6. FRACTURE BEHAVIOUR

2.6.1. INTRODUCTION

When a fibre is loaded in tension beyond a certain limit, its microstructure and internal organisation change irreversibly, giving rise to permanent deformation, as has already been noted. If the loading continues, the material separates and breaks, first on a microscopic scale, and ultimately fracturing and breaking the fibre. The process of deformation and degradation prior to rupture is complex and depends as much on the type of material and its microstructure as the geometry and applied load. Therefore, the measured failure loads and strains often vary widely, much more than other mechanical properties (such as the elastic modulus, for example)

A detailed analysis of the principal fracture mechanisms of materials, and models which address the mechanical description which have little effect on the mcicr, are presented in Section III. For the moment it is enough to differentiate between the two main types of fracture behaviour: *brittle* fracture and *ductile* fracture, and identify the implications for testing and characterisation of biological fibres.

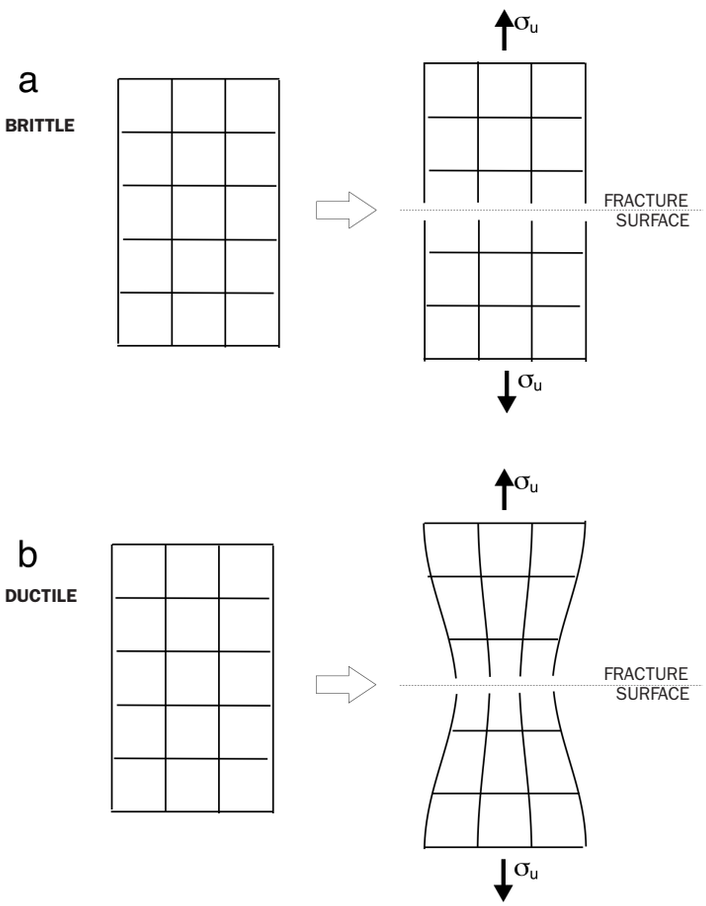

Fig. 28. *Fracture behaviour*
a. brittle
b. ductile

Brittle fracture is characterised by the absence of permanent deformation prior to rupture. That is, the material behaves elastically up to failure and it suddenly fractures. The material suffers large very localised strains which have hardly any effect upon the microstructure away from the fracture surface. These deformations happen so rapidly relative to the time scale of the test that they can be considered instantaneous (Figure 28a).

Ductile fracture, on the other hand, occurs when the material suffers large plastic deformations during the fracture process (Figure 28b). The appearance of irreversible deformations usually induces significant changes in the microstructure beyond the fracture zone and even the geometry of the specimen. These changes alter the stress distribution and, if not taken into account, may give rise to serious errors in estimating the values of the load and/or failure strain.

The boundary between brittle and ductile fracture is not well-defined and depends not only upon the type of material but also the geometry of the specimen, its size and the manner in which the load is applied and the surrounding environment. The phenomenon is complex and the interested reader can consult specialist texts on the fracture mechanisms of fibres (for example Elices and Llorca 2002). Simplistically, as a general rule, it is possible to indicate that–for the same material– the larger the size of the specimen relative to its microstructure the more likely the behaviour will be brittle.

As can been seen, the type of fracture–brittle or ductile– is linked to the (microscopic) deformation which takes place in the fracture zone (Figure 28) and may bear little relation to the elongation (macroscopic deformation) of the specimen. It is wrong to establish –as is sometimes done– that a fracture is ductile when there is a large elongation before rupture. An obvious example is the rupture of an elastomer, whose elastic elongation can be more than 100% before brittle fracture. By the same token, the definition of tenacity as the area under the macroscopic stress-strain curve up to the point of rupture can give an erroneous estimate of the ductility of the material.

In the particular case of a test on fibres, ductile behaviour brings with it the appearance of a localised deformation, a process known as *necking*, which was described in paragraph 2.2.1. It has to be borne in mind that once necking has occurred, the values of fibre stress and strain are not the same throughout the specimen, so that it becomes difficult to define a value of rupture stress or strain.

When the behaviour of the fibre can be treated as brittle, or while ductile the plastic deformation is limited and failure is rapid, it is possible to approximate fracture behaviour by means of a probabilistic model based on the Weibull theory of the weakest link. This model, which will be explained later, is useful in handling the variability of the experimental values of the rupture stress or strain and to predict the behaviour of specimens of different sizes.

2.6.2. Weibull model

Weibull theory[16] assumes that the failure of a structure happens as a sudden random event with the appearance of the first macroscopic crack and whose probability increases with the volume of the structure and the level of the applied stress. It is also based on the supposition that the material is brittle, so that there are no changes in geometry, and therefore the stress distribution, before failure. The model does not consider time dependent effects.

Figure 29a shows a fibre of volume V_T subjected to a stress σ. Its probability of fracture $P_f(\sigma, V_T)$ will depend as much on the level of the applied stress as the volume and is, in principle, an unknown fuction that needs to be determined.

If the volume of the fibre is notionally divided into two parts V and $V_T - V$ respectively (Figure 29b), the probability of survival of the fibre is $1-P_f(\sigma, V_T)$ which can be expressed as the product of the probabilities of survival of the two parts into which the specimen was divided, given that the fibre fails when one of its parts fail and that these are statistically independent events, then

$$1-P_f(\sigma,V_T)=[1-P_f(\sigma,V)][1-P_f(\sigma,V_T-V)] \tag{59}$$

in which the same probability function has been used for each part of the fibre because it is the same material.

Equation (59) must be true for any chosen division, that is, any V *between 0* and V_T, which yields an equation which is a differentiable function of V, leading to:

$$\frac{P_f'(\sigma,V)}{1-P_f(\sigma,V)}=\frac{P_f'(\sigma,V_T-V)}{1-P_f(\sigma,V_T-V)} \tag{60}$$

In which $(')$ indicates the partial derivative with respect to V. Since V and $V_T - V$ can take on arbitrary values between *0 and* V_T, the above fractions must be independent of the volume, so that

$$\frac{P_f'(\sigma,V)}{1-P_f(\sigma,V)}=c(\sigma) \tag{61}$$

where $c(\sigma)$ is a function only the stress, called the *defect concentration function*. Equation (61) can be integrated to obtain:

$$P_f(\sigma,V)=1-e^{-c(\sigma)V} \tag{62}$$

which is the Weibull probability of failure (1939, 1951). $c(\sigma)$ usually interpreted as the density of microdefects present whose failure stress is less than or equal to σ.

The function $P_f(\sigma,V)$ provides that probability that a fibre of volume V loaded to s stress σ will suffer brittle fracture or, in other words, the probability that the rupture stress of the fibre is less than or equal to σ. Therefore, $P_f(\sigma,V)$ is the probability distribution function of the random variable "rupture stress" of the fibre.

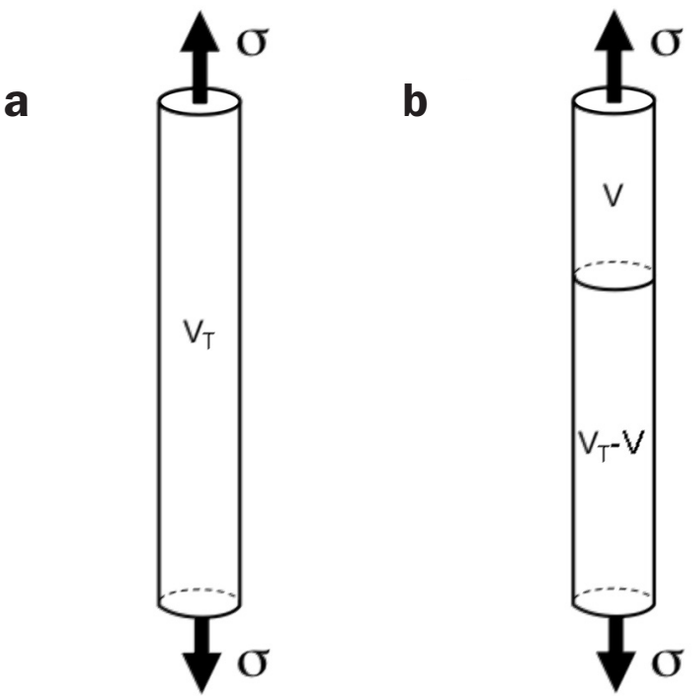

Fig. 29. *Tensile test on a fibre*
a. Original fibre volume V_T
b. Notional division of the fibre into two parts $V_T - V$ *and* V

[16] Ernst Hjalmar Waloddi Weibull (1887-1979) was a Swedish engineer interested in the fatigue and fracture of materials, who in 1951 published the statistical distribution that bears his name. The concept was suggested earlier by Fréchet (1927) and by Rosin and Rammler (1933).

The *probability density* function $\phi(\sigma,V)$ is obtained by differentiating equation (62) with respect to σ:

$$\phi(\sigma,V) = V\frac{dc}{d\sigma}e^{-c(\sigma)V} \tag{63}$$

The quantity $\phi(\sigma,V)d\sigma$ represents the probability of failure of a fibre of volume V subjected to a stress between σ and $\sigma+d\sigma$ or, in other words, the probability that the value of the rupture stress of the fibre will be between σ and $\sigma+d\sigma$. Weibull roved that a good fit with experimental data is obtained by assuming a possible defect concentration function of the form.

$$c(\sigma) = \frac{1}{V_0}\left\langle\frac{\sigma-\sigma_{th}}{\sigma_0}\right\rangle^m \tag{64}$$

where V_0 and σ_0 are two constants denoted reference volume and stress, σ_{th} is the rupture threshold stresses and m is a nondimensional constant known as the Weibull modulus. The brackets $\langle\rangle$ indicate that only positive values of the argument are taken, and otherwise zero. If the applied stress is less than the threshold stress σ_{th} the probability of failure is zero.

With the concentration function in equation (64), the probability of failure and the probability density become:

$$P_f(\sigma,V) = 1-e^{-\frac{V}{V_0}\left\langle\frac{\sigma-\sigma_{th}}{\sigma_0}\right\rangle^m} \tag{65}$$

$$\phi(\sigma,V) = \frac{Vm}{V_0\sigma_0}\left\langle\frac{\sigma-\sigma_{th}}{\sigma_0}\right\rangle^{m-1} e^{-\frac{V}{V_0}\left\langle\frac{\sigma-\sigma_{th}}{\sigma_0}\right\rangle^m} \tag{66}$$

which are represented in figures 30 and 31 for various values of the parameters in them. In these figures it is clear that the Weibull modulus, m, controls the distribution of the failure stresses, with them being more defined the great the modulus. The Weibull modulus for several fibres are presented in Table 1.

TABLE 1. WEIBULL MODULUS FOR SEVERAL FIBRES

FIBRE	WEIBULL MODULUS	REFERENCE
Spider silk	3 - 4	Pérez-Rigueiro et al. (2001)
Silkworm silk	5.8	Pérez-Rigueiro et al. (1998)
Semolina (dry)	10 – 15	Guinea et al. (2004)
Glass*	10 – 30	Le Bourhis (2008)
Jute	2.7	Fidelis et al. (2013)
Pita	3.7	Fidelis et al. (2013)
Flax	3-5	Andersons et al. (2005)

* For specimens which are not of fibre form the Weibull modulus lies between 3 and 7

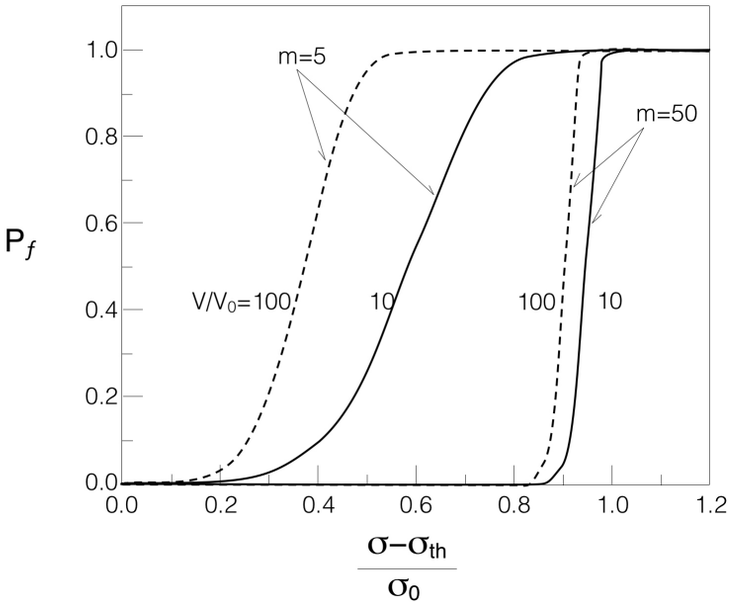

Fig. 30. *Weibull model for the probability of failure*

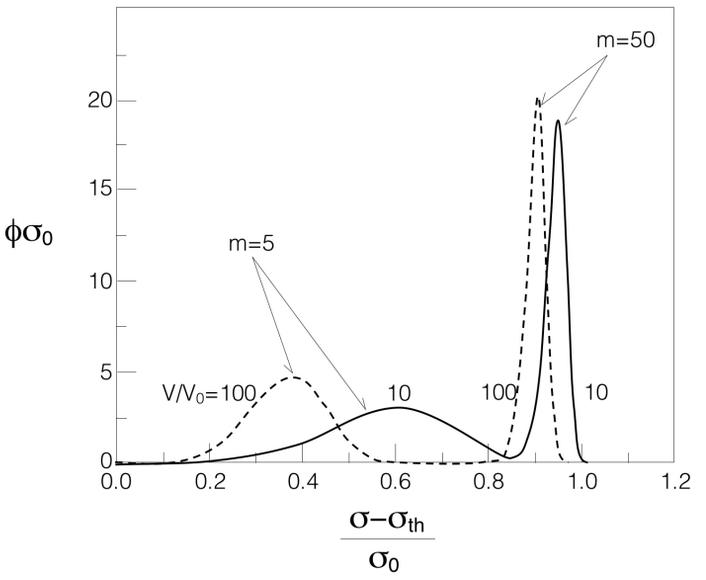

Fig. 31. *Weibull model for the probability density of failure*

It is usual to employ the Weibull modulus without the value of the threshold stress σ_{th} setting it to zero. This parameter normally has very little influence on the results, and the assumption simplifies the calculation of the statistical parameters from equation (66). The mean failure stress σ_u then becomes

$$\sigma_u = \int_0^\infty \sigma\ \phi(\sigma) d\sigma = \Gamma(1+1/m)\ \sigma_0 \left(\frac{V_0}{V}\right)^{1/m} \tag{67}$$

and the coefficient of variation of the failure stress, ω, is given by

$$\omega^2 = \frac{\int_{\sigma_{th}}^\infty (\sigma - \sigma_u)^2\ \phi(\sigma) d\sigma}{\sigma_u^2} = \frac{\Gamma(1+2/m)}{\Gamma^2(1+1/m)} - 1 \tag{68}$$

where $\Gamma(z)$ is Euler's Gamma function which is defined as

$$\Gamma(z) = \int_0^\infty t^{z-1} e^{-t}\, dt$$

which, for values $5 < m < 50$, can be approximated to $\Gamma(1+1/m) \approx 0.6366^{1/m}$ with which

$$\sigma_u = \sigma_0 \left(0.6366 \frac{V_0}{V}\right)^{\frac{1}{m}}$$

with an error of less than 0.5%. Equally

$$\omega = \frac{1}{0.462 + 0.783m}$$

With a error of less than 0.25% for the same range of values of m (Bazant and Planas 1997).

Equations (67) and (68) provide a simple means of calculating the Weibull parameters from statistical values of rupture and making estimates of the mean stress for fibres of different lengths.

EXERCISE

Integrate equation (61) and obtain equation (62).

Recall the model hypothesis, for V tending to 0, P_f must also tend to zero.

Solution:

If we write equation (61) in differential form and separate the variables

$$\frac{dP_f(\sigma,V)}{1 - P_f(\sigma,V)} = c(\sigma) dV$$

the equation can be easily integrated

$$-\ln\left(1 - P_f(\sigma,V)\right) = c(\sigma)V + C(\sigma)$$

where C is a constant of integration. The condition $P_f(\sigma, V=0)=0$ yields the value $C=0$, so that

$$1 - P_f(\sigma,V) = e^{-c(\sigma)V}$$

which is equation (62).

EXERCISE

Pérez-Rigueiro et al. (1998) recorded the values for the rupture of silk fibres presented in the Table. Calculate the Weibull modulus of silk thread assuming that there is no stress threshold: a) from the probability of failure, using equation (65) and the given data; b) from equations (67) and (68).

TABLE (A) : FAILURE STRESS (MPa)

203	280	280	319	327	336	346	366	375	375	392	401	415	419	426	433	436	454	455	457	464	471	471	523

Solution

a) Equation (65) with σ_{th} =0 gives: $P_f = 1 - e^{-\frac{V}{V_0}\left(\frac{\sigma}{\sigma_0}\right)^m}$ or $\ln\left(\ln\left(\frac{1}{1-P_f}\right)\right) = m\ln(\sigma) + \ln\left(\frac{V}{V_0{\sigma_0}^m}\right)$

Plotting ln(ln(1/(1- P_f))) against a ln(σ) gives a straight line of slope m.

Estimation of the probability exceeding a determined value from a series of experimental data is a subject of great engineering interest, and there are many expression for this, as well as the two referenced in the text. An extensive discussion of the best method can be found in (Barnett 1975).

In order to assign probabilities $P_f(\sigma)$ to the measured values of failure stress Hazen's equation (1930) is usually employed.

$$P_f(\sigma) = \frac{i(\sigma) - 0.5}{N}$$

where i is the ordinal of each value of the failure stress, onced ordered from smallest to largest and N is the total number of measurements. In Table (b) the values obtained are presented, together with value of the probability calculated with the alternative expression (Weibull 1939)

$$P^*_f(\sigma) = \frac{i(\sigma)}{N+1}$$

which is also often used. The previous expressions differ above all in the assignment of probabilities at the extremes (large and small values) and are more precise approximations as the size of the specimen increases, converging for $N \to \infty$.

TABLE B. STRESS σ (MPa)	Order (i)	P_f	P_f*
203	1	0.020833	0.04
280	2	0.062500	0.08
280	3	0.104170	0.12
319	4	0.145830	0.16
327	5	0.187500	0.20
336	6	0.229170	0.24
346	7	0.270830	0.28
366	8	0.312500	0.32
375	9	0.354170	0.36
375	10	0.395830	0.40
392	11	0.437500	0.44
401	12	0.479170	0.48
415	13	0.520830	0.52
419	14	0.562500	0.56
426	15	0.604170	0.60
433	16	0.645830	0.64
436	17	0.687500	0.68
454	18	0.729170	0.72
455	19	0.770830	0.76
457	20	0.812500	0.80
464	21	0.854170	0.84
471	22	0.895830	0.88
471	23	0.937500	0.92
523	24	0.979170	0.96

The graph presents the data with two estimated probabilities P_f *and* P_f* and their corresponding straight-line approximations. The slope of the lines (Weibull modulus) lies between **5.76** for P_f and **5.08** for P_f*.

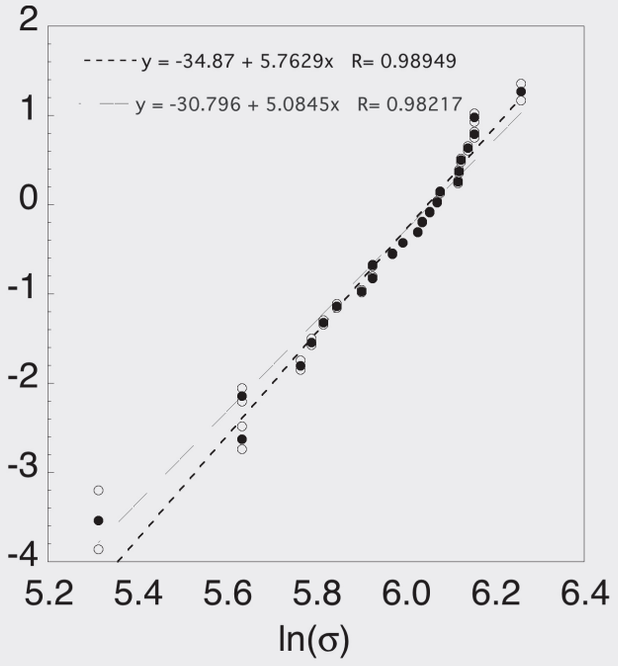

b) With the data in Table (a) we can calculate the mean value (= 392.67 MPa) and standard deviation (= 75.133 MPa) of the failure stress.

The coefficient of variation of the failure stress is

ω = standard deviation / mean value = 75.133 / 392.67 = 0.1913

and since $\omega \approx (0.462+0.783m)^{-1}$ we see that m= **6.09**.

EXERCISE
Tensile tests on a batch of fibres have provided a value for the mean failure stress of 203MPa, with a standard deviation of 17.3 MPa. Calculate the value of the Weibull modulus of the materialCalcule el valor del módulo. Neglect the threshold stress.

Solution
The ratio of the standard deviation and the mean value,ω gives ω = 17.3/203=0.0852. Using the equation of Bazant & Planas $\omega \approx (0.462+0.783m)^{-1}$ we see that m= 14.4.

EXERCISE
If the fibres in the previous exercise are divided in half before testing, what will the mean stress to failure be according to the Weibull model?

Solution
Equation (67) provides the average breaking stress $\sigma_u = \Gamma(1+1/m)\ \sigma_0(V_0/V)^{1/m}$

Then, for a length L and diameter $\emptyset$ the volume is $V=\pi L\emptyset^2/4$ and the mean stress to failure will be

$$\sigma_u = \Gamma(1+1/m)\ \sigma_0(4V_0/(\pi L\emptyset^2))^{1/m}$$

For a length L' of the same diameter $\emptyset$ the volume will be $V'=\pi L'\emptyset^2/4$ and

$$\sigma_u' = \Gamma(1+1/m)\ \sigma_0(4V_0/(\pi L'\emptyset^2))^{1/m}$$

dividing both expressions

$$\sigma_u'/\ \sigma_u = (L/L')^{1/m} = (2)^{1/m} = 1.05$$

If σ_u=203 MPa then σ_u=213 MPa

2.6.3. Final remarks

The rupture of a material is a complex phenomenon in which the deformation processesin the fracture zone and its surroundings play an important role. The models used to describe failure depend upon the type of deformation produced (reversible, irreversible, time-dependent etc.) and the extent of the affected zone.

Brittle fracture, in which ideally it is assumed that the material does not suffer any plastic (irreversible) deformation, is perhaps the simplest case to analyse. Even so, the appearance of discontinuities inside the material enormously complicates the mechanical analysis and requires the use of empirical information (location and geometry of defects, for example) which are rarely easy to obtain.

Probabilistic failure models such as that of simplify the situation assuming that the defects are randomly distributed in the material and when one of these reaches a critical stress the entire structure collapses. Although this is not normally the case for most structures (which can usually sustain a certain degree of defect, and a resulting redistribution of stresses and strains). If usually a more realistic situation in the case of brittle fibres, and hence the moderate success obtained in said models, including in the field of biological materials. A study which used the Weibull model to characterise the properties of serrano ham (*jamón serrano*) has been recently published (Romero de Ávila et al. 2014).

When it is required to perform a deeper analysis of fracture and to be able adequately predict the rupture load and strain it becomes indispensible to delve more deeply into the material and its deformation and failure mechanisms. Section III of this book deals with this.

3 CHAPTER Examples

3.1. COTTON FIBRES

3.1.1. Introduction and fibre structure

Cotton fibres are polysaccharides. They come from the hairs that cover the seeds of plants of the genus *Gossypium*. The structure of the fibres is shown in Figure 1. The fibres have a diameter of about 25 μm and lengths which vary between 1 and 5 cm. In their natural state the cross section of the fibre is circular, exhibiting daily growth rings (Figure 1a). Once picked, they lose water and collapse, adopting the twisted form with the kidney-shaped cross section shown in Figures 1b and 1c.

From plant to fabric, cotton fibres pass through the following stages: *harvest* (*picking*), in which the fibres are extracted from the seed capsule, manually or by machine;

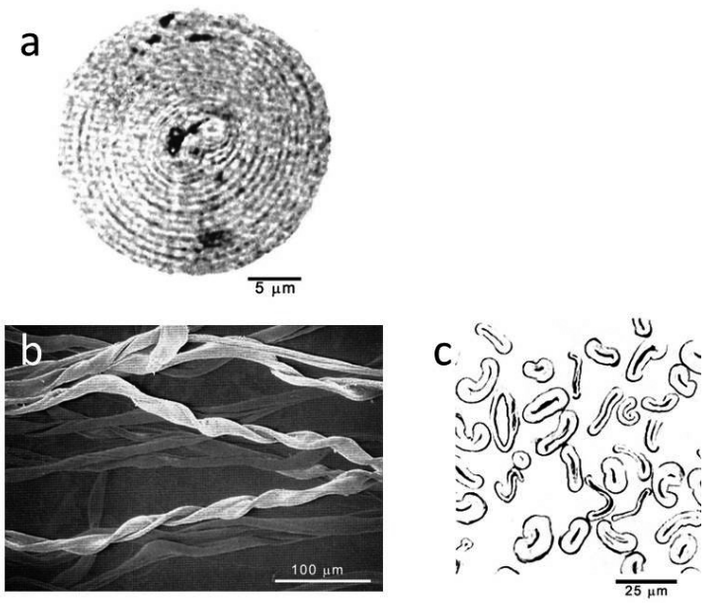

Fig. 1. *Form of cotton fibres.*
a. Cross section of a fibre with water, in which the growth rings are apparent (T. Kerr 1937).
Dry fibres; longitudinal view (b) and transverse view (c).

ginning, the process by which the fibres are separated from the seeds; *yarn*, manipulation when the fibres are stretched, twisted, folded and pressed against each other in order to create threads with distinct characteristics; and, finally, the *fabric* made from the fibres. In some cases the fibres are subjected to a preparation process for later manipulation, called *mercerisation* (due to John Mercer, 1844), and which consists of dousing them in an 18% solution of NaOH which causes a swelling of the fibres. By the end of the treatment the fibres are thicker, less twisted, and stronger, more lustrous and absorb colour better.

The use of cotton goes back to prehistoric times. There is evidence that it was cultivated in the Indus valley, in India, around 3000 BC. The ancient Egyptians and Chinese spun and wove cotton. In the Middle Ages, the Arabs introduced cotton to Europe, among other routes through Spain. They called it *qutn*, from which it became *algodón* in Spanish, *cotó* in Catalan, or *cotton* in English. The invention of the mechanical cotton gin in 1793, by the American Eli Whitney, revolutionised its production; it took production from 3,000 bales per year to 73,000, in 1800. According to some historians, cotton production played a role in triggering the American Civil War, because of the need for slave labour. Currently more than 26 million tons of cotton are produced annually, a clear indication of the importance of this fibre.

Cotton fibres have a hierarchical structure—as do all natural fibres— represented, in a simplified form, in figure 2. In a mature cotton fibre six levels can be identified: The first is the *cuticule*, a fine shell —of several molecules— which contains waxes, pectin and proteins. The second is the *primary wall*, with a thickness of about 0.1 μm, formed of a network of cellulose fibrils arranged helically with an angle between 20 and 30˚ to the fibre axis. The thickness of this wall depends upon the maturity of the fibre; the more mature, the thicker, and, in general, the more mature, the stronger the fibre. The third level is known as the *layer S1*, it is another, but simpler, network of fibrils aligned to the axis of the fibre forming angles between 40 and 70˚. The thickness is about 0.1 μm. The fourth level, called *layer* S2, is the *secondary wall* which has a greater thickness, of about 4 μm, and is, to a large extent, responsible for the stiffness of the fibre. It is also composed of cellulose fibrils which lie, approximately, at an angle of 45˚ to the fibre axis. The fifth level is the *lumen wall*, or *layer* S3. And the sixth level is the *lumen* itself, a channel which runs down the centre of the fibre and which, in a mature fibre when the calyx of the plant is opened , the interior dries, the lumen collapses, and the cross section takes on the kidney-shaped form shown in figure 2.

The purest form of cellulose that nature produces is in cotton fibres, with a content of about 90%. The remaining components (waxes, proteins, *etc*.) are located in the external shell or inside the lumen.

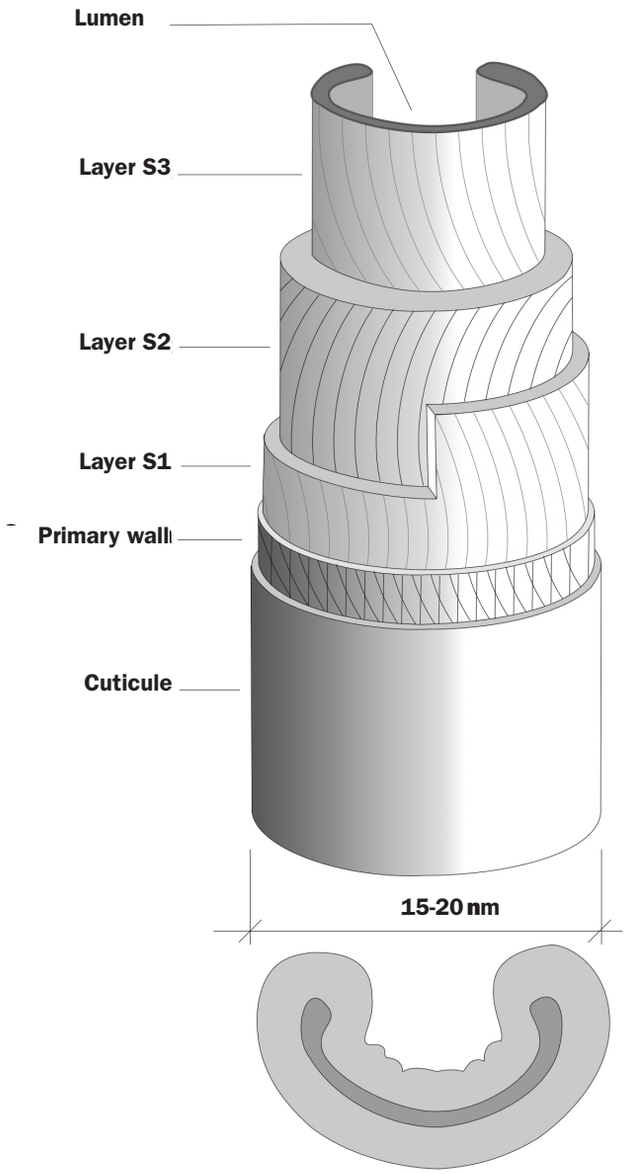

Fig. 2. *Hierarchical structure of cotton fibres (R. Jefferies et al. 1969).*

3.1.2. Mechanical properties

The mechanical behaviour of cotton fibres are derived from tensile tests, tests which are not without their difficulties because of the small dimensions of the fibres; the diameter in particular. The characteristics of the these tests and their peculiarities are not the purpose of this chapter, but the interested reader can consult the articles of Sasser *et al*. (1991), Hebert *et al*. (1995), or Thibodeaux *et al*. (1998).

When testing natural, rather than artificial, fibres a significant spread in the results is obtained, a factor that must be taken into account when modelling their behaviour. Figure 3 is a typical example of the distribution of the results when the strength of fibres and threads (a bundle of fibres) are measured.

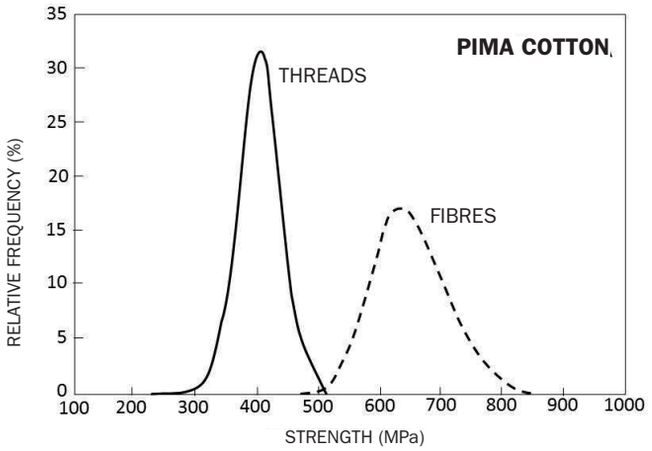

Fig. 3. *Spread of results from the measurement of the strengths of Pima[1] cotton fibres and threads (Faray and Elmogahzy, 2009)*

Several examples of the stress-strain curves for cotton fibres are shown in figure 4. The behaviour is practically linear elastic, although at large strains, on unloading, the deformation is not completely recovered, as will be discussed later.

Strength values can range from 200 to 800 MPa. The strength of these fibres is attributed to the cellulose chain stiffness, the fibrillar structure and the multiple hydrogen bonds; as much intermolecular as intramolecular. However, there is no reliable model for the prediction of the failure load, owing to the hierarchical structure of the fibre, shown in figure 1.

Strains in tensile tests may reach as much as 6 to 14%. These values are small in absolute terms, allowing the use of small deformation mechanical models. Strain measurement is tricky since the fibre is initially wavy, as can be seen in figure 1, and during straightening, in the first phase of loading, an erroneous elongation is recorded as a result of this process. For this reason it is common the "comb" the fibres a little to try to unravel them prior to testing. Fibres with larger elongations before rupture produce more flexible threads and, also, larger failure strains. Both characteristics are desirable for fabric production because the fibres are subjected to a conditioning process before weaving in order to increase their stiffness.

The elastic modulus of cotton fibres typically lies between 5 and 12 GPa. Given the shape of the stress-strain curves, which are essential straight lines, the initial modulus is valid for the whole curve. Measurement of the initial modulus presents the same difficulties mentioned above with measurement of the initial strains, because the fibres are wavy.

As has already been mentioned, the mechanical response of the fibres is not completely elastic, beyond a certain strain the fibres do not recover their original length on unloading. This characteristic is very important because the fibre suffer repeated loading and unloading cycles during handling, weaving and later use. Linen fibres are more elastic and, for large deformations, recover up to 80%. Cotton fibres, under the same circumstances, only recover 50% (elastic recovery is measured as the quotient of the difference between the

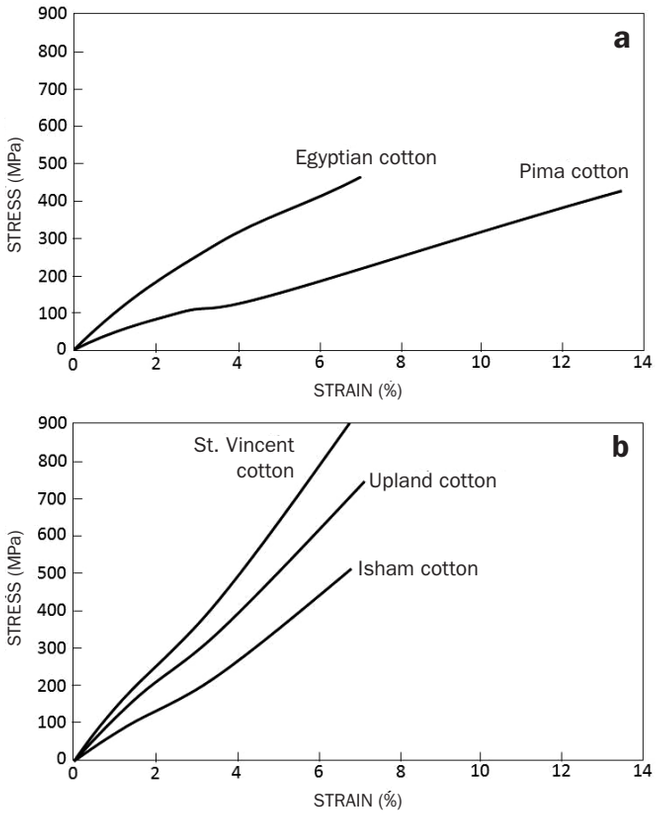

Fig. 4. *Engineering stress-strain curves for cotton fibres.*
a. Following Farag and Elmogahzy (2009).
b. Following Sparrow (1973).

[1] Pima cotton is type of cotton with a longer fiber than conventional cotton. Pima cotton fibers measure between 1.4 to 2 inches in length, while conventional cotton fibers measure up to 1.1 inches long. Pima cotton fabric comes out softer and more durable than if it were made from a shorter staple cotton.

maximum and final strains after one cycle of loading and unloading, and the maximum strain to which the fibre was subjected). An approximate picture of the elastic recovery of cotton fibres can be obtained from the work of Meredith (1945); if the strain is less than 2% the recovery will be typically about 80%. For strains of about 5% recovery is about 50% and for large strains, of the order of 10%, recovery does not exceed 30%.

Another factor which influences the mechanical properties of the fibres is humidity. It affects the dimensions, strength and flexibility. The effects of humidity on the stress-strain curves are shown in figure 5. Increasing the humidity increases the strength, strain to failure and the flexibility.

The tensile test on cotton fibres, as well as providing data on their quality, can give an indication of the strength of threads manufactured from the fibres. The contribution of the fibres to the strength of threads is due to their own strength, and the friction between them. A detailed analysis of the strengths of threads can be found in Farag (2009) and in Schwartz (2008). The conclusion is that the strength of threads is less than that of the fibres, as indicated in figure 3, although the dispersion in the data is usually less than that of fibres (as is also apparent in the figure).

One conclusion of this study is that the value of the elastic modulus of a thread E_h is a function of the modulus of the fibre E_f and the angle α which the fibre forms with the axis of the thread. The result is given by

$$E_h = E_f \left[\cos^2 \alpha \left(1 - k \operatorname{cosec} \alpha\right)\right]$$

where k, is a constant which depends up on the geometry of the fibre and the coefficient of friction between the fibres (see the exercise).

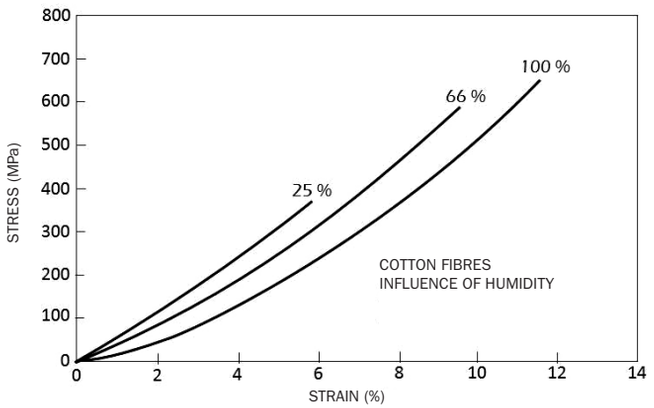

Fig. 5. *Engineering stress-strain curves of cotton fibres. Influence of humidity (Meredith, in Fibre Science, J.M. Preston (Ed.), The Textile Institute 1953, p. 246).*

If all of the fibres have the same length as the thread, only the first factor appears $-\cos^2 \alpha-$, which indicates that the stiffness can be reduced by increasing the angle. The second factor $-(1 - k\ cosec\ \alpha)-$ takes into account the dimensions of the fibres and the friction between them through the parameter k, which is given by

$$k = A\ (a/\mu)^{1/2}\ L^{-1}$$

where A is a constant, a and L the diameter and length of the fibres, respectively, and μ is the coefficient of friction between them.

3.1.3. Concluding remarks

One of the reasons for the continued use of cotton is the large number of applications that it has. From a 230 kg bale of cotton it is possible to make about 700 shirts, 1,200 T-shirts, 6,000 pairs of knickers, 22,000 handkerchiefs, 4,000 socks, 200 pairs of jeans, 240 sheets, 600 towels, 1,200 pillowcases or 3,000 nappies.

The vast range of cotton products is due, in great part, to its physicochemical properties and the organoleptics of this fibre. The smooth texture of cotton makes it very suitable for underwear, because it feels like skin. It is absorbent, durable against abrasion, and resistant to many chemical agents.

Non-woven cotton products also have a future –for example; wipes, cloths, and cleaning gauzes– because of their great powers of absorption and wet strengths, and they have many application in daily use, in hospitals and in cosmetics. Other articles fabricated by punching, such as serviettes, tablecloths or sheets, are economical and can be used as disposable products, although some can be washed as many as six times. The challenge is to make them economically competitive by means of the appropriate selection of fibres and manufacturing processes.

Biotechnology has also played a part in the production of cotton fibres and may have an even greater role in the future. Currently, varieties of cotton have been produced that are more resistant to certain herbicides and insects, and attempts will be made to produce longer, finer and stronger fibres and, if possible, of different colours.

Another challenge for the cotton industry is to optimise production and to be able to recycle the waste products. Transformation of cotton products into cellulose, by dissolving or chemical processing, is another challenging technology.

EXERCISE

The curves in the figure show the degree of **elastic recovery** (in Ishan cotton fibre) measured by Meredith (1945), as a function of the load, and strain reached in each cycle of loading and unloading.

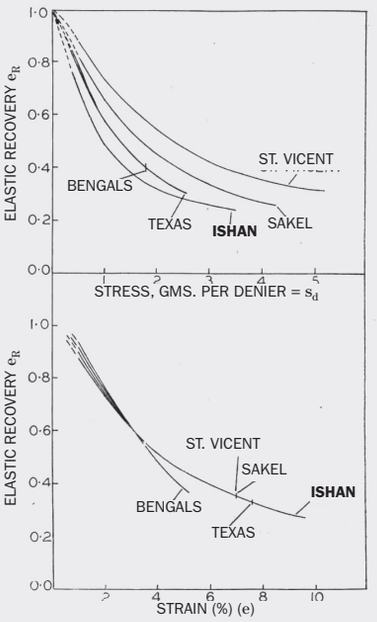

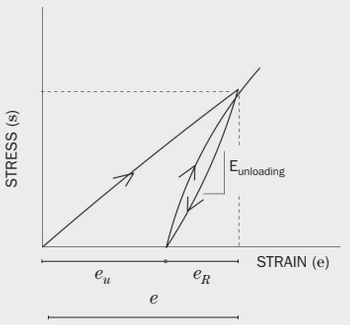

$R_E = e_R/e$

Derive the engineering stress-strain curves for the fibres and the value of the elastic modulus of the unloading-reloading branches as a function of the maximum strain reached in the cycles. Assume that the behaviour is linear during unloading and reloading.

Data for Ishan cotton fibres: mass = 2.4 denier; density of cotton =1.54g/cm^3

Solution:

The engineering stress-strain curves is obtained by plotting pairs of stress-strain points corresponding to the same value of the elastic recovery. This will be the new curve of the fibre.

The resulting curve is shown in the **figure a** with the stress expressed in MPa. In order to obtain it, the definition of *denier* given in paragraph 2.2.1 has been used. If *A* is the cross sectional area of the fibre and ρ its density, the linear density will be $\mu = \rho A$ so the engineering stress *s* is then

$$s = \frac{F}{A} = \frac{\mu}{A}\frac{F}{\mu} = \rho\frac{F}{\mu} = \rho s_d$$

stress expressed in units of force per linear density. In Meredith's chart we see that s_d is given in grammes-force/denier and, for that, we will write

$$s = 1540\frac{kg}{m^3}\ s_d\left(\frac{g_f}{denier}\right) = 1540\ s_d\frac{kg}{m^3}\frac{10^{-3}kg_f}{\left(2.4g/9km\right)}\frac{9.81N}{kg_f} = 56.65\ s_d MPa$$

In order to obtain the elastic modulus of the unloading branch E_u, we simply divide the stress s at each point by by the value of the elastic strain e - e_u = e . e_R:

$$E_u = \frac{s}{e.e_R}$$

Then, the strain recovered on unloading is the product of the elastic recovery $e_R = (e - e_u)/e$ and the strain *e* reached in each cycle. The results are shown in **figure b,** in which the secant elastic modulus is also shown, defined as the ratio of the stress and the maximum strain reached in each cycle s / e.

a

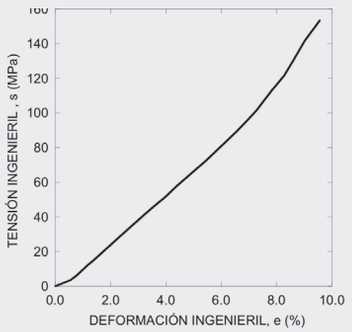

b

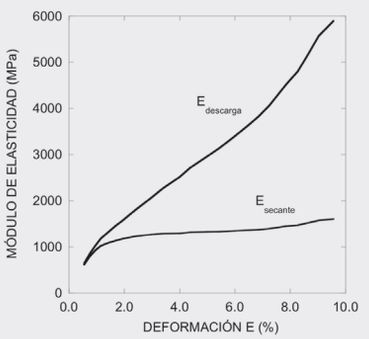

As can be seen in figure b (above), when the fibre undergoes larger strains, the response hardens –as much in new loading as in the unloading and reloading branches– probably as a result of the forced alignment of its microfibrils.

If we compare the curve in figure a with that of figure 4b, obtained by Sparrow (1973) we see significant differences, probably attributable to the different threading and moisture content during the experiments.

EXERCISE

In the case of fibres of equal length, determine the value of the elastic modulus of a thread E_h from the elastic modulus of a fibre E_f

Solution:

Consider a thread, of length L, consisting of a bundle of N fibres which form a cylindrical helix of angle α with the axis of the thread, as shown in the figure. A straight line element of a single fibre is shown in the figure. We shall assume that all of the fibres have the same length L_f and cross sectional area A_f. We shall also assume that the strain in the thread is small enough that any change in the angle α can be ignored, and that there is no friction between the fibres.

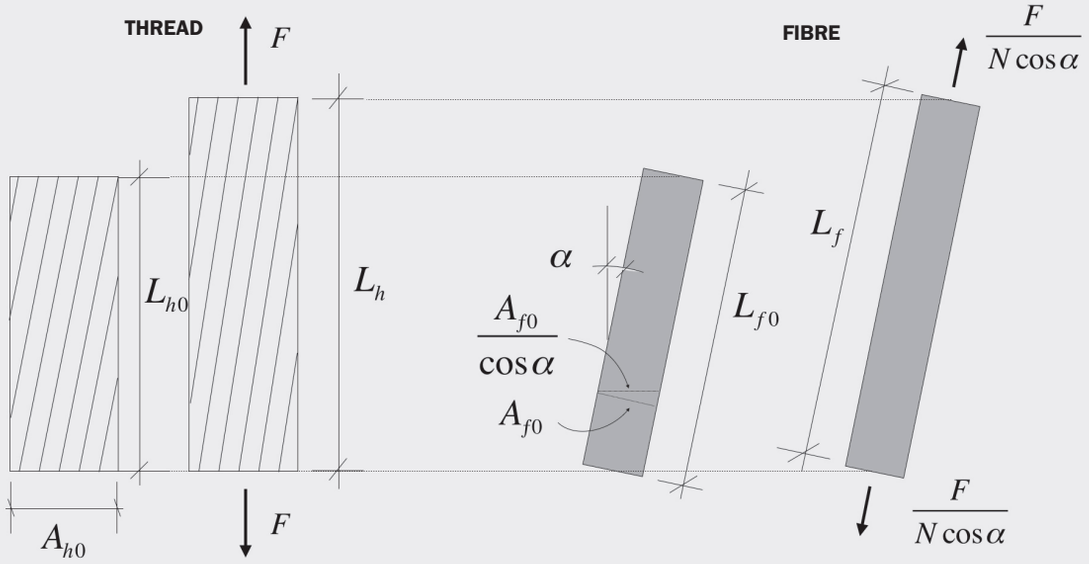

Under these conditions, if the thread is subjected to a tensile force F, the engineering stress in the thread will be:

$$s_h = \frac{F}{A_{h0}} = \frac{F\cos\alpha}{NA_{f0}}$$

where A_{h0} and A_{f0} are the initial cross sectional areas of the thread and fibre, respectively. In order to obtain A_{h0} we note that the cross sectional area of the thread will be the sum of the oblique cross sections of the fibres $A_{f0}/cos\alpha$.

If the initial length of the thread is L_{h0}, the engineering strain will be $e_h = \frac{L_h}{L_{h0}}$

In the fibres, the stress state will also be tensile and the force carried by each of them will be $F / (N\ cos\alpha)$ since there is no friction. Note that the vector sum of the forces on all of the fibres must be equal to the external force and that the components perpendicular to the axis of the thread must cancel out.

The engineering stress in a fibre will be $s_f = \frac{F}{NA_{f0}\cos\alpha}$ and its engineering strain $e_f = \frac{L_f}{L_{f0}} = \frac{L_h}{L_{h0}} = e_h$

since $cos\alpha = L_h/L_f = L_{h0}/L_{f0}$, and the ratio of the height of a helix and its length is the cosine of the angle which the helix forms with its axis.

From these results, the elastic modulus of the thread and fibre must be related by

$$E_h = \frac{s_h}{e_h} = \frac{F\cos\alpha}{NA_{f0}}\frac{1}{e_h} = \frac{F}{NA_{f0}\cos\alpha}\frac{1}{e_h}\cos^2\alpha = \frac{s_f}{e_f}\cos^2\alpha = E_f\cos^2\alpha$$

which is the required relationship.

3.2. WOOL FIBRES

3.2.1. Introduction and fibre structure

Wool fibres are proteins; amino acid polymers. They come from the hair of domesticated sheep of the genus *Ovis aries*. The name has been generalised and is also used for the fine hair of some goats (*cashmere*, from Himalayan goats, and *angora* or *mohair*, from goats of Ankara), from camels, vicunas, alpacas and yaks, and also Angora rabbits.

From wool to fabric, the fibres pass through the following stages: *cleaning*, since they contain impurities (grease, earth, excrement and vegetable material); *mechanical* treatment consisting of disentangling the fibres by carding, combing and drawing; *chemical* treatments, such as carbonising (this process destroys the vegetable residues) bleaching (the process of removing the natural colouring of the fibres) and, sometimes, dyeing. The final product, made from the fibres, may be subjected to moth and stabilisation treatments. For more detailed information see, for example, Simpson and Crawshaw (2002).

Wool was, probably, the first fibre used for clothing by mankind, initially in the form of felt, from cut or torn hair. Spinning of fibres and then fabric came later. It is difficult to track down the origins of the use of woollens because they do not survive well, but it is known that in ancient Babylon (which according to some sources means “land of wool”) there was an active market in this product. One of the oldest woollen fabric remains, dating from around 1800 BC, comes from a tomb in Denmark, which has been preserved in a reasonable state thanks to an acid soil (Barber, 1992).

The Phoenicians introduced sheep from Asia Minor as far as North Africa. They entered Spain about the XII century by the hand of the Beni-Merines tribe and, quite possibly, from this comes the name of sheep (merino) which produce very fine wool of excellent quality. Spain had a monopoly of wool between the XII and XVI Centuries, and the export of merino sheep was severely punished. The Napoleonic wars almost ended the Spanish merino breed. At the beginning of the XIX Century, this breed began to proliferate in Germany, the United States, Australia and South Africa.

An ideal wool fibre has a circular cross section, whose diameter ranges from 20 to 40 μm, a length which varies from 5 to 50 cm, and is curly.

The actual structure of wool fibres is very complicated, as shown in figure 6a. The components of the fibre are: the cortical cells, the extracellular complex (*cell membrane complex* CMC) and the cuticle that surrounds the fibre. The three components are shown schematically in figure 6b.

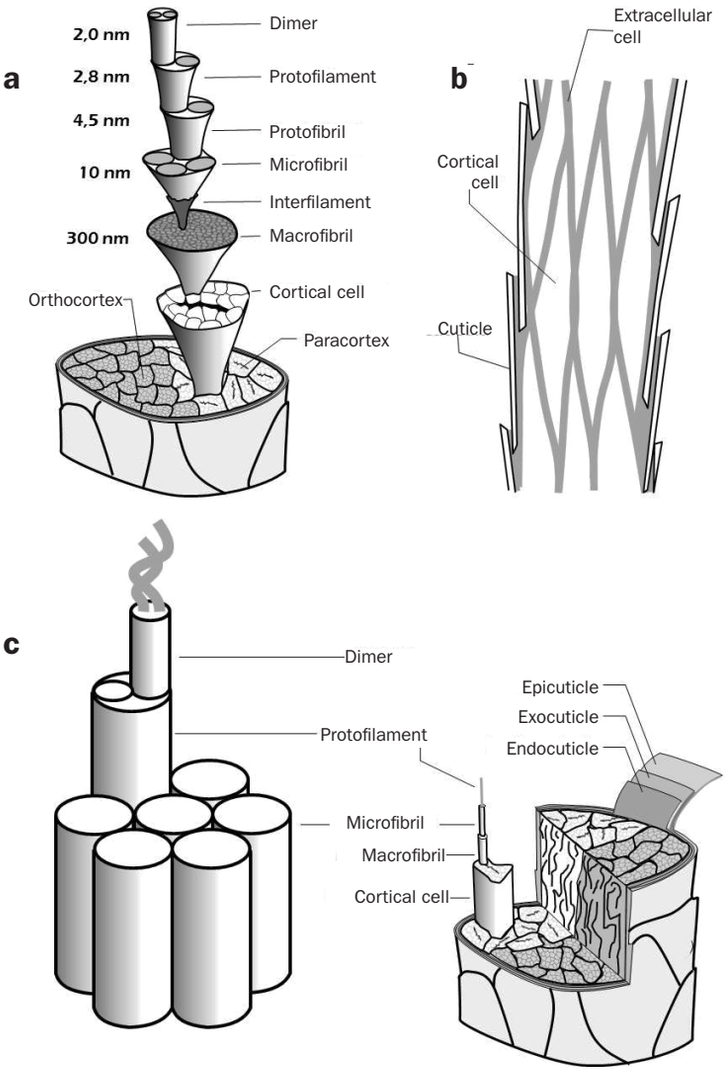

Fig. 6. *Hierarchical structure of wool fibre (after Eichner et al. 1985).*
b. Longitudinal section of a fibre with its principal components; cuticle, cortical cells and extracellular matrix.
c. Schematic of the hierarchical structure.

The cuticle is formed of flattened cells, interleaved like (roof) tiles, whose tips point towards the fibre end. The approximate dimension are 20 x 30 x 0.8 μm. In each cell four layers can be distinguished; the surface, or *epicuticle*, which is a thin membrane (about 5 nm) strong and hydrophobic, the α *layer*, the *exocuticle* and the *endocuticle* (figure 6c). In figure 6c the α *layer* is not shown.

The extracellular complex covers all of the cortical cells, and ensures its stability by means of intercellular links via proteins known as *desmosomes* (binding bodies or *maculae adherentes*).

Examining the cross section of a cortical cell it is possible to identify *macrofibrils* which are aligned in the direction of the fibre axis (figure 6c) and embedded in an intermacrofibrilar matrix. The macrofibrils, in turn, are formed of hundreds of *microfibrils* , a sort of protein which is present in the cell cytoskeleton and which is usually called *intermediate keratin filaments* (IKF), embedded in a *keratin associated protein* (KAP) matrix. It is possible to identify two classes of cortical cells by their different appearances after staining with silver nitrate; the *orthocortical* cells, which que appear clearer compared to the darker stained *paracorticals*.

The cortical cells are spindle-shaped, (figure 6b), with lengths between 45 and 95 μm and a width of between 2 and 6 μm. The combined cortical cells occupy 90% of the fibre, the *orth-* type being more abundant than the *para-*.

In each cortical cell between 5 and 20 macrofibrils can be observed. Each microfibril has a diameter of between 0.1 and 0.3 μm and is composed of a stack of 500 to 800 microfibrils (figures 1a and 1c).

Microfibrils are formed of 7 or 8 protofilaments and each protofilament is composed of four chains of intermediate keratin filaments (IKF) grouped in two helically wound pairs (Simpson and Crawshaw 2002) (figure 6c).

When observed by X-ray diffraction microfibrils show peaks which indicate a certain order. If the fibres are stretched to about 50% and immersed in a steam bath, the X-ray diffraction pattern changes and other peaks appear. For this reason the undeformed fibres are called α-*keratins* and the deformed ones, β-*keratins*.

In α-keratin the peptide chain forms a right-handed helix whose stability is ensured by intramolecular hydrogen bonds (Pauling *et al*. 1951). Two helices of this type are wound and form a left-handed super-helix with hydrophobic amino acid residues facing outwards (Letai and Fuchs, 1995). These dimers are the smallest units of the microfibril, as shown in figure 6a.

In β-keratin, the peptide chain is more stretched and forms a different structure called β-leaf in which the chains are joined transversely by means of hydrogen bonds (Pauling, 1953).

3.2.2. Mechanical properties

The density of wool is about 1.31 g cm^{-3}, at 25˚C and relative humidity of 65%.

Moisture absorption

The protein in wool contains hydrophilic groups which attract water molecules, so that water absorption depends upon the ambient relative humidity, the temperature and, also, the history of the wool. The process of water absorption is exothermic and the water absorption curves as a function of relative humidity are almost reversible: that is there is very little hysteresis, barely 2%.

Although wool is hygroscopic, the surface of the fibre is hydrophobic, as has already been observed, which makes the penetration of water in the liquid phase difficult. The shrinkage caused by water absorption is not the same in the radial direction as the longitudinal; with a relative humidity of 100%, the fibre may extend by only 2% but increase in radius by 16% (Onions, 1962).

Tensile test

The mechanical properties of wool fibre depend upon the ambient relative humidity (as would be expected), the temperature and prior history. For example, a dry wool fibre, at room temperature and which has not previously been deformed might have a breaking load of between130 and 210 MPa, but, if tested wet, these values may decrease by 20%. The extension to failure has the opposite tendency; when dry this can vary between 28 and 48%, but if wet the value increases by between 40 to 60%.

Figure 7 shows two stress-strain curves for a wool fibre tested at 20˚C, with a relative humidity of 65%, and another tested in water at the same temperature. The general shape of the curves is typical of tensile response of these fibres, in which distinct regions are apparent:

In the first phase (OA), where the stress increases rapidly with strain, up to values of 1 to 2%, the initial elastic modulus decreases with humidity. This first tranche is usually called “Hookean” but this is not strictly correct, since, as will be seen later, although the behaviour is linear, it is viscoelastic.

The second phase (AB) (note that point B is not on the curve, rather it is a reference point) is known as the flow region; the load increases very slowly with strain, reaching strains of the order of 25 to 30%.

In the third phase (BC) the stress increases more quickly with strain, until rupture at point C. In general the curves

are quite reproducible up to point B. Tranche BC is more variable because it is affected by imperfections which may precipitate breakage. A good fibre can reach strains as great as 60%.

X-ray diffraction spectra indicate that after point A, that is the initiation of flow, the lines corresponding to the α-helices weaken and those of the β-leaves develop (Bendit, 1960). This transition is, to some extent, reversible, as noted by Feughelman (1997) showing that if the fibre is deformed up to point B, at room temperature, it can recover its mechanical properties completely if the duration of straining is less than an hour. If the fibre is unloaded and immersed in water at room temperature for 10 hours (or one hour at 50˚C), not only is the initial length recovered, the same stress-strain response is obtained on reloading.

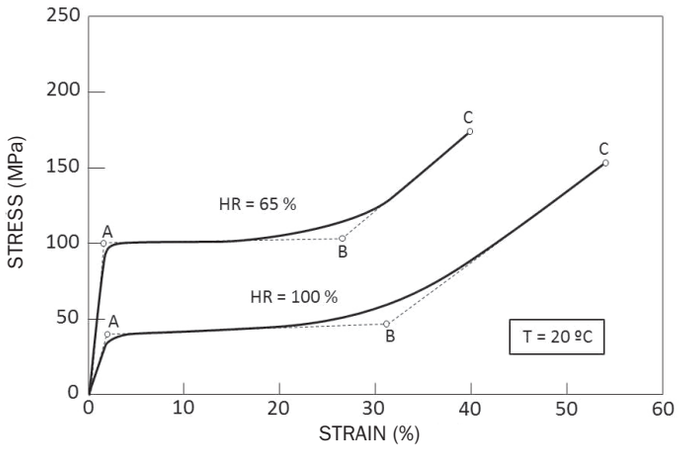

Fig. 7. *Engineering stress-strain curves for wool fibre (Zahn et al. 1996).*

EXERCISE

The figure shows a typical load (in grammes)-engineering strain curve for wool fibre in water at 20 °C subjected to tensile loading in a test lasting 25 days (Feughelman 1997). The strain rate was 0.375%/hour from the beginning to the end of the Hookean region/initiation of the flow plateau, and 1.875%/day from that point on.

If the fibre has an average diameter of 30 μm derive the engineering and true stress-strain curves and determine salient values.

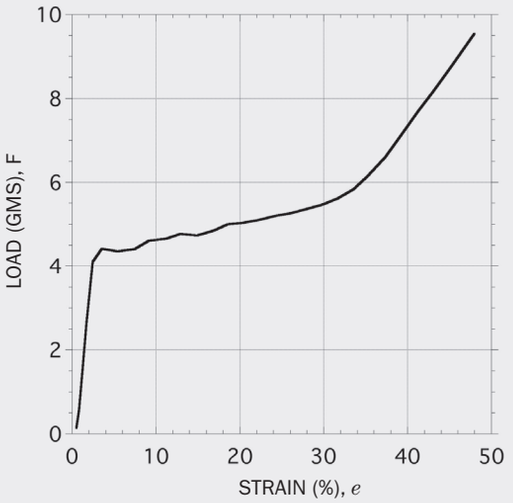

Solution:

The engineering stress is calculated using equation (1) of section 2.2:

$$s = \frac{F}{A_0} = \frac{4F}{\pi D_0^2}$$

where F is the force on the specimen and A_0 is its cross sectional area, which we calculate from its diameter D_0. The resulting s-e curve is sketched in the figure (below). From equations (6) and (7) we obtain the true strains and stresses $\varepsilon = \ln(1+e)$ and $\sigma = s(1+e)$ which are also drawn in the figure.

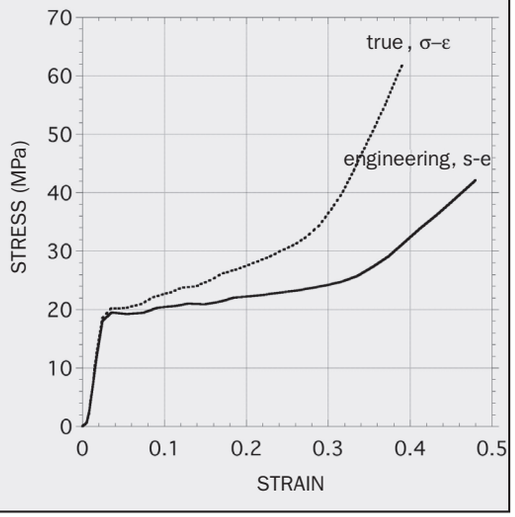

The salient values of these curves are:

	Engineering	True
Initial modulus E(GPa):	970	1013
Flow stress, s_y or σ_y (MPa)	19.4	20.2
Modulus in flow region E_2(GPa)	20	52
Modulus post flow E_3(GPa)	120	300

Note that when values for the parameters of the stress-strain curves are given it is important to specify from which curves they have been obtained, whether from true or engineering, the data will be different, especially for strains above 5%.

Influence of humidity, temperature and ambient conditions

Figure 8 shows the effect of **humidity** on the stress-strain curves, according to data from Speakeman (1927). The drier the fibre, the greater the elastic limit, the slope of the flow region, the initial modulus and the breaking stress, but the smaller the strain to failure.

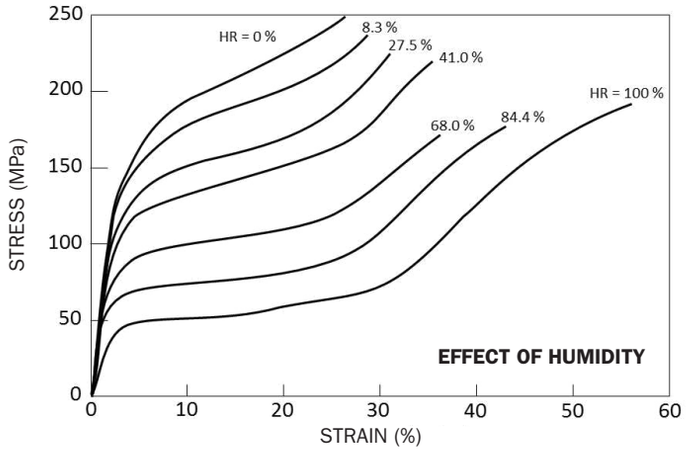

Fig. 8. *Engineering stress-strain curves for wool fibres at 24.4ºC as a function of the relative humidity (after Speakman 1927).*

Figure 9 shows the effect of **temperature** on the stress-strain curves, again using data from Speakeman (1927). When the test temperature increases, the elastic limit decreases, as do the slope of the flow region and the breaking stress. Note that these changes are more pronounced between 40 and 80˚C.

Figures 8 and 9 justify the use of water and temperature to facilitate combing, although this assistance is temporary since the hairs recover their initial properties when the humidity and /or temperature are reestablished. Thanks to the presence of the amino acids with sulphur (cistein), it is possible to form

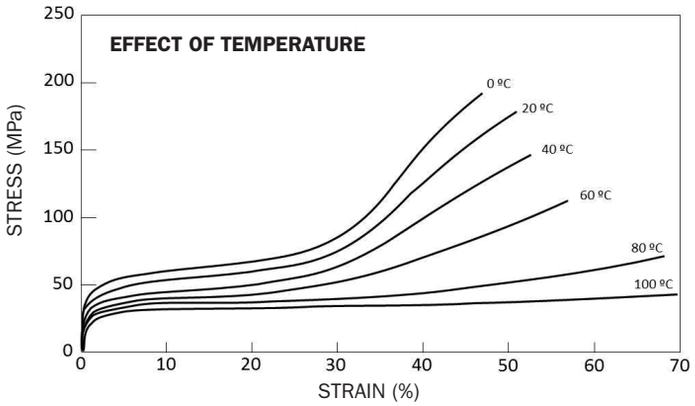

Fig. 9. *Engineering stress-strain curves for wool fibres tested in water as a function of temperature (after Speakman 1927).*

permanent bonds between the keratin fibres through disulphur bridges (–S–S–) , which allow *permanent* changes to the form and properties of the hairs. This is precisely the name that hairdressers have given to the treatment, in which a reducing agent first (generally tyoglicolic acid) and then another oxidant (oxygenated water) break the existing disulphur bridges and then reform them in hair with the desired shape.

Figure 10 shows the effect of various ambient media **(acids and alcohols)** on the stress-strain curves, using data from Peters and Woods (1956). Figure 10a illustrates the effect of alcohols. Since the alcohol molecules are larger than that of water they do not cause the reduction in the stiffness evident in Figure 8. However, the larger the alcohol molecule the smaller the plastifying effect, and the mechanical properties improve. The effect of alcohols is similar to that of humidity; the larger molecules behave as if the environment were dryer. Figure 10b shows the effect of acids. Everything indicates that if the molecules are small they have less difficulty in penetrating the fibre, and therefore, weaken the material.

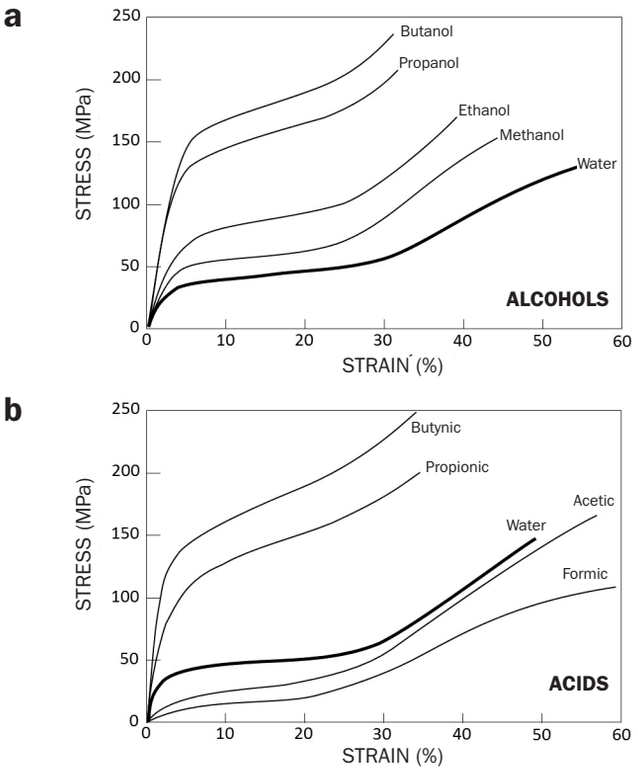

Fig. 10. *Engineering stress-strain curves for wool fibres immersed in several media: a.- alcohols, b.- acids (after Peters and Woods 1956).*

In 1894 the Spaniard A. Borrás produced "*El fraile del tiempo*" a weather forecasting device which is still on sale. This is based on the sketch of a monk on cardboard (see the figure) who has a wand and mobile hood. These items rise and fall according to whether or not it is going to rain.

Actually it is a hair hygrometer, which measures the ambient humidity thanks to the extension induced in a fibre –usually human hair– by the atmospheric moisture. The wand and hood are usually rigidly connected and rotate together about a point. In order to keep the fibre in a state of tension at all times, a counterweight is usually included.

Weather forecasting is based on the correlation between humidity and atmospheric pressure, since the latter is sensitive to the presence of anticyclones (high pressure phenomena) which are normally accompanied by dry stable weather, and low pressure systems (troughs) which usually bring changeable weather and squalls.

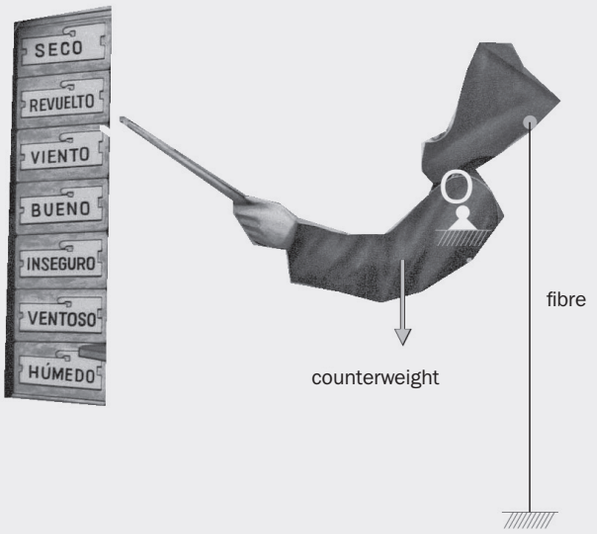

The influence of humidity on human hair has been known since ancient times (people with long hair notice that their hair curls and expands in bulk when the humidity is high) but it was not until 1783 when the Swiss physicist and geologist Horace Bénédict de Saussure built the first hygrometer from human hair very similar to the one described above.

If we take as reference values those of figure 8 (which are for wool fibres) we see that the initial modulus changes from ~2GPa to ~6GPa when the relative humidity changes from 100% to 0%. This implies that elongation of the fibres (under the same load) will be (6/2 = 3) three times bigger when saturated compared to that in the absence of moisture. The hair hygrometer takes advantage of this change to precisely measure humidity on a graduated scale.

Influence of time

The stress-strain curves of wool fibres are like those of many other polymers, but only during the loading process. On unloading, if the elastic limit has been exceeded, a permanent deformation occurs in many polymers, but not in the case of wool fibres; if tested wet and before the strain has surpassed 30%, as illustrated in figure 11, due to Morton and Hearle (1993), the strain is completely recovered. In this example, the unloading curve does not follow that of loading, and only rejoins it for values of about one third of the elastic limit.

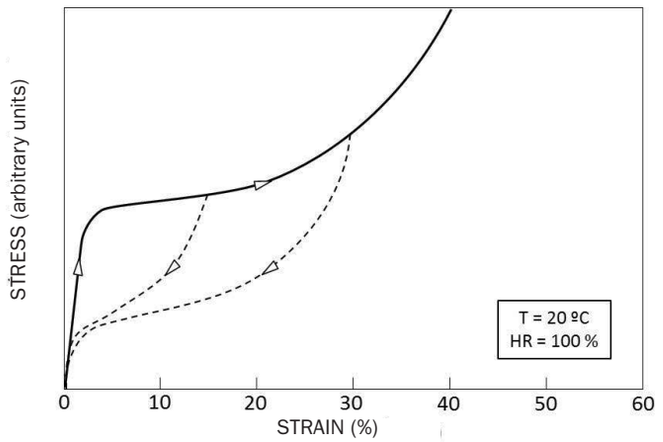

Fig. 11. *Loading and unloading curves for a wet wool fibre (after Morton and Hearle 1993. The stress is in arbitrary units).*

Other experiments have demonstrated this recovery capacity, which decreases with the degree of relative humidity (Meredith, 1945. Beste and Hoffman, 1950). All this indicates that **time** is a factor to take into account in the deformation of these fibres.

Figure 12 shows the results of several **relaxation** experiments. This phenomenon occurs even in the "elastic" region. For this reason it was noted above that it is not correct to call this first part of the curve the "Hookean region", even though it is straight. Figure 12a indicates how the stress relaxes from an initial strain of 0.8% (which in this fibre is in the initial straight section). The data are from Feughelman and Robinson (1971), and the stresses are normalised with the respect to the value limited by the fibre humidity. The effect of humidity on the relaxation is also shown in the figure.

Figure 12b shows the relaxation in stress for different values of strain beyond the elastic zone, in experiments on human hair (which behaves similar to wool), wet and at a temperature of 35˚C. The shape of the curves seem to indicate that there are several different relaxation mechanisms; initially there is a rapid reduction in the stress (in less than one second), then there is a slow reduction lasting about 100 seconds, after which there is another rapid decline, between 100 and 10,000 seconds, and, finally, it seems to approach an asymptote (Peters and Wood, 1956).

Figure 12c shows how the relaxation, in wet human hair, varies with temperature for a deformation of 40%, according to Peters and Wood (1956).

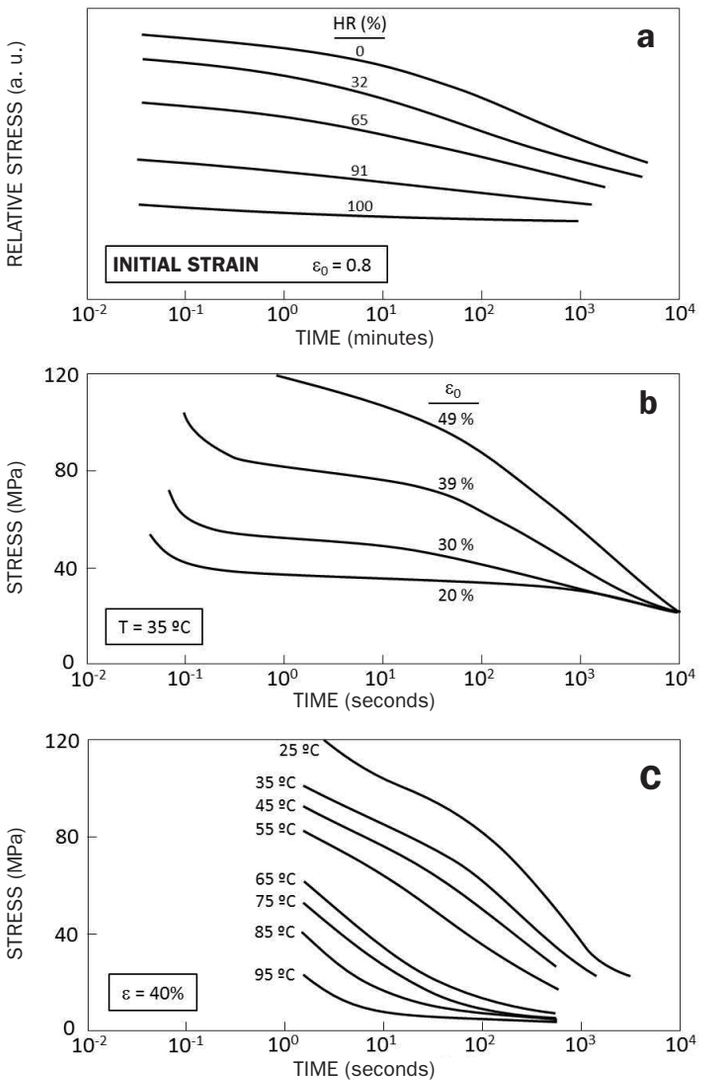

Fig. 12. *Relaxation curves of engineering stresses*

a. Influence of humidity in wool fibres at 20ºC (initial strain in the linear zone; 0,8%) (after Feughelman and Robinson 1971).

b. Influence of the initial strain. Wet human hair at 35˚C (after Peters and Woods 1956).

c. Influence of temperature. Wet human hair with an initial strain of 40% (after Peters and Woods 1956).

Creep test results are presented in figures 13a and 13b for short duration tests (2.5 minutes) and in figure 13c for tests which lasted a week. The effect of the initial stress is shown in figure 13a, for wet wool at 18.5˚C. The influence of temperature, for the same wet wool tested subjected to an initial stress of 38.5MPa is illustrated in figure 13b (Feughelman, 1954). These results—obtained with a low initial stress, of the order of the elastic limit— seems to suggest that, after a short while, an asymptote is reached and the strain stabilises. This does not happen when the experiments are performed with higher initial stresses –about 70MPa instead of 40MPa– and longer duration, as is apparent in figure 13c (taken from Peters and Woods, 1956), in which there seems to be a new creep mechanism coming into play after roughly 100 minutes.

Viscoelastic behaviour of wool fibres is also observed in the **dynamic** behaviour, even in the "Hookean" region. Figure 14 presents dynamic data for wool fibre tested under low amplitude vibrations, with a frequency of 116Hz, at 25˚C and different levels of relative humidity (from Danilatos and Feughelman, 1979). Figure 14a shows the variation in the storage modulus, G_1; note that the maximum occurs in the Hookean region, then it decreases in the flow region in order to increase again in the hardening zone. Figure14b represents the loss angle δ and is a mirror image of the previous one; minimum values in the Hookean and hardening regions, and maximum in the flow region.

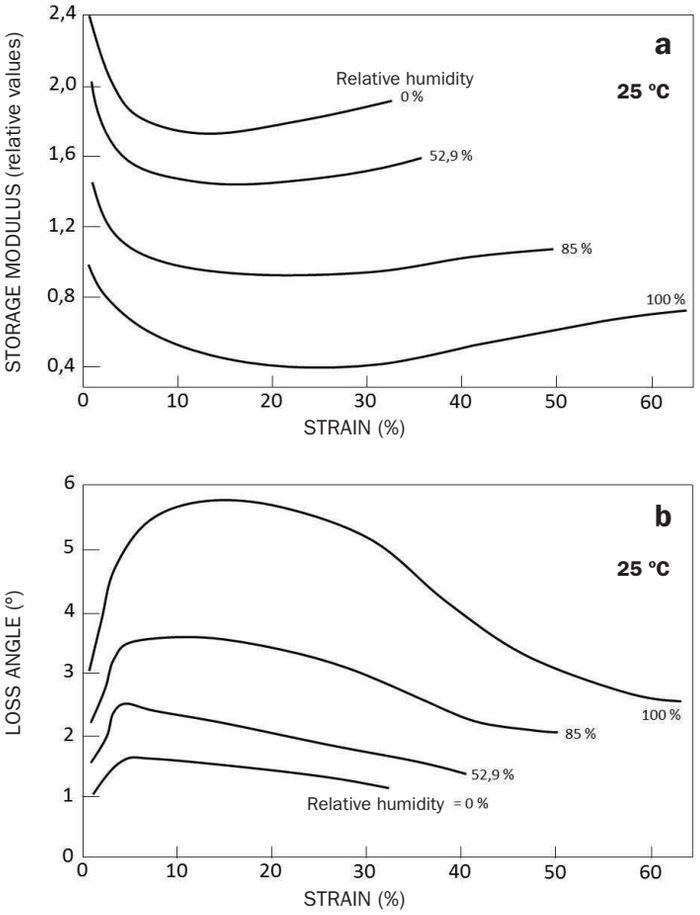

Fig. 14. *Dynamic tests on wool thread. Frequency 116 Hz. Temperature 25˚C and engineering strains (after Danilatos and Feughelman 1979).*
a. Variation of storage modulus G_1 with strain, as a function of relative humidity.
b. Variation of loss angle, δ, with strain, as a function of relative humidity.

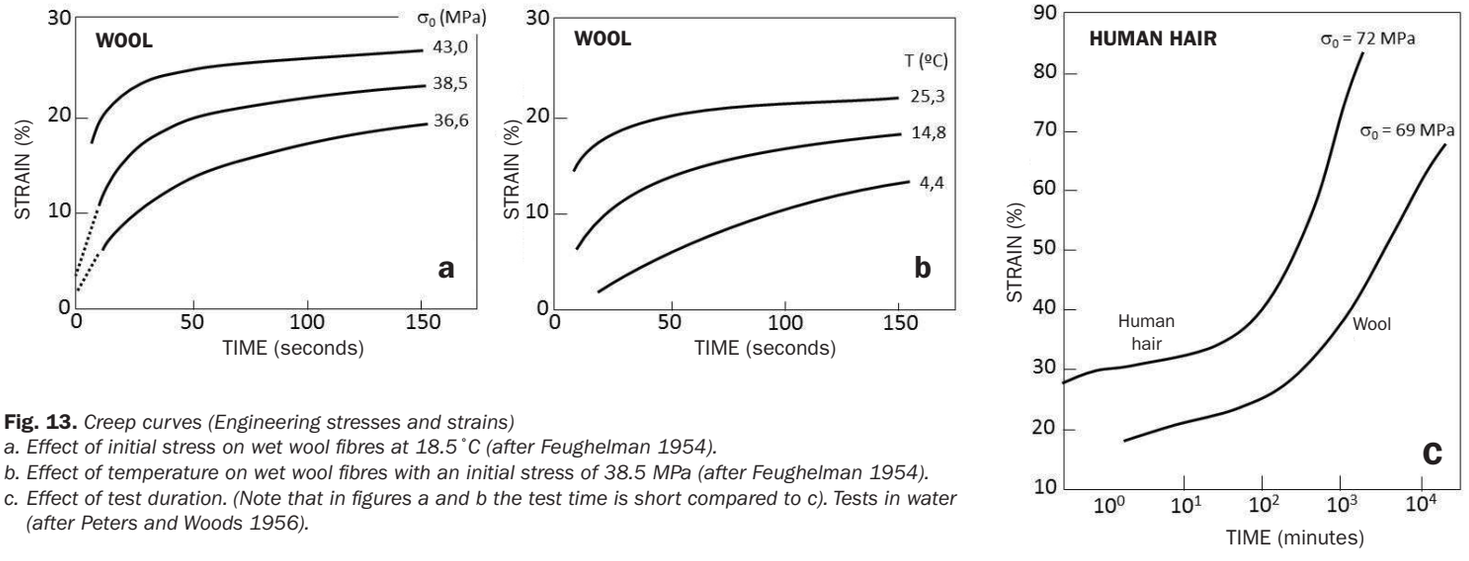

Fig. 13. *Creep curves (Engineering stresses and strains)*
a. Effect of initial stress on wet wool fibres at 18.5˚C (after Feughelman 1954).
b. Effect of temperature on wet wool fibres with an initial stress of 38.5 MPa (after Feughelman 1954).
c. Effect of test duration. (Note that in figures a and b the test time is short compared to c). Tests in water (after Peters and Woods 1956).

EXERCISE

Assess the validity of the linear viscoelastic model for the study of wool fibres in a short duration test from the curves shown in figure 13a. Investigate the influence of temperature using the data in figure 13b.

Solution:

The linear viscoelastic hypothesis proposes that in a creep test under a load σ_0 the creep function is $J(t)=\varepsilon(t)/\sigma_0$, a function which is a material property and independent of the test conditions. Therefore, if we divide the data in the curves of figure 13a by the values of the applied stress in each case all the curves must collapse on to a single curve which gives the creep function $J(t)$.

As we see in figure (a), this is not the case and the curves $\varepsilon(t)/\sigma_0$ remain quite separate. This is common in the majority of viscoelastic materials, particularly biological materials. We shall revisit this in more detail in the next section, when we examine the viscoelastic behaviour of collagen.

In order to study the effect of temperature, we draw the curves in figure 13b in figure b with a logarithmic time scale and strain values divided by the creep stress (38.5MPa) with the aim of obtaining the creep modulus $J(t)=\varepsilon(t)/\sigma_0$. We see that it is possible to identify a time shift which superimposes the curves. Taking the curve for T=14.8º C as a reference we see that $J(t;14.8º)=J(6.4t;25.5º)=J(0.22t;4.4º)$. The dashed line corresponds to the displaced curves. It can be seen that the fit between the two higher temperatures is better but, even so, it seems that for T=14.8º we can deduce the creep curves for times ranging from somewhat less than 10s to more than 15 minutes (900s).

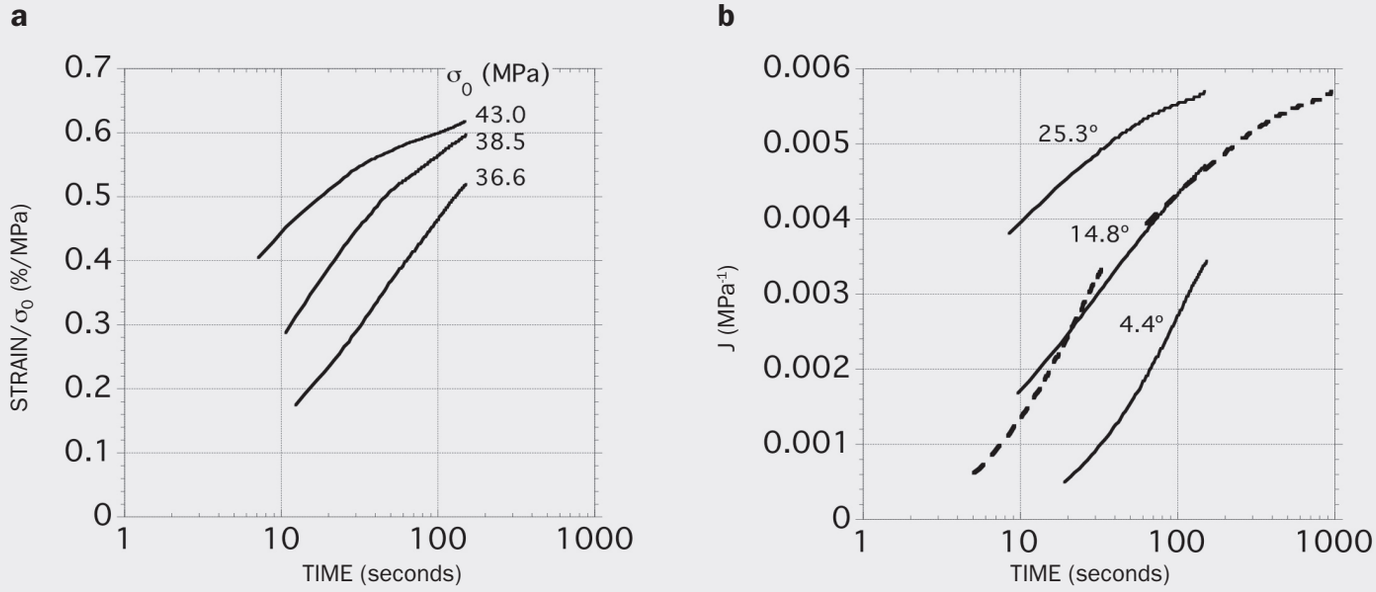

Although attempts have been made to introduce models that provide a better representation of experimental behaviour (such as Fung's linear quasi-viscoelastic model (Fung, 1972)) the linear viscoelastic model and parameters are still widely used for the characterisation of biological materials.

Currently there is extensive information on the chemical composition and mechanical behaviour of wool fibres as a function of humidity, temperature , time and environment, but much remains to be done to achieve a model that provides a detailed description of their behaviour. This is not surprising given the complex hierarchical structure shown in figure 6. Nonetheless, approximations have been made in this direction and one of the simplest is a two phase model, due to Feughleman, which explains some of the experimental features discussed above. The interested reader will find details in Feughleman (1997). A summary of some ideas extracted from this book follow.

Feughelman's model, described schematically in figure 15, provides reasonably satisfactory results in the small deformation regime; up to values of 1% strain. The model of a keratin-water system assumes that the fibre is composed of three interpenetrating polymer networks: a) a microfibril network (IKF) formed of α-keratin fibres orientated parallel to the fibre axis, b) an amorphous globular protein (KAP) matrix with a high sulphur, glycine and tyrosine content, c) water, in the form of a network of hydrogen bonds, which interact with the residual surface hydrofils of the proteins of a and b. Increasing the water content (humidity) produces a constriction in the matrix and the model accounts for the larger increase in radial strain compared to the axial strain.

For small deformations the strength is due to the strain energy in the hydrogen bonds with the α-helices more than the strength provided by the matrix. However, the shear strength, or value of the shear modulus, is principally due to the properties of the matrix.

For large deformations the model is more complicated because there are three phases: the α-helices destabilise and are transformed into β-leaves, the *gel* type matrix structure collapses into a state more like a *sol*, but when the fibre is unloaded, the structures recover again to form a polymer with the three networks. It is not the aim of this chapter to analyse the model in detail. In the reference cited above (Feughelman 1997) calculations based on this model, which coincide with the publishes experimental data, can be found.

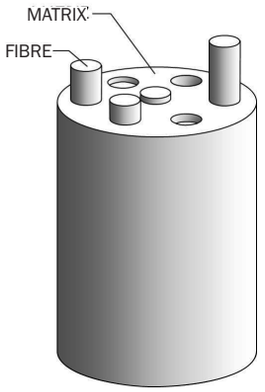

Fig. 15. *Feughleman's model (1997).*

3.2.3. Concluding remarks

The worldwide production of clean wool in 1992 was 1.7 million tonnes (Mt), in 1995 1.5 Mt, in 2000 1.4 Mt and in 2017 it did not reach 1.2Mt. The trend is decreasing although it seems that in the last few years it has tended to stabilise. The production of wool is modest in comparison with cotton and synthetic fibres, the percentage of wool fibres is about 3% of all fibres. However, the current trend is towards quality rather than quantity.

In the last few years, with the introduction of synthetic fibres, there has been increased emphasis on producing smoother and lighter wool fibres, and in a simpler manner, by reducing the fibre diameter.

Wool fibres are classified by their diameter; *fine* fibres have a diameter between 17 and 23μm, *medium* fibres between 23 and 33μm, and *thick* between 33 and 42μm. The preference for fine fibres has been notable in the last few years; in Australia, for example, in 1994 only 8.5% of fibres had a diameter of less than 19μm, twelve years later the percentage was 31%. The finest fibres have strength problems; if a fibre has an intrinsic strength of 200MPa, for example, and a dimeter of 18μm it will only support 50mN. In order to improve the strength of fine fibres several techniques have been used, principally employing genetic engineering (Rogers, 2000) but so far progress has been slow.

3.3. SILK FIBRES

3.3.1. Introduction and fibre structure

Silk fibres –like wool fibres– are proteins; amino acid polymers. Silk is usually associated with the fibre produced by the larva of the silkworm *Bombyx mori* but it is also produced by many arthopods, in particular some insects and spiders. There are more than 30,000 species of spiders and 100,000 species of insects (of the order *Lepidopteros)* which produce silk. In general, any proteic fibre produced by extrusion of a viscous liquid through a fine orifice can be considered as silk.

Silk fibres can be obtained directly from spider webs, from silkworm cocoons or the yarn forced through the glands of the creatures. From a cocoon it is possible to obtain about 1,000 metres of silk, while that from a spider's forced yarn about100 m –in several extractions– and only 10 m from the larger cobwebs.

Silks have multiple uses; to produce cocoons which protect and thermally insulate the larvae, to fabricate lairs, or to construct webs to catch prey. The most studied silks are those that come from domesticated silkworms *Bombyx mori* and the silk from some spider webs, particularly those from the genera *Nephila*, *Argiope* and *Araneus*

Silkworm silk

About 5,000 years ago, according to Chinese legend, Princess Xi Ling Shi was walking in her garden with a cup of tea in her hand. As luck would have it a silkworm fell into her cup. While trying to remove it, she saw that she could get a delicate shiny and iridescent thread from the soft mass formed by the heat of the infusion. This accident was the origin of the silk art and industry.

It is not surprising that this interesting polymer attracted the interest of peoples throughout history. For centuries the Chinese jealously guarded the secret of sericulture, an imperial law decreed death to those who revealed it. Silk was unknown in Europe 2,000 years ago, and until the VIth Century the when the techniques of sericulture reached the West, thanks to industrial espionage by one of the monks encouraged by the emperor Justinian (Feltwell, 1990). Currently, the textile industry consumes , annually, more than 400,000 tonnes of silk cocoons.

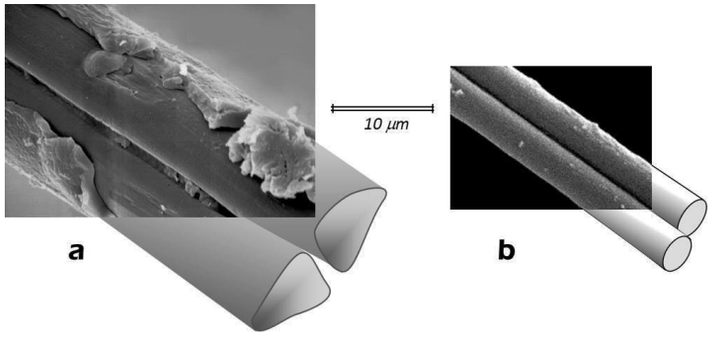

Fig. 16. *a. Silkworm silk; fibres of fibroin coated sericin. b. Spider silk; fibres of spidroin.*

Most of the silkworms belong to the domesticated species *Bombyx mori* and produce silk during one stage of its life cycle. Domestication of the *Bombyx mori* has reached the point that the insect is totally dependent on humans for food and protection, perhaps the only insect that has reached this extreme.

The thread that silkworms spin –moving their head in a figure of eight– is formed of two filaments of fibroin coated with a sericin adhesive (see figure 16a). The thickness of the fibres is about 10 μm. Silk fibres are extracted from the cocoons which have been previously boiled in soapy water to remove the sericin coating.

From each cocoon de 300 to 1200 metres of fibre are obtained, with the Japanese holding the record which they achieved, at the start of the Twentieth century, from a variety of silkworm whose cocoon produced two kilometres of fibre. In order to make a tie about 100 cocoons are needed, 650 for a shirt and more than 3,000 for a high quality kimono, for the last the silkworms must consume about 60 kilos of mulberry leaves.

The microstructure of silk thread is not known in great detail; the threads are formed by two fibres of triangular cross section, covered with a layer of sericin (figure 16a). Little is known about the hierarchical structure inside the fibres.

The protein of the silkworm –also called *fibroin*– contains two proteic chains (a heavy one, H, and the another lighter one, L) joined by sulphur crosslinks, together with a glycoprotein called P25. The molecular weights of these chains are, approximately, 350 kDa for H, 26 kDa for L, and 30 kDa for P25. These chains are connected to form a single large molecule, with respective proportions 6:6:1. The percentages of amino acid which comprise the fibroin are presented in Table 1.

The primary structure of H chain is known (Zhou *et al*. 2000) and the GlyAlaGlyAlaGlySer motif is repeated many times. It is believed that this amino acid chain is folded on itself in a structure known as β folding and which ends with the formation of nanocrystals.

Silk fibres can be modelled as a semi-crystalline material in which the macromolecules are, more or less, orientated in the direction of the fibre axis. In this model the crystalline

TABLE 1. PERCENTAGE OF AMINO ACID IN SILK FROM B. MORI, N. CLAVIPES AND A. TRIFASCIATA

AMINO ACID	B. MORI[a]	N. CLAVIPES[b]	A. TRIFASCIATA[c]
Ala	30.0	22.71	22.8
Gly	42.9	49.96	33.7
Tyr	4.8	2.99	3.4
Ser	12.2	2.24	8.7
Asp	1.9	1.06	0.5
Arg	0.5	1.76	1.4
His	0.2	0.21	0.1
Glu	1.4	11.02	1.0
Lys	0.4	0.10	0.5
Val	2.5	0.89	1.9
Leu	0.6	4.26	3.1
Ile	0.6	0.07	1.4
Phe	0.7	0.26	0.9
Pro	0.5	2.04	5.7
Thr	0.9	0.34	1.4
Met	0.1	0.04	0.5
Cys	0.0	0.06	0.1

a. Y. Nakazawa (2002), b. R.W. Work (1987), c. Average values of MaSp1 and MaSp2 for Gatesy et al (2001) and Motriuk et al. (2005).

regions play a dominant role in the stiffness and strength, while the amorphous regions contribute to the elasticity and deformation of the fibre. The crystallinity of *B. mori* is estimated to be about 50% (Drummy *et al*. 2007).

The textile industry is a unique consumer of silk fibres, but currently it is thought that the use of silk is expanding –dissolved and respun silk– for multiple applications, in particular in the field of medicine (Murphy and Kaplan, 2009).

Spider silk

Spider silk is, possibly, the natural fibre with the greatest mechanical performance. However, so far, it has not been possible to use it in the textile industry because spiders are, by their nature, solitary predators, and it is not known how to domesticate them, as the Chinese did with the silkworm.

Until the middle of the Twentieth century spider silk fibres—because of their fineness— were only used to make reticules in optical instruments. The natives of New Guinea, New Hebrides and the Solomon Islands used plaited strings with silk threads from spiders of the species *Nephila* to make nets and fishing implements. In 1709, Bon de Saint-Hilaire made gloves and stockings from silk taken from the ovigenous sacks, but the French Academy thought that silk based on siders would never be viable. Three hundred years later, because of the extraordinary properties of this material, industrial production of silk proteins from genetically modified organisms is being considered.

The production of spider silk threads is quite different from that of silkworms, since, as mentioned earlier it has not been possible to domesticate spiders; the threads obtained directly from webs or extracting the rows situated in the abdomen of spiders by forced silking (Guinea *et al*. 2005), which is how the spider makes it using its legs. For this reason spider silk thread has not been exploited industrially and is used only for research with the aim of determining the causes of their excellent mechanical properties, and to try to make it artificially.

Spiders can make, at least, seven types of silk threads (Vollrath and Porter, 2006); that from the web spokes (the strongest), the circumferential (elastic and sticky), that which envelopes the prey, that from the cocoon, *etc*. One of the most studied is that which is made for the web spokes, which is also used for the mooring network and as a safety line for moving. Most ampullate is secreted from the gland, conveniently designated *MAS* (major ampullate silk). In the following discussion attention is centred around silks of the genera *Nephila* and *Argiope*, since they are the best documented.

The microstructure of these threads is also not known in much detail; the MAS threads are formed of two fibres of almost circular cross section with a diameter of about 3.5 μm, without the coating, as shown in figure 16b. Some authors believe that they have detected a hierarchical structure in the fibres consisting of a multilayer coating (Sponner *et al*. 2007).

MAS fibres contain at least two types of protein which are usually called *spidroins*; *MaSp1* (for major ampullate spidroin) and *MaSp2*. The molecular weight of these spidroins is several hundred kDa, of the same order as the heavy H chain of the fibroin of the *B. mori* (Hakimi et al. 2007). The motifs which appear in these spidroins are typically grouped in four modules; $(\text{Gly Ala})_n(\text{Ala})_m$, … GlyGlyX, … GlyProGlyXX, and spacers. The two motifs of the first module are believed to be composed of β-nanocrystals, just like the fibroin motif mentioned above. The second module probably adopts a helicoidal configuration of type 3_1. The third is believed to involve more flexible helicoidal structures than the previous ones, and which are responsible for the elastic behaviour and large deformations in these fibres. The percentage of amino acids spidroins of *Nephila clavipes* and *Argiope trifasciata* are given in Table 1.

Like silkworm silk, spider silk fibres can be modelled as a semi-crystalline material in which the macromolecules are, more or less, aligned with the fibre axis. The estimated crystallinity of the MAS threads of *Nephila* and *Argiope* varies between 11 and 15% (Hakimi *et al*. 2007), rising to more than 20% (Plaza, G. R. *et al*. 2012).

3.3.2. Mechanical properties

The tenacity of silk fibres (measured approximately as the area under the stress strain curve) is far higher than that of the best synthetic fibres, as shown in figure 17. This property is a consequence of a good combination of strength and deformation; the strength is due, in part, to the β-nanocrystals and the deformability of the amorphous regions between these crystals. The tenacity depends not only upon the chemical composition of the fibres but also the processing: that is, how they are generated, since the orientation of the macromolecules during spinning has a great influence.

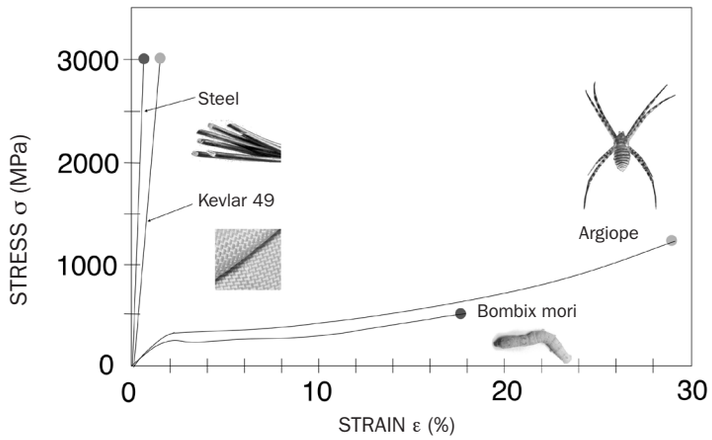

Fig. 17. *True stress-strain curves for different types of fibre.*

Silkworm silk

Silk fibre can be obtained from the cocoons of the silkworm or by extracting it directly from the worm when it begins to spin. Both techniques are described in detail in (Pérez-Rigueiro *et al*. 2002), in which the usual procedure for tensile testing these fibres is also presented

A typical stress-strain curve of silk thread is represented in figure 17. Such curves depend upon the relative humidity, temperature and strain rate; the data shown are for a test at room temperature, 60% relative humidity and a strain rate of 0.0002 s^{-1}.

The means of extraction has relatively little effect upon the behaviour of the fibres, as indicated in figure 18, which depicts force displacement curves for fibres obtained by forced silking and those produced directly by the worm.

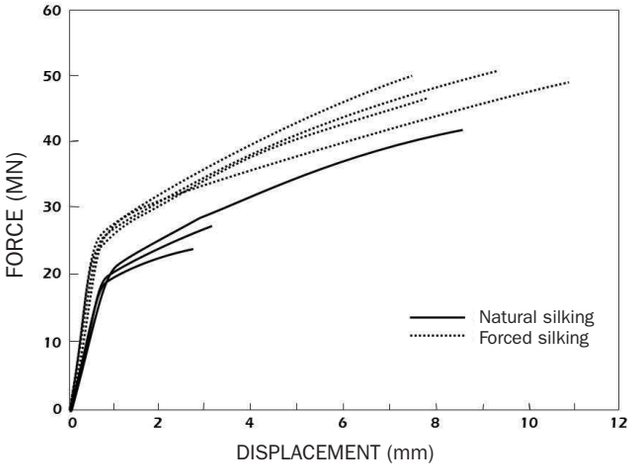

Fig. 18. *Force-displacement curves for silk fibres of B. mori obtained naturally by the worm and by forced silking (both from the same worm).*

Fibres obtained by degumming –boiling the cocoons in a detergent solution– have a similar behaviour, although the initial modulus is less, as are the elastic limit and the strain to failure (Pérez-Rigueiro *et al*. 2002). The degumming process reduces the size of the protein chains and worsens the properties of the fibre. Nonetheless, its use is essential for the elimination of sericin which binds the fibres and can also produce an allergy in contact the skin.

Martel *et al*. (2007) details the effect of temperature on tensile tests. It seems that the initial modulus increases gradually up to 227˚C, the temperature at which the tiny crystals degrade. On the other hand, the failure load and strain to failure remain constant up to 127˚C, the temperature above which both parameters begin to decrease.

EXERCISE

Sketch the stress-strain curves corresponding to the data in figure 18, and comment on the results. All of the fibres have a diameter of 10μm and the initial tensile test specimen length is 30mm.

Solution:

Taking the two curves with the greatest stress for each fibre, we calculate the true stresses and strains using equations (4) and (7), based on the usual constant volume assumption. In this way

$$\varepsilon = \ln\frac{L}{L_0} = \ln\frac{L_0+\Delta L}{L_0} \quad \text{and} \quad \sigma = \frac{F}{\pi\ {}^{2}_{0}/4}\frac{L_0+\Delta L}{L_0}$$

with L_0 = 30mm and D_0 = 10μm, where F and ΔL lare the force and displacement , respectively, presented in figure 18. Hence we obtain the curves in figure a.

If that has happened the curve is no longer representative of a material property beyond that point since the geometry of the fibre is not uniform. Since it is difficult to determine the condition $\sigma = d\sigma/d\varepsilon$ at every point, because numerical differentiation would be needed, we will use Considère's construction (see the exercise in section 2.2).

The procedure is based on writing equation (8) in terms of the true stress σ and the elongation $\lambda = L/L_0$. Since $d\varepsilon = d\lambda/\lambda$ equation (8) become $\sigma = (d\sigma/d\lambda)\lambda$ which can be written as

$$\frac{\sigma}{\lambda} = \frac{d\sigma}{d\lambda}$$

an equation which indicates when the slope of the (σ,λ) curve coincides, at the point of instability, with the tangent to the curve drawn from the origin. The construction is shown in figure b

As we see from the curves instability is never achieved, so that the specimens break while maintaining a uniform geometry.

a

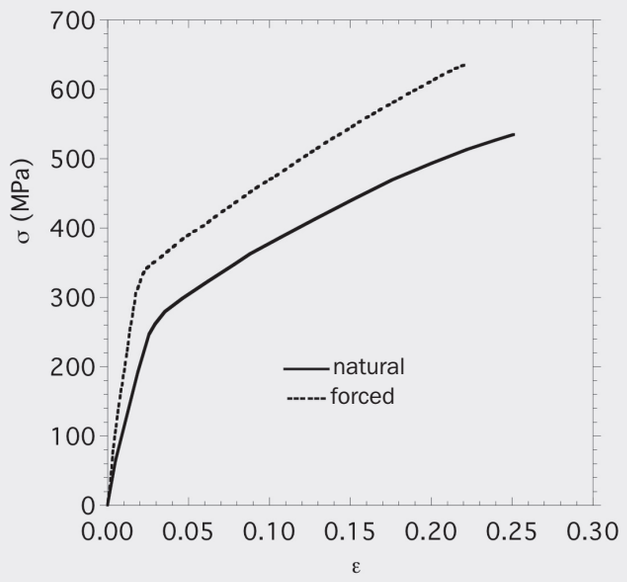

b

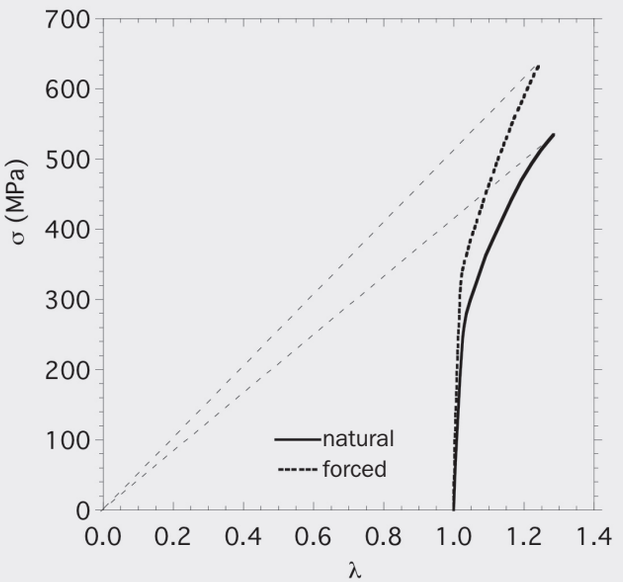

Experimental data on the influence of strain rate on the stress-strain curves are not available.

The influence of various aqueous media on tensile tests is shown in figure 19 (Pérez-Rigueiro *et al*. 2000). Testing in water reduces the stiffness of the fibre and increases the deformability. Ethanol, on the other hand, increased the rigidity and reduces the strain to failure. These results seem to indicate that water breaks the hydrogen bonds present in the amorphous phase , while other solvents (ethanol, acetone, isopropanol) remove water and promote the formation of new hydrogen bonds in the amorphous phase.

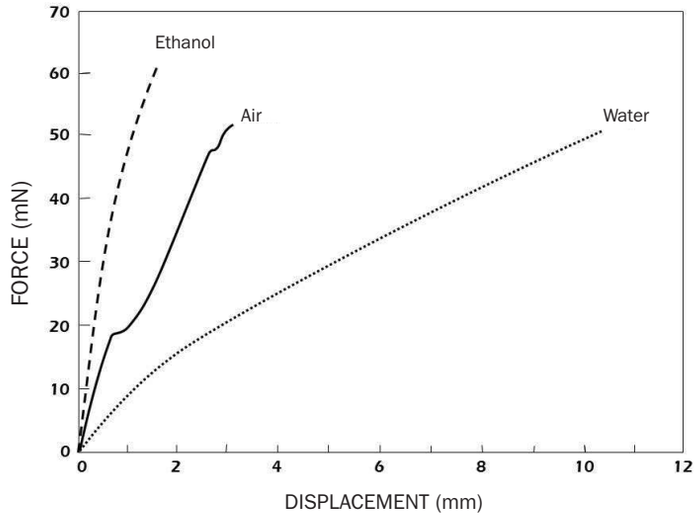

Fig. 19. *Force-displacement curves for silk fibres of B. mori in different media; ethanol, air and water.*

Spider silk

Silk fibres can be obtained directly from the web or also by forced silking. This technique is described in detail by Pérez-Rigueiro *et al*. (2005). The tensile test method is the same as that used for silkworm silk. For calculation of the true stress it is assumed that the volume is constant during the test (Guinea *et al*. 2006).

The mechanical behaviour of the fibres obtained from the two processes is rather different, as shown in figure 20 (Guinea *et al*. 2005a). Fibres obtained by forced silking are stiffer and have a lower strain to failure. It is thought that these differences are due to the orientation of the polymer chains during processing; this will be greater in forced silking than in the natural fibre. Fibres which the spider spins have a larger dispersion between stress-strain curves since the spider exerts active control during spinning according to the end use of the fibre; the fibre for weaving a web is not the same as that for when the spider need to jump off quickly to flee from a threat (Garrido *et al*. 2002).

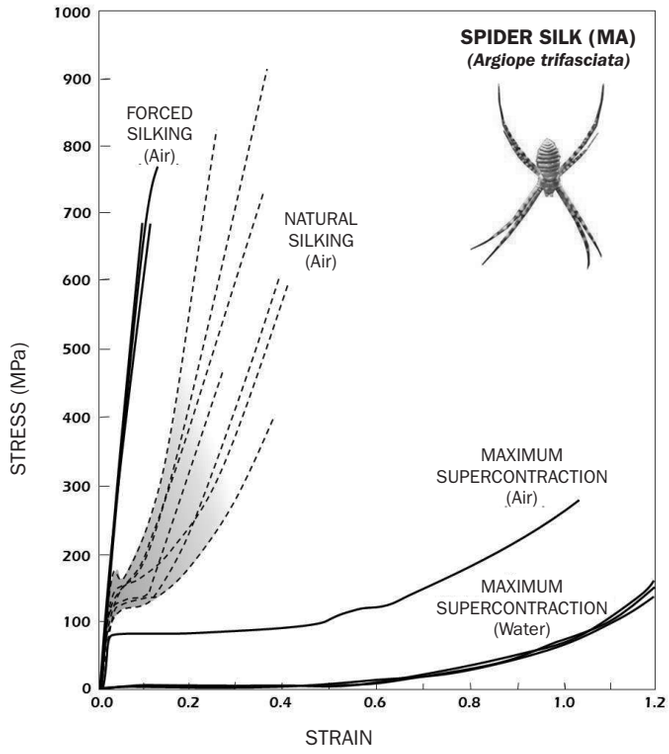

Fig. 20. *Engineering stress-strain curves of MAS silk fibres of A. trifasciata obtained under various conditions (see the text).*

The test conditions influence to stress-strain curves. In figure 21 (Plaza *et al*., 2006) the effects of **temperature** on tests performed with a relative humidity of 50% are shown. It is apparent that increasing the temperature softens the fibres, and reduces the rupture stress.

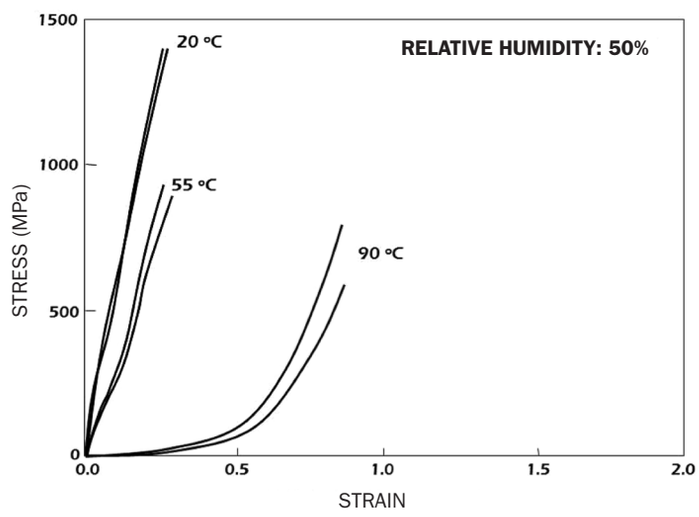

Fig. 21. *Engineering stress-strain curves for silk fibres (MA of* A. trifasciata *) for different temperatures (at a constant 50% relative humidity).*

In figure 22 (Plaza *et al*., 2006) the effect of **humidity** on tests carried out at 55˚C are shown. Here, the effect of an increase in the humidity on fibre softening and rupture stress are more marked than in the case of temperature.

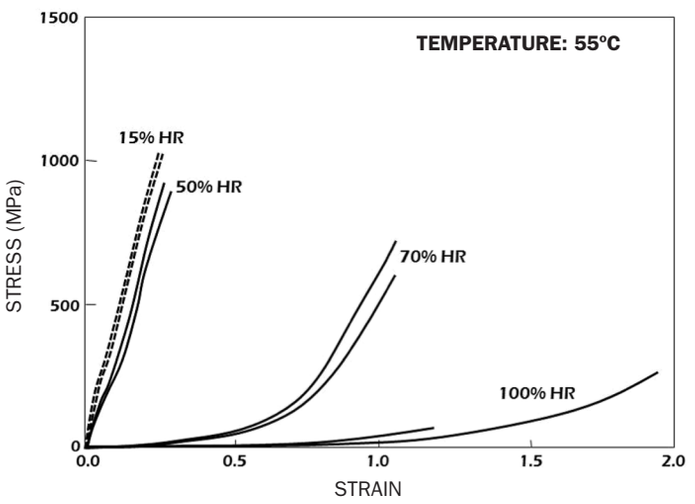

Fig. 22. *Engineering stress-strain curves for MA silk from* A. trifasciata *for different values of relative humidity HR (at a constant temperature, 55 ˚C).*

The effect of the **loading rate** is illustrated in figure 23. For moderate velocities –between 10^{-5} and 10^{-1} s^{-1}– a small increase in all of the characteristic parameters of the stress-strain curve is produced, as may be observed in figure 23a (Elices *et al*. 2005). For greater values –between 10^{-3} and 10^{3} s^{-1}– the increase is more marked and there is a change in the shape of the curve (a plateau appears in the last section) as shown in figure 23b (Hudspeth *et al*. 2012).

One of the most striking characteristics of the spider MAS thread is the huge contraction which it experiences when submerged in water, a phenomenon known as **super-contraction** and whose microscopic mechanisms are not fully understood (Elices *et al*. 2011). This phenomenon can be quantified by means of the super-contraction index SC, defined as $(L_0 - L_C)/L_0$, where L_0 is the initial length if the fibre and L_C is the length of the fully contracted unstressed fibre. Table 2 contains values of the maximum observed contraction (usually called the super-contraction) for the MAS fibres of *Argiope* and *Nephila*.

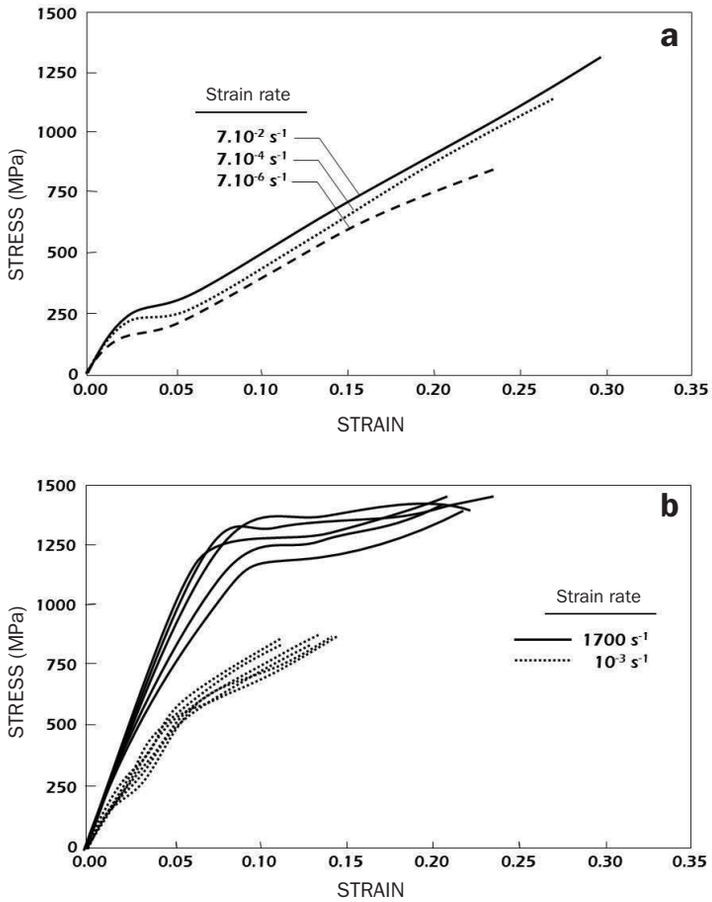

Fig. 23. *Engineering stress-strain curves of MA silk fibres for different values of strain rate.*
a. Moderate speeds (A. trifasciata).
b. High speed (N. clavipes)

TABLE 2. SUPER-CONTRACTION INDICES FOR SOME SPIDER MAS FIBRES

TYPE OF SPIDER	SC INDEX = $(L_0–L_C)/L_0$	REFERENCE
Argiope trifasciata	0.31	Pérez-Rigueiro et
Natural thread	0.52	al. 2003
Forced spun		Elices et al. 2009
Nephila sp	0.20	Work 1985
Natural thread	0.40	Elices et al. 2009
Forced spun	0.44	Liu et al. 2005
		Jelinski et al. 1999

The tensile behaviour, in **water**, of the super-contracted fibres is typical of an elastomer (see figure 20), characterised by small values of the initial elastic modulus and a marked increase in the stiffness for large deformations. When the super-contracted fibre is dry the behaviour is totally different, as illustrated in figure 20 (fibre Maximum Super-contraction tested in **air**).

Super-contraction modifies the tensile behaviour of the fibre and provides ways of understanding the mechanical properties (Guinea *et al*. 2005a,b, and Elices *et al*. 2011). The stress-strain curves of a dry super-contracted fibre (figure 20, curve MS) are independent of the previous load history; that is, the curve is the same after the super-contraction, independent of whether the fibre has been loaded or unloaded several times, or if the fibre was obtained from the web by forced silking. This property allows the use of the MS fibre curves as **reference curves** since, from these, it is possible to obtain all of the others (that which the spider spun and those obtained by forced silking) by means of a process of controlled loading in water (Guinea *et al*. 2005a) characterised by an alignment parameter α ; in the initial state, unstretched, α = 0 and its value increases with the deformation of the fibre during treatment. It has been observed that for the fibres that spiders weave, α ranges from 0.45 to 0.9, approximately. The largest values correspond to fibres obtained by forced silking. These results are presented in figure 24 (Elices *et al*., 2011), for MAS fibres of the *Argiope trifasciata*.

Next exercise shows the meaning of the α parameter.

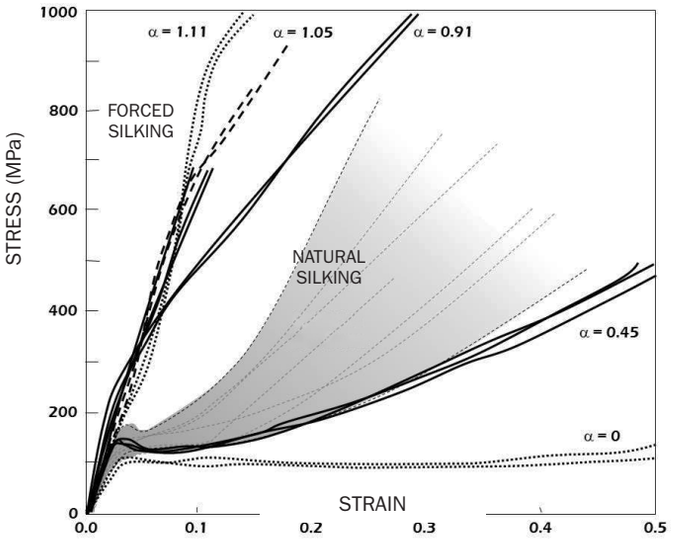

Fig. 24. *Engineering stress-strain curves of MA silk fibres of* A. trifasciata *obtained from MS fibres (see text) by straining under humidity (different values of* α*).*

The mechanical behaviour of silks can be modelled by a semi-crystalline composite material, as has already been mentioned:

At the molecular level, Termonia's model, (Termonia, 2000), gives results that provide reasonable agreement with experiment; for small strains (less than 0.2%) it predicts a linear response, with a modulus of 10 GPa, agreeing with experimental observation. Beyond this strain, the hydrogen bonds between the chains in the amorphous regions begin to break and a yielding phenomenon appears accompanied by a plateau. After a strain of approximately 0.1%, After a strain of approximately 0.1%, the stress begins to increase with strain until it reaches about 0.3%, at which it breaks. The model is also capable of reproducing the effect of water by eliminating the hydrogen bonds between the amorphous phase chains.

In a continuum mechanics based treatment, the fibre can be modelled as a composite of microfibrils dispersed in a deformable matrix (Planas *et al*. 2007). The microfibrils are modelled as nonlinear springs in parallel with a system formed of a slider and a linear spring; the nonlinear spring represents the behaviour of the molecular chains in the elastomeric state (with the network of hydrogen bonds deactivated), while the slider-spring system attempts to reproduce rupture of the hydrogen bonds and sliding of the chains when the fibre is above the glass transition temperature. This model is not only able to reproduce tensile tests it can also simulate tests on super-contracted fibres and stressed with different values of α.

EXERCISE

A simple way of understanding the behaviour of spider thread is to consider the protein chains which form it as tangled creating an elastic (nonlinear) network which is stable thanks to the weak bonds between the chains. These bonds break easily in the presence of humidity. Therefore, when the fibre is submerged in water the network unlocks and tends to shrink to its maximum value. If the network is stretched in **water** up to a certain value and the fibre dried in this new position, the bonds recombine to provide stiffness, so that we obtain a longer fibre than the initial one but with a certain internal "pre-stress", which can be relieved if it is wetted again.

With these ideas, explain figures 20 and 24, and the effect of the alignment parameter α, defined as $\alpha = L_0 / L_C - 1$ (Guinea et al., 2005a) where L_0 is the length of the relaxed dry fibre L_C is relaxed dry length when it is totally constrained (state of maximum contraction, MS).

Posing the problem:

A explained, the stress-strain curve in water, shown in figure 20 **(Maximum super-contraction-water)** represents the behaviour of a molecular network, free from the effects of the bonds between the chains, and therefore a material characteristic, same in all of the fibres. We shall call this curve $s_{net}(e)$ (Figure a).

If we let the fibre contract **freely** in water, and then test it dry (in air) we will obtain the **maximum super-contraction-air** (curve MS air) which will be the combined of the effect of the elastic molecular network and the network of weak bond. The subtraction of the two Maximum super-contraction curves in Figure 20 shows the behaviour of the network of weak bonds. The result is shown in figure a. This engineering stress-strain curve will be called $s_{bonds}(e)$.

We now consider a test in which we **stretch** a fibre of initial length and area L_C and A_C, in **water,** until the strain $e_S = 0.6$ the corresponding stress is $(s_S \approx 13.5\text{MPa})$ and at this point allow it to dry.

What will the shape of the stress-strain curve be, for a new tensile test performed on this fibre?

a

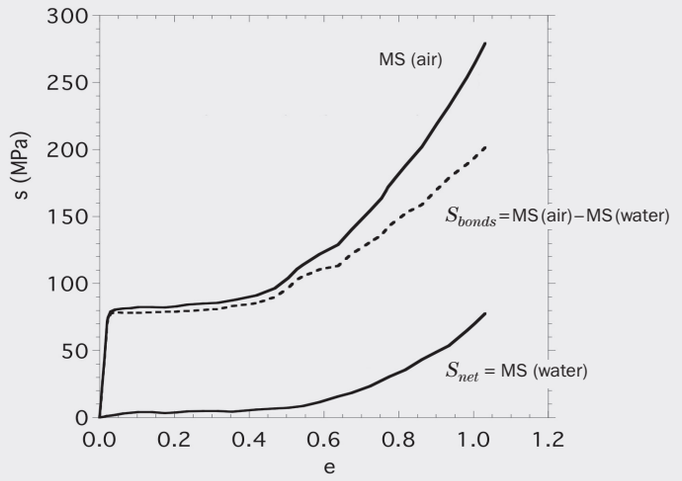

b

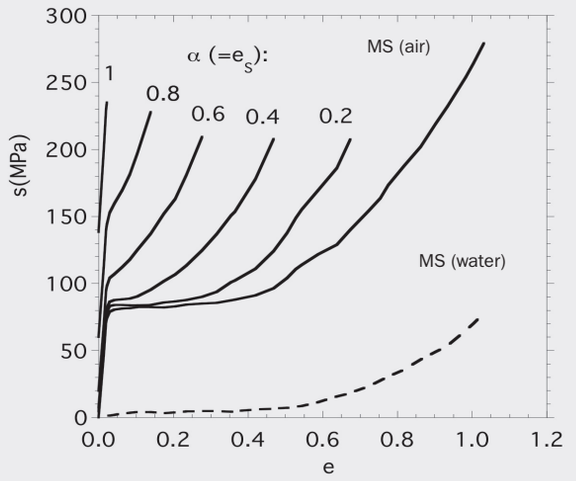

Solution:

To answer this question, suppose that by drying the fibre the residual strain is e_S, without producing any contraction during drying, which is not strictly true, but which we can take as a first approximation.

The stretched dry fibre will now have a length $L_S = (1+e_S)\, L_C = 1.6\, L_C$ and a cross sectional area $A_S = A_C/(1+e_S)$, which we obtained from conservation of volume. Note that L_S and A_S become the initial reference length and area for the new tensile test.

To stretch the fibre we must apply a force greater than the internal residual forces created when drying the fibre F_S. Its value can be calculated from the stress at the point of drying $F_S = s_{net}(e_S)\, A_C$. Note that this value of the force now gives, in the new test, an engineering stress $s_{net}(e_S)\, A_C / A_S = s_{net}(e_S)\, (1+e_S)$, having to refer the force to a smaller area A_S.

The force exerted in the test must overcome the behaviour of the polymer network, represented by the load curve in water and also must overcome the forces in the network of weak links, whose stress-strain curve we assume to be approximated by the calculation shown in figure a. In both cases, the forces must be referred to the initial cross sectional area in the new test, that is A_S and not A_C.

Bringing this together, the force due to the molecular chain **network** will be

$$F_{net} = A_C s_{net}\left(\frac{L}{L_C}-1\right) = A_C s_{net}\left[\frac{L}{L_S}\frac{L_S}{L_C}-1\right] = A_C s_{net}\left[\left(1+e\right)\left(1+e_S\right)-1\right]$$

So now $e=(L-L_S)/L_S$, and $L_S/L_C = 1+e_S$.

On the other hand, the force due to the **weak links** will be

$$F_{bonds} = A_S s_{bonds}\left(\frac{L-L_S}{L_S}\right) = A_S s_{bonds}\left(e\right)$$

in this case we consider that the links are completely restored when the water is eliminated, with no memory of its previous state.

Therefore, the engineering stress becomes $s = \frac{F_{net}+F_{bonds}}{A_S} = \frac{A_C}{A_S} s_{net}\left[\left(1+e\right)\left(1+e_S\right)-1\right] + s_{bonds}\left(e\right) = (1+e_S) s_{net}\left[\left(1+e\right)\left(1+e_S\right)-1\right] + s_{bonds}\left(e\right)$

The result for different values of $\alpha = e_S$ is represented in figure b. Note that, according to the definition given for the alignment parameter, this result will be equal to e_S.

3.3.3. Concluding remarks

Silkworm fibres have been principally destined for the textile industry although recent interest has developed in biomedical applications, particularly in regenerated fibroin threads.

Silkworm fibres are covered with a layer of sericin which provokes an inflammatory response *in vivo*. For this reason when used for stiches they must be de-gummed, eliminating this coating. In these circumstances it seems that the inflammatory response is less than with traditional biomaterials, such as collagen or polylactic acid.

Another form of use of the fibre is regenerating; the de-gummed fibres dissolve at high temperature (between 60 and 80˚C) in various watery solutions, dialysed in water and the fibroin solution is processed in the form of fibres, films or sponge structures which can be used as scaffolds in engineering of textiles. The potential of these scaffolds to function chemically makes them attractive for controlling the interaction between fibroin and living systems. The surface chemistry of the fibroin scaffolds can greatly influence the cellular response in many ways; from changes in adhesion to modifying the cellular proliferation processes, differentiation or survival (Murphy and Kaplan, 2009).

Spider silk threads have many attractive features, among them its huge tenacity (energy absorbing capacity when strained, represented by the area under the stress-strain curve) as can be inferred from figure 17. The tenacity of a MAS thread from *Argiope* is about 130 kJ/kg compared to 30 kJ/kg of Kevlar® and 4 kJ/kg of steel. However, they have the disadvantage that it is not possible to obtain large quantities for the reasons noted above, a motive for the growing interest in obtaining these fibres through genetic engineering.

The route forward has two stages: in the first, attempts are made to identify the spider genes responsible for the production of silk proteins, synthesise them and express them in other organisms. The second stage consists of producing a protein solution, spinning it and fabricating the fibre.

With this strategy, several related amino acid sequences with the composition of silk threads have been identified, and artificial genes which mimic the most characteristic aspects of the natural have been prepared. These genes have been expressed in bacteria, in several micro-organisms, in plants such as sunflowers and in the mammary cells of genetically modified goats from which milk rich in spider protein has been produced. After spinning the protein solutions, the mechanical properties of these artificial fibres are quite different from those of the natural fibres, possibly because the spider protein has not been completely reproduced, and because the spinning process has not recreated the natural spinning strategy.

The spinning difficulties could be avoided if it were possible to insert in the genome of the worm the genes responsible for the enhanced properties of spider silk. This process has already begun in several research laboratories but, as of now, the results obtained are inferior to those of natural fibres.

Despite not achieving the excellent mechanical properties of natural silk, the silk thread obtained from these processes may have important applications in the medical field (Kluge *et al*. 2008, Elices *et al*. 2011), in particular in the textile technology and in pharmacology (in the form of microcapsules for the administration of medication).

3.4. COLLAGEN FIBRES

3.4.1. Introduction and fibre structure

Collagen is the most abundant fibrous protein in vertebrates and is present in the throughout the animal kingdom, except for the simplest eukaryotes (protists). About 25% of all mammal proteins are some sort of collagen molecule (Smith 1991). It is the protein that provides strength and resistance to biological tissues, and appears in practically all organs from bones to skin, in tendons, the cornea, blood vessels, the uterus or epithelia.

The name collagen comes from the Greek κόλλα (cola, glue) and literally means "generator of adhesion". Since ancient times, glue has been made by cooking skin, cartilage, tendons and ligaments of horses and other animals, and also the skin and bones of fish. Collagen glue was used to give strength and impermeability to everyday utensils, and also as funeral decoration. Up to now, the oldest preserved remains, more than 8,00 years old, come from the Nahal Hemar cave near the Dead Sea (Nissenbaum 1997). Nowadays musical instrument makers still use animal glue in more elaborate string instruments in order to be able to re-open them without damaging the wood when needed, since it is a thermoplastic adhesive which softens with heat.

Currently 29 types of collagen are known, and are codified by 44 different genes (Soderhall 2007). All of them are trimers (generally called tropocollagen) composed of three levorotatory chains. In each chain, the most common amino acid repeating unit is Gly-X-Y, in which the proline amino acids or hydroxyproline and, to a lesser extent, lysine or hydroxylysine occupy positions X and Y *(*Ramshaw 1998*)*. Each type possesses a characteristic structure in which the chains that form the triple helix can be the same or different. Table 3 contains the composition of the most common types of collagen, its preferred location, the cells that secrete them and their principal function.

Type I collagen is by far the most important in vertebrates, by constituting about 90% of the total and being the major part of organs such as the skin, tendons, ligaments, bones, blood vessels and the cornea. Its microstructure is shown in figure 25. Each molecular chain consists of about 1,000 amino acids which take on the form of a levorotary helix of 3.6 amino acids per turn. Two α1[I][17] chains and one α2[I] chain link together to form a triple helix with a right-hand rotation. The molecular weight of the α1[I] chain is about 139 kDa and that of the α2[I] chain 129kDa, yielding a value approaching 400 kDa for the trimer (Cowan 1955).

TABLE 3 – PRINCIPAL TYPES OF COLLAGEN IN VERTEBRATES (BRINCKMANN 2005)

TYPE	COMPOSITION*	STRUCTURE	TISSUES	PRODUCTION	FUNCTION
I	α1[I]$_2$ α2[I]	Fibrillar	Dermis, tendons, ligaments, bones, blood vessels, cornea, scar tissue	Fibroblasts, chondroblasts and osteoblasts	Thick structural fibres: tension
II	α1[II]$_3$	Fibrillar	Cartilage, vitreous humour	Chondroblasts	Very fine structural fibres: tension and compression
III	α1[III]$_3$	Fibrillar	Accompanies Type I, in arterial veins, skin, intestine and uterus	Smooth muscle cells, fibroblasts	Spongey mass support and support of other cells: expandible bodies
IV	α1[IV]$_2$ α2[IV] α3[IV] α4[IV] α5[IV] 5[IV]$_2$ α6[IV]	Reticulated	Basal lamina under the epithelia	Epithelial cells and endothelia	Support and filtration

(*) Indicates the type of chain–same or different– which forms the tropocollagen molecule

[17] Although the symbol α is used for helices which form collagen molecules, it must be remembered that its structure is different from the alpha helix which forms the secondary structure of proteins, and is dextrorotatory.

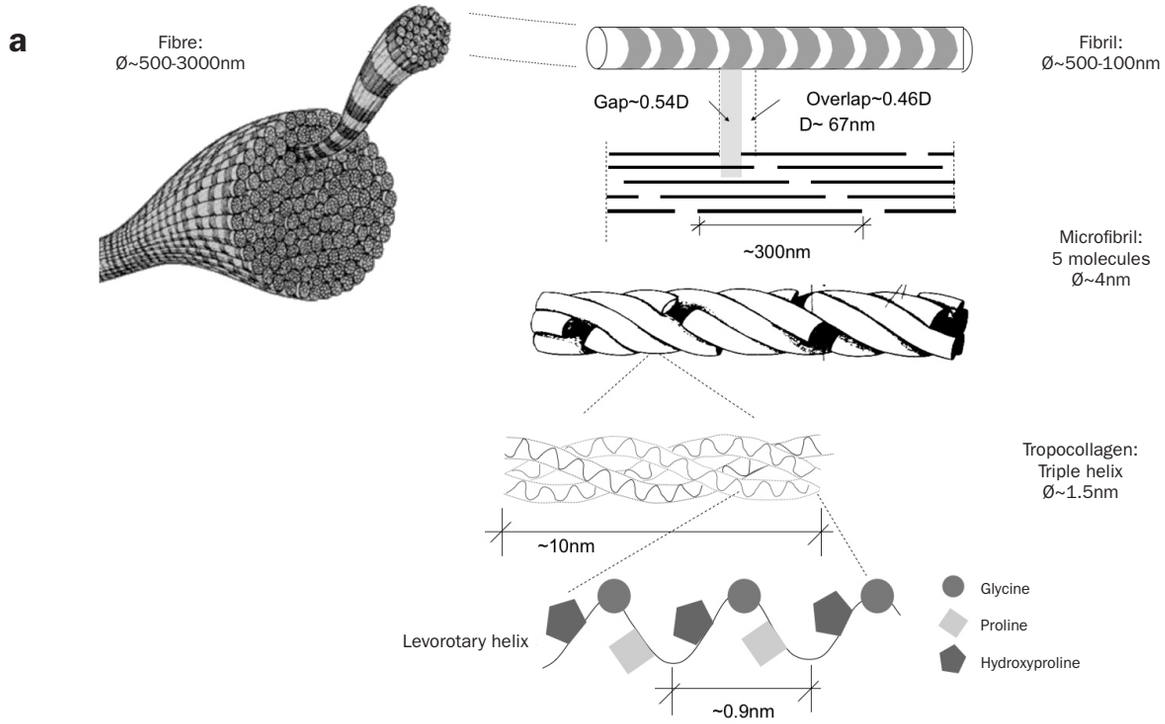

Fig. 25. *a) Typical microstructure of Type I collagen fibres. b) Electron microscopic image which shows the typical striated fibres.*

A single α chain is not stable, and must combine with two similar ones to form the tropocollagen triple helix. Nor is Type I tropocollagen stable at body temperature *(*Leikina 2002*)*, so five molecules combine (figure 25a) to form a stable structure *(*Orgel 2006*)*. The packing is such that adjacent molecules are shifted by approximately ¼ of their length (67nm), and this arrangement produces the striated effect which can be observed under an electron microscope (figure 25b).

The stability of tropocollagen molecules is achieved by means of hydrogen bonds, principally between the proline residues and hydroxyproline. The lack of this last amino acid destabilises the chains and causes weakening, with grave consequences for the tissues (malformations, weakness and bleeding). Human beings, like the rest of primates, are incapable of producing their own vitamin C–essential for the synthesis of hydroxyproline– and a diet deficient in this vitamin triggers the serious disease of scurvy. It is calculated that about two million sailors died between 1600 and 1800 through a lack of vitamin C, resulting from the difficulty of transporting fresh fruit and vegetables in ocean crossings *(*Drymon 2008*)*.

Some genetic illnesses directly affect the production and assembly of collagen causing very severe syndromes which are difficult to treat. For example, Ehlers-Danlos syndrome originates in an extreme loosening of the skin and tendons– rubber men– and promotes the formation of aortic aneurisms. The Osteogenesis Imperfecta syndrome impedes the correct assembly of the triple helix and causes bone brittleness (the so-called glass children). Nor is the overproduction of collagen synonymous with good health, since fibrosis (for example in the liver and lungs) produced as a response of the organ to an attack on its tissues can inhibit the function of the affected organ.

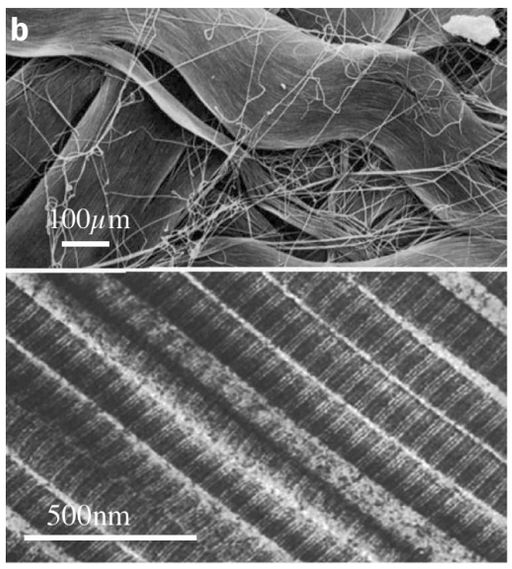

3.4.2. Mechanical properties

Collagen represents a paradigm example of the hierarchical structure of biological materials, in which –as mentioned above– it is difficult, and always a matter of judgement, to distinguish between the structure and the material. Figure 26 shows the structural organisation of tendon, in which continuity is not observed from the atomic and molecular up to the macroscopic level of the insertion into the bone or muscle. Therefore, to talk in general about the mechanical properties of collagen is very difficult and it must always be done with care to specify clearly the structure studied. In this section attention is focussed on the two extremes of the hierarchical organisation: fibril and microfibrils, almost molecular collagen, and tendons and ligaments.

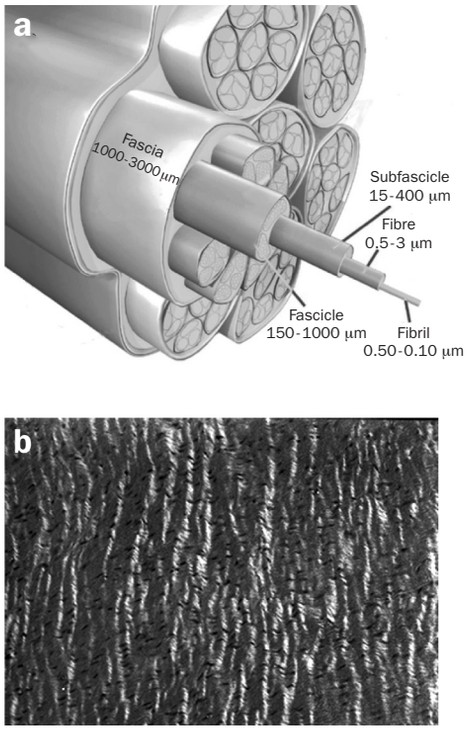

Fig. 26. *Typical structure of a tendon.*
a. Hierarchical organisation.
b. Wave pattern on collagen fibres (Weiss 2001).

Mechanical behaviour of collagen fibrils

Collagen fibrils are formed by the addition of tropocollagen microfibrils, (figure 25a) and their diameter varies depending upon the tissue and the production. In figure 27 the stress-strain curves of *the skin of the holothuria* are shown. The fibril diameter is about 300 nm and the length 10μm. The tests were performed using a micro-electro-mechanical system (MEMS) (Shen 2008).

In general it can be said that the behaviour of the fibrils is linear elastic until the yield stress, probably due to sliding between the microfibrils. It can also be seen that unloading of the fibre is linear elastic, and that there is a small recovery of the plastic strain if the fibre rests in a humid environment (*Shen 2008)*. Figure 27c shows that the value of the yield stress depends upon the volume of the fibril, decreasing with size.

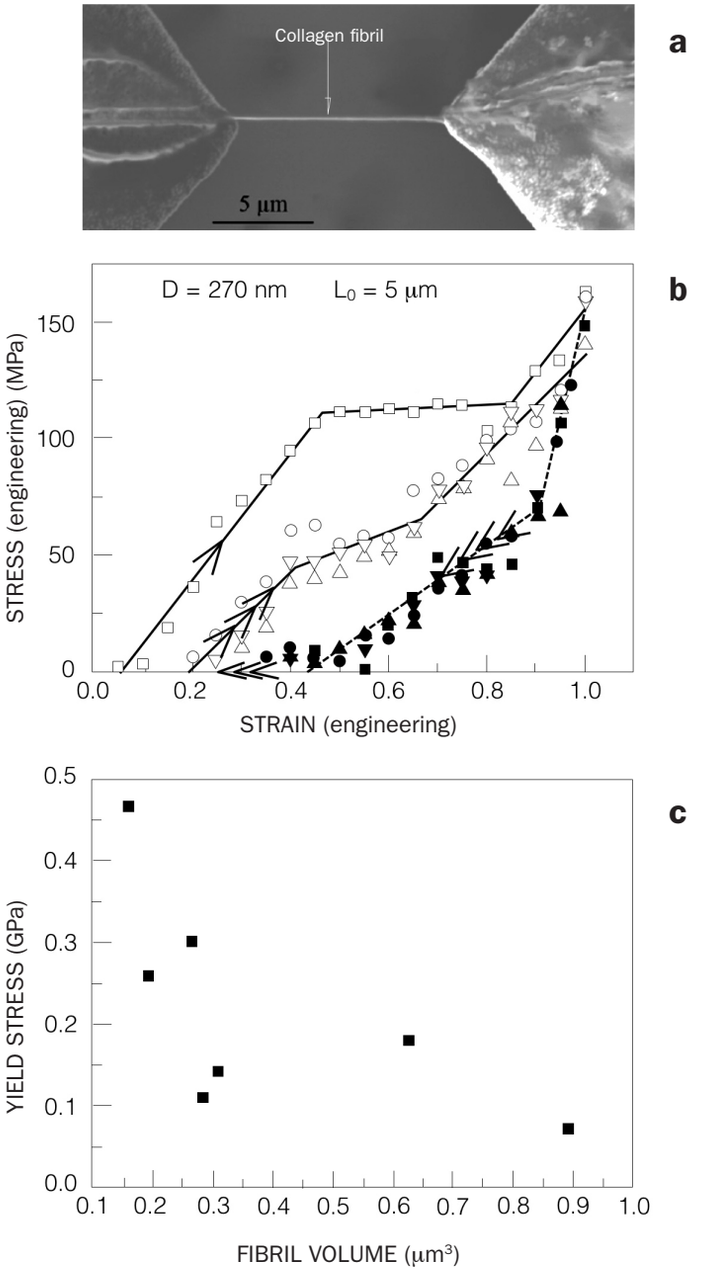

Fig. 27. *Tensile tests on collagen fibrils (Shen 2008).*
a. Photograph of the test.
b. Cyclic stress-strain curves loading (open symbols)-unloading (filled symbols). Each symbols represents one test.
c. Yield stress.

TABLE 4. ELASTIC MODULUS OF COLLAGEN FIBRILS

TYPE OF FIBRIL (REF.)	TECHNIQUES USED	STATE	E(GPa)
Rat tail tendon *(Wenger 2007)*	Nanoindentation	Dehydrated	3.75–11.5
Rat tail tendon *(Harley 1977)*	Brillouin spectroscopy	0.15 M NaCl	9.0
		30% humidity	14.7
		0% humidity	21.5
Bovine Achilles tendon (*Sasaki 1996*)	X-ray diffraction	0.15 M NaCl	2.9
Bovine Achilles tendon (*van der Rijt 2006*)	Brillouin spectroscopy	0% humidity	2-7
		PBS	0.2–0.5
Holothuria (*Eppell 2006*)	Tensile test (MEMS)	water	12
Holothuria (*Heim 2006*)	Nanoindentation	45% humidity	1-2
Holothuria (*Shen 2008*)	Tensile test (MEMS)	30-60% humidity	0.86

Table 4 contains the values of the elastic moduli of collagen fibrils measured by different researchers. The values are quite dispersed and go from about 200 MPa to somewhat more than 21 GPa. The elastic modulus is, in general, high indicating that the fibrils are quite stiff, especially in the absence of moisture. Experimental data show wide degree of variability owing to the different conditions in which the fibrils were tested, the difficulty in preparing the test specimens and the test methods themselves, which include micromechanical tests, optical techniques and X-rays.

In the tests mentioned, as much as because of the techniques used –some non-destructive– as the handling difficulty and size of the fibrils, the strength has not been measured. The determination of this parameter is much more difficult than the elastic modulus but the reference data cited and numerical simulations performed with molecular models show that the strength of collagen fibrils is more than 0.6GPa and probably greater than 1 GPa. On the other hand, the estimated failure stress of the tropocollagen molecule is more than 10GPa (*Buehler 2006, 2008)*.

Mechanical behaviour of tendon

Tendon is a very uniform fibrous connective tissue which joins the bones and muscles in order to transmit the mechanical forces that permit movement. Its organisation is complex (figure 26a) being composed of collagen fibres arranged in fascicules. The composition of tendon is by mass 90% Type I collagen, although this varies in the vicinity of its insertion into the bone –osteotendinous junction– or to the muscle –miotendinous junction (Amiel 1984).

Collagen fibres in the interior of tendons adopt a position parallel to the axis a typical undulation of wavelengths between 100 and 300μm (figure 26b) which has clear repercusions on the mechanical behaviour, as will be seen below.

Tests on tendon are usually done immersed in serum and at 37°, in order to reproduce, as closely as possible, the physiological condition. Figure 28 shows the stress-strain curve of human tendon of the extensor digitorum longus muscle (Schechtman 1997*)*. In that figure four distinct zones are apparent (labelled from I to IV in the figure) corresponding to different fibre strain states. In the initial zone (I) the curve takes on a concave shape and the stresses increase slowly with the strain. In this zone, whose limits lie between 1 and 4% strain, the collagen fibres gradually lose their initial rippled texture, and they regroup and re-orientate themselves in the loading direction. From this point in which all the fibres are stretched the behaviour of the tendon is practically linear elastic, as shown in zone (II) of figure 28, up to strains of around 10%. The first fibre failures signal the start of zone (III), in which there is a gradual loss of stiffness by the weakening of the tendon up to its rupture in zone (IV).

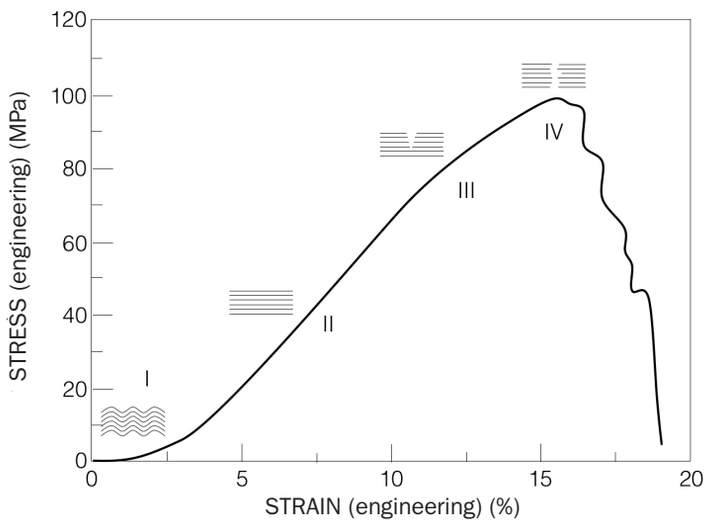

Fig. 28. *Tensile test on the tendon of the extensor digitorum longus muscle (Schechtman 1997).*

The average values of the elastic modulus in the linear zone are quite variable, possibly due to the different experimental techniques used and the difficulty in estimating the cross sectional area of the specimens, given that tendons are soft tissues which deform under pressure. In general the elastic modulus ranges from 0.3 to 1GPa (Cowin 2007) and is sensitive– like the rest of the loading curve– to the strain rate.

Tests with strain rates from 0.05 to 150 %/s have shown that the initial zone (I) hardly changes while the slope of the linear zone (II) and also the rupture stress increase with the loading rate. The strain to failure, however, remains essentially constant (Abrahams 1967, Ng *et al*. 2004). Figure 29 shows the experiments of Abrahams (1967) for the human Achilles tendon. The values obtained by Cowin (2007) can be taken as a reference for the rupture stress (70-100MPa) and the strain to failure (~11%). The values of the elastic modulus of tendon are generally an order of magnitude less than those of collagen fibrils, and a similar ratio is maintained in the values of the rupture stress.a.

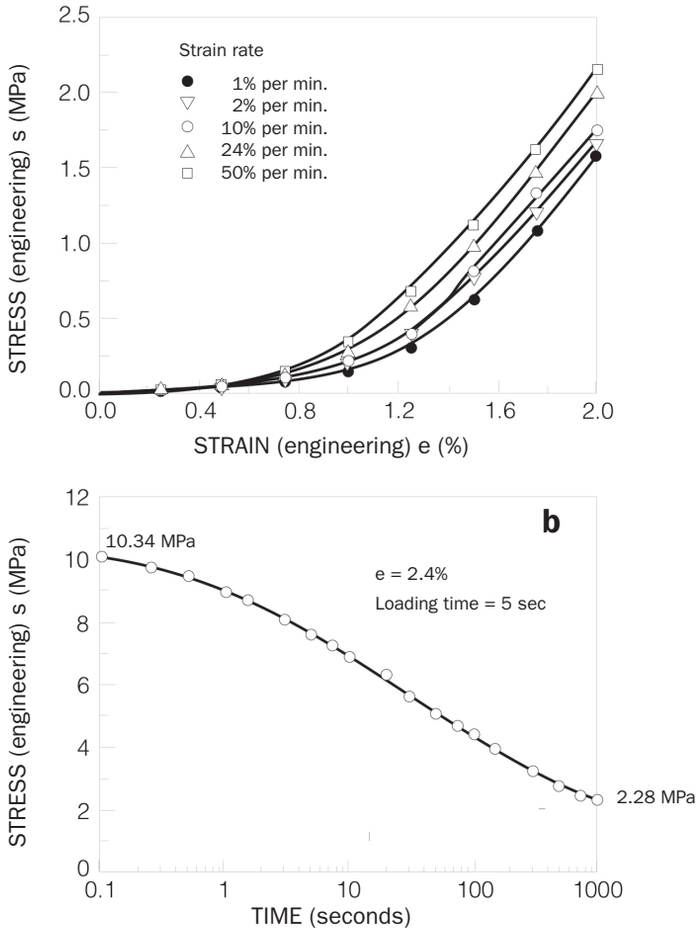

Fig. 29. *Experiments on the human Achilles tendon (Abrahams 1967). a) Effect of strain rate. The experiments were stopped at a strain of 2% b) Relaxation test. The tendon was loaded to e=2.4% in 5 seconds.*

EXERCISE

Estimate the elastic modulus of collagen fibrils from holothurian skin using the curves of figure 27b.

Solution:

Using figure 27b we can identify several sections in which we can easily calculate the slope, as shown in the figure below. The values are:

section	E(MPa)
1	275
2	204
3	150
4	82
5	212
6	933
7	275

Given the difficulty in the testing, and the dispersion in the values, care must be taken when considering the values above since, for example, section 4 could be influenced by spurious effects associated with the experimental technique such as microslip in the glue regions of the grips. However, the values obtained (with the exception of section 4) lie reasonably within the range observed in other experiments.

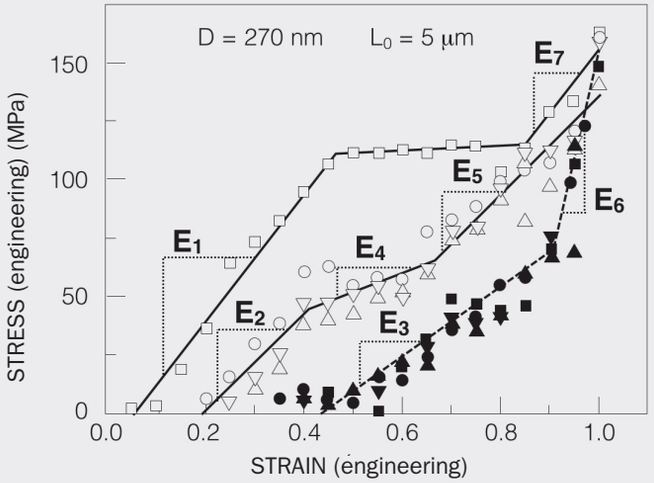

Tendon exhibits a viscous behaviour, illustrated in figure 29, which is for a *relaxation test.* Unfortunately, and like many other soft tissues, tendon is not linear viscoelastic. In figure 30 experimental results are presented for relaxation tests performed by Hingorani (2004) on the lateral median ligament of rabbit at different strain levels Although not for tendon these results are perfectly extrapolatable since ligaments and tendons share the same structure of aligned collagen fibres.

It can be observed, in the figure, that the relaxation is not proportional to the level of the applied strain since the relaxation modulus $G(t)$ (obtained by dividing the stress by the initial strain, $G(t)=\sigma(t)/\varepsilon_0$) does not remain constant in all of the tests (figure 30b).

The tendon strain is not elastic much beyond zone (I) (Abrahams 1967). Even so, and neglecting the different unloading behaviour and time dependency, hyper-elastic models have been proposed to represent the nonlinear behaviour of tendon. Details can be found in Cowin (2007). In general, three-dimensional transversely isotropic models are used, in which the contribution of the collagen fibres is separated from that of the matrix which is assumed isotropic. The study of these models lies outside the scope of this chapter and the interested reader is left to consult the cited reference.

When it is required to model time-dependent behaviour, given the *nonlinearity* of the viscoelastic response and its dependency of the load level, it is common to adopt an "ad-hoc" linear viscoelastic model for the range of desired loadings. Obviously the validity of the approximation and its accuracy are compromised by the underlying hypothesis. In this case the modelling is exclusively one-dimensional.

Another possibility is the use of more elaborate models developed to account for the dependency of the relaxation (or creep) on the loading state, such as the quasi-linear viscoelastic model of Fung (1972). The interested reader can find its application in Cowin (2007).

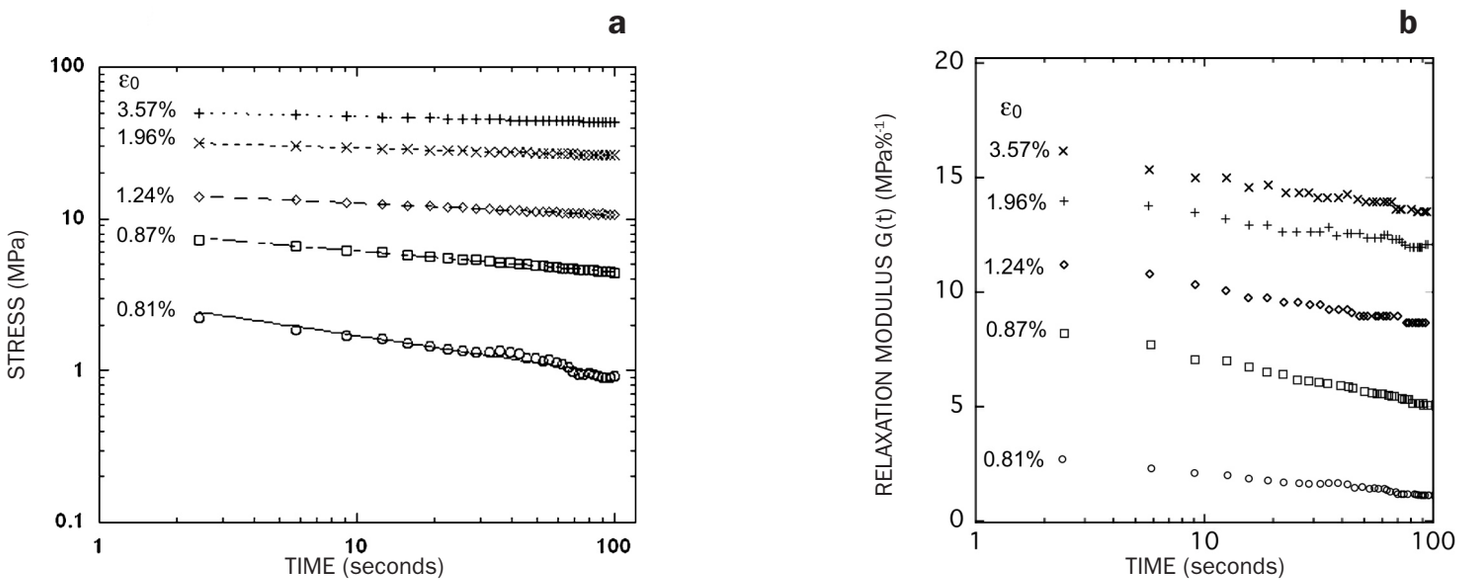

Fig. 30. *Relaxation tests on the lateral median ligament of rabbit and on the human Achilles tendon for different levels of strain* ε_0 (Hingorani et al. 2004)
a) Stress as a function of time $\sigma(t)$
b) Relaxation modulus $G(t) = \sigma(t)/\varepsilon_0$.

3.4.3. Final remarks

Collagen is a biological material of huge mechanical capacity and with numerous applications in medicine, bioengineering and in the cosmetics and food industries.

Using processes of alkaline, acid or enzyme hydrolysis collagen is obtained industrially from tendons and skin of bovines, equines and pigs and it is commercialised in liquid solution or –more commonly– in powder. Its molecular weight varies from 1kDa to 10kDa and the molecules have a globular disordered structure.

Being a component of the extracellular matrix, collagen possesses haemostatic wound-healing properties and promotes cell growth. Therefore it is used in the treatment of severe burns and is a frequent ingredient of scaffolds used in tissue engineering and as an implant coating (Lee 2001). It can be used on its own or in combination with silicones, glycosaminoglycans, fibroblasts, growth agents and other substances *(*Parenteau-Bareil 2010*)*.

Hydrolysed collagen is also commercialised for use in cosmetics as a skin moisturiser and conditioner, and as a dietetic supplement to promote bone growth and maintain articular joints (Oesser 2008).

If reconstituted with water, hydrolysed collagen forms gelatine, a viscoelastic birefringent gel below its melting point whose uses are many and varied; from the preparation of desserts to pharmaceutical capsules, supplements for low calorie products, adhesives and photographic emulsions *(*Ward 1977*).*

When it is required to take advantage of the mechanical potential of collagen fibres it is necessary to use animal tissues directly, changing their elaborate hierarchical structure as little as possible. In these cases it is possible to opt to use the entire organ, as has been done for years with simple elements like porcine blood valves, and there are more advanced studies with such sophisticated organs as the kidneys or the heart *(*Maher 2013*).* The strategy used is simple: it aims to eliminate completely the cellular component of the donor preserving the collagen matrix, so that that can be colonised by the cells of the patient. For the first time, a human has been given a transplant of a pig´s heart that had been genetically modified to boost the chances of acceptance in a human body. (New Scientist, 2022).

Otherwise tissues rich in collagen are used, generally membranes such as the bovine pericardium or dura, to repair veins or hernias, or as prosthetic elements like heart valve vanes. In these cases, the collagen tissues are usually treated with glutaraldehyde to crosslink and delay its biodegradation *(*Nimni 1987*).*

Collagen is one of the most versatile and useful natural fibres, with applications in very diverse sectors. Moreover, their excellent mechanical and biological properties mark them out as one of the most important biomaterials of the present and with great future development potential.

4 CHAPTER

Complementary exercices

EXERCISE

Derive equation (26a).

Solution:

Consider a chain with one end at the origin of coordinates and formed by n links l_i, all of equal length l_0, oriented randomly as shown in figure 12. We consider the random variation of their positions over a sufficently long time. Let $p(\boldsymbol{r})$ be the probability density function of r= l, the sum of the vectors corresponding to each link. If the chain is very long –theoretically infinitely long– we can assume that the probability $p(\boldsymbol{r})dV$ of finding the end of $\mathbf{r} = \sum_n \mathbf{l}_i$ in a volume dV centred at location $\boldsymbol{r}$ (figure 12) will be equal to

$$p(\mathbf{r})dV = w_x(x)dx\, w_y(y)dy\, w_z(z)dz$$

with $w_x(x)dx$ being the probabilty of finding the component x in an interval dx centred at position x, and $w_y(y)dy$ and $w_z(z)dz$ defined in a similar way. Since the chain is very long we can treat the components (x,y,z) as statistically independent variables and, therefore, the combined probability is the product of the the individual probabilities. On the other hand, the symmetry of the problem requires that density functions be identical

$$w_x = w_y = w_z = w$$

and also that $p(\boldsymbol{r})$ depends only on the distance to the origin, r, and not the orientation of the vector $\boldsymbol{r}$. Therefore we can write

$$p(\mathbf{r}) = p(r^2) = w(x)w(y)w(z)$$

since $r^2 = x^2 + y^2 + z^2$. The previous equation can only be satisfied if the function w is of the form (see the following exercise)

$$w(x) = ce^{ax^2}$$

this only has a physical meaning if a is a negative constant, since the probability must tend to zero for large values of x. If $a=-b^2$, we can write

$$p(\mathbf{r}) = p(r^2) = c^3 e^{-b^2 r^2}$$

Also, the normalisation condition (i.e. the probability of finding the end of $\boldsymbol{r}$ somewhere in space is 1) requires that the value of c satisfies

$$\int_{espacio} p(\mathbf{r})dV = 1 = \int_0^\infty c^3 e^{-b^2 r^2} 4\pi r^2\, dr = \left(\frac{c\sqrt{\pi}}{b}\right)^3$$

from which $c = b/\pi^{1/2}$ and therefore

$$p(\mathbf{r}) = p(r^2) = \frac{b^3}{\pi^{3/2}} e^{-b^2 r^2}$$

which is equation (26a).

EXERCISE

Show that the equation $w(x)w(y)w(z)=p(r^2)$ can only be satisfied if the function w has the form $w(x) = c\ exp(a\ x^2)$, where c and a are constants.

Note: Application of this result allows inference of the probability distribution function, as shown in the previous exercise.

Solution:

For values $y=z=0$ in the equation we see that $w(x)w^2(0)=p(x^2)$. From this expression it can be deduced that

$$w(x)w(y)w(z) = \frac{p(x^2)p(y^2)p(z^2)}{w^6(0)} = p(r^2)$$

Again, putting $y=0$ in this last expression (and with $z^2=r^2-x^2$) we arrive at

$$\frac{p(x^2)p(r^2-x^2)}{w^3(0)} = p(r^2)$$

or

$$\frac{p(x^2)}{w^3(0)} = \frac{p(r^2)}{p(r^2-x^2)}$$

Since the left hand side does not depend upon r^2, the derivative with respect to r^2 must be zero, from which we obtain

$$0 = \frac{dp(r^2)}{d(r^2)}p(r^2-x^2) - \frac{dp(r^2-x^2)}{d(r^2)}p(r^2) = \frac{dp(r^2)}{d(r^2)}p(r^2-x^2) - \frac{dp(r^2-x^2)}{d(r^2-x^2)}p(r^2)$$

and then

$$\frac{dp(r^2)/d(r^2)}{p(r^2)} = \frac{dp(r^2-x^2)/d(r^2-x^2)}{p(r^2-x^2)} = cte = a$$

since the equality must be true for any value of r^2 and r^2-x^2. Integrating we see that

$$p(r^2) = k\ \mathrm{e}^{a\,r^2}$$

where k is a constant of integration. The expression sought comes from the last equation and

$$w(x) = \frac{1}{w^2(0)}p(x^2) = \frac{k}{w^2(0)}\mathrm{e}^{a\,x^2} = c\ \mathrm{e}^{a\,x^2}$$

EXERCISE
Derive equations (28) and (29).

Solution:
The mean distance $\langle r \rangle$ between two ends of a chain, is calculated from the integral given in equation (28),

$$\langle r \rangle = \int_0^\infty rP(r)dr = \int_0^\infty r\frac{4b^3}{\pi^{1/2}} r^2 e^{-b^2r^2}\, dr = \frac{4b^3}{\pi^{1/2}}\int_0^\infty r^3 e^{-b^2r^2}\, dr$$

which can be solved using integration by parts,

$$\langle r \rangle = \frac{4b^3}{\pi^{1/2}}\int_0^\infty r^3 e^{-b^2r^2}\, dr = \frac{4b^3}{\pi^{1/2}}\int_0^\infty r^2 d\left(\frac{e^{-b^2r^2}}{-2b^2}\right) = \frac{4b^3}{\pi^{1/2}}\left[r^2\frac{e^{-b^2r^2}}{-2b^2}\bigg|_0^\infty + \frac{1}{2b^2}\int_0^\infty 2re^{-b^2r^2}\, dr\right] = \frac{4b}{\pi^{1/2}}\int_0^\infty re^{-b^2r^2}\, dr = \frac{2}{b\pi^{1/2}}$$

which is equation (28).

The mean square distance $\langle r^2 \rangle$ is given by integral (29)

$$\langle r^2 \rangle = \int_0^\infty r^2 P(r)dr = \int_0^\infty r^2\frac{4b^3}{\pi^{1/2}} r^2 e^{-b^2r^2}\, dr = \frac{4b^3}{\pi^{1/2}}\int_0^\infty r^4 e^{-b^2r^2}\, dr$$

A double integration by parts gives us

$$\langle r^2 \rangle = \frac{4b^3}{\pi^{1/2}}\int_0^\infty r^4 e^{-b^2r^2}\, dr = \frac{-2b}{\pi^{1/2}}\left[r^3e^{-b^2r^2}\bigg|_0^\infty - \int_0^\infty 3r^2e^{-b^2r^2}\, dr\right] = \frac{6b}{\pi^{1/2}}\int_0^\infty r^2e^{-b^2r^2}\, dr = \frac{-3}{b\pi^{1/2}}\left[re^{-b^2r^2}\bigg|_0^\infty - \int_0^\infty e^{-b^2r^2}\, dr\right] = \frac{3}{b\pi^{1/2}}\int_0^\infty e^{-b^2r^2}\, dr$$

This last integral can be performed more easily if it is borne in mind that

$$\int_0^\infty e^{-b^2r^2}\, 4\pi r^2\, dr = \int_{-\infty}^\infty e^{-b^2(x^2+y^2+z^2)}\, dxdydz = \left(\int_{-\infty}^\infty e^{-b^2x^2}\, dx\right)\left(\int_{-\infty}^\infty e^{-b^2y^2}\, dy\right)\left(\int_{-\infty}^\infty e^{-b^2z^2}\, dz\right) = \left(\int_{-\infty}^\infty e^{-b^2x^2}\, dx\right)^3 = \left(2\int_0^\infty e^{-b^2x^2}\, dx\right)^3 = 8\left(\int_0^\infty e^{-b^2r^2}\, dr\right)^3$$

with $$\langle r^2 \rangle = \frac{6b}{\pi^{1/2}}\int_0^\infty r^2e^{-b^2r^2}\, dr = \frac{3}{b\pi^{1/2}}\int_0^\infty e^{-b^2r^2}\, dr$$

we can see that $$\int_0^\infty e^{-b^2r^2}\, 4\pi r^2\, dr = \frac{2\pi}{b^2}\int_0^\infty e^{-b^2r^2}\, dr = 8\left(\int_0^\infty e^{-b^2r^2}\, dr\right)^3$$

from which we deduce that $$\int_0^\infty e^{-b^2r^2}\, dr = \frac{\pi^{1/2}}{2b}$$

and also $$\int_0^\infty e^{-b^2r^2}\, 4\pi r^2\, dr = \frac{\pi^{3/2}}{b^3}$$

resulting in $$\langle r^2 \rangle = \frac{3}{2b^2}$$

In order to determine the constant b, we can calculate $\langle r^2 \rangle$ directly from the scalar product of the vector $\boldsymbol{r}$

$$r^2 = \mathbf{r}\cdot\mathbf{r} = \sum_n \mathbf{l}_i \sum_n \mathbf{l}_j = \sum_n (\mathbf{l}_i\cdot\mathbf{l}_i) + 2\sum_{i\neq j}(\mathbf{l}_i\cdot\mathbf{l}_j)$$

which turns out to be $$r^2 = nl_0^2 + 2l_0^2\sum_{i\neq j}\cos(i,j)$$

then $\boldsymbol{l}_i\,\boldsymbol{l}_i = l_0^2$ and $\boldsymbol{l}_i\,\boldsymbol{l}_j = l_0^2\cos(i,j)$.

When determining the mean $\langle r^2 \rangle$, the sum of the cosines is zero since the distribution of angles is random, which finally gives equation (29)

$$\langle r^2 \rangle = nl_0^2 = \frac{3}{2b^2}$$

And the constant b will be $$b^2 = \frac{3}{2nl_0^2}$$

EXERCISE
Show that the value $<r^2>$ given by equation (29) remains valid for the freely articulated chain model. Hint: use generic reasoning without integrating equation (26b).

Solution:
Repeating the arguments of the previous exercise, we have

$$r^2 = \mathbf{r} \cdot \mathbf{r} = \sum_n \mathbf{l}_i \sum_n \mathbf{l}_j = nl_0^2 + 2l_0^2 \sum_{i \neq j} \cos(i,j)$$

Again, when calculating the mean $<r^2>$, the sum of the cosines is zero because there is a random distribution of angles and therefore we finally have

$$\left\langle r^2 \right\rangle = nl_0^2$$

EXERCISE
Show that, in the limit of a very large n, equation (26b) reduces to equation (26a).

Solution:
As has been noted, parameter β s defined by the Langevin function

$$\mathcal{L}(\beta) = \coth(\beta) - \frac{1}{\beta} = \frac{r}{nl_0}$$

which is a monotonically increasing function and confirms that $L(0) = 0$. As a result, for large values of n, we are in the region of $\beta \approx 0$ where the Langevin function can be approximated by

$$\mathcal{L}(\beta) = \frac{\beta}{3} + 0(\beta^3)$$

so we have

$$\beta \approx \frac{3r}{nl_0}$$

On the other hand, also for small β

$$\ln\left(\frac{\beta}{\sinh(\beta)}\right) \approx -\frac{\beta^2}{6} + 0(\beta^4) = -\frac{1}{6}\left(\frac{3r}{nl_0}\right)^2 = -\frac{3}{2}\frac{r^2}{n^2 l_0^2}$$

hence, equation (26b) becomes

$$p(\mathbf{r}) = C\exp\left[-n\left\{\frac{r\beta}{nl_0} + \ln\left(\frac{\beta}{\sinh(\beta)}\right)\right\}\right] \approx C\exp\left[-n\left\{\frac{3r^2}{n^2 l_0^2} - \frac{3r^2}{2n^2 l_0^2}\right\}\right] = C\exp\left[-\frac{3r^2}{2nl_0^2}\right]$$

which we recognise as equation (26a), when

$$b = \left(\frac{3}{2nl_0^2}\right)^{1/2}$$

and

$$C = \frac{1}{\pi^{3/2}}\left(\frac{3}{2nl_0^2}\right)^{3/2}$$

as required by the normalisation of the probability.

EXERCISE

Prove that for small deformations equation (40) reduces to equation (39).

Note: For that, an approximate expression for the inverse of the Langevin function

$$\mathcal{L}^{-1}(x) = x\frac{3-x^2}{1\quad x^2}$$

can be used in the range (−1, 1) with an error of less than 5%[1]

Solution:

Equation (40), written with Cohen's approximation for L^{-1} gives

$$\sigma = \frac{NkT}{3}\lambda\sqrt{n}\left[\frac{\lambda}{\sqrt{n}}\frac{3-\lambda^2/n}{1-\lambda^2/n} - \lambda^{-3/2}\frac{1}{\sqrt{\lambda}\sqrt{n}}\frac{3-(\lambda n)^{-1}}{1-(\lambda n)^{-1}}\right]$$

Since $\lambda \approx 1$ we can write

$$\sigma \approx \frac{NkT}{3}\left[\lambda^2\frac{3-1/n}{1-1/n} - \lambda^{-1}\frac{3-1/n}{1-1/n}\right]$$

and as $(1/n) << 1$ we have

$$\sigma \approx \frac{NkT}{3}\left[\lambda^2\frac{3}{1} - \lambda^{-1}\frac{3}{1}\right] = NkT\left[\lambda^2 - \lambda^{-1}\right]$$

which is equation (39)

[1] Cohen, A. (1991). "A Padé approximant to the inverse Langevin function". Rheologica Acta. 30 (3): 270–273

EXERCISE

Deduce equations (43b) and (44b).

Solution:

Consider the load curve $\sigma(t)$ in figure a, in which $\sigma=0$ for $t < 0$ and $\sigma(0) = \sigma_0$. Note that on decomposing it into stress steps as is required for the application of the principle of superposition, all of these will be infinitesimal except for the first, which will have a finite value σ_0. As a result the strain will be given by equation (44) –which takes into account all of the infinitesimal steps $d\sigma$– as well as a term $\sigma_0 J(t)$ due to the first step. In this way equation (44b) is obtained. In an analogous manner equation (43b) is obtained.

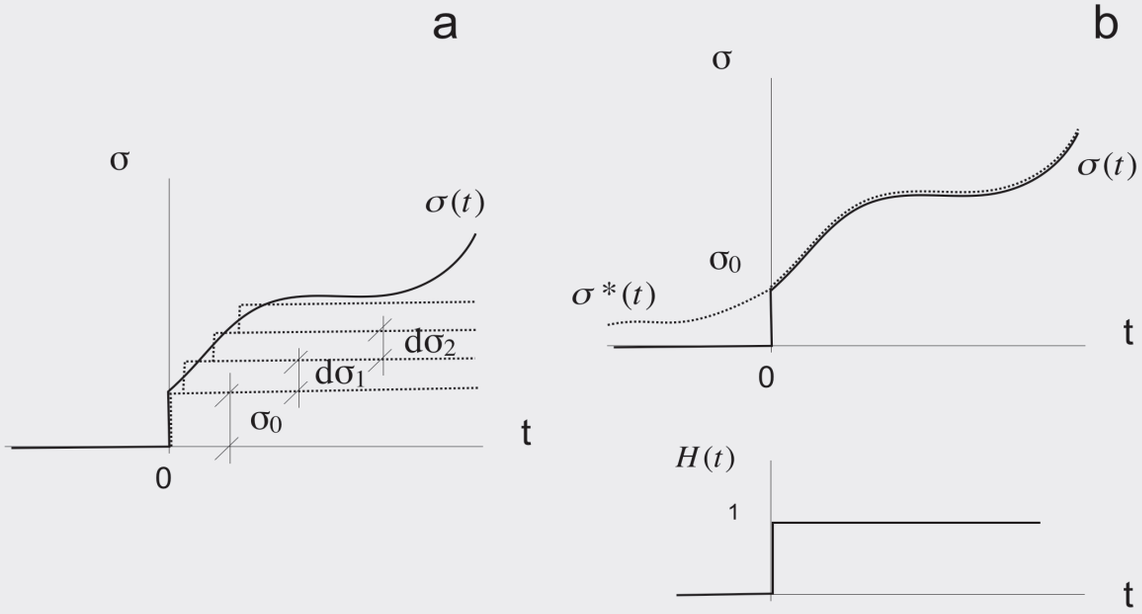

Equations (43b) and (44b) do not appear in many specialist texts since they use equations (43) and (44) extending the lower limit of integration from the negative side of 0 (0^-). Thus presenting the problem of superposition, the difficulty lies in calculating the derivative, $d\sigma/dt$ at the initial instant, t=0, since $\sigma(t)$ is discontinuous at the origin. In order to remove this difficulty an arbitrary function $\sigma^*(t)$ is defined, which is continuous and differentiable at $t=0$ (figure b, line of points), and has the same values as $\sigma(t)$ for $t > 0$.

Our function $\sigma(t)$ could then be written as $\sigma(t)= \sigma^*(t)\, H(t)$, where $H(t)$ is the Heaviside step function, which is zero for $t < 0$ and has the value 1 for $t > 0$.

Then: $$\frac{d\sigma}{dt}=\frac{d\sigma^*(t)}{dt}H(t)+\frac{dH(t)}{dt}\sigma^*(t)=\dot{\sigma}^*(t)H(t)+\delta(t)\sigma^*(t)$$

Since the derivative of the Heaviside step function is the Dirac delta function, $\delta(t)$. Equation (44), with given value of strain, becomes

$$\varepsilon(t)=\int_0^t J(t-\tau)\frac{d\sigma(\tau)}{d\tau}d\tau=\int_0^t J(t-\tau)\left(\frac{d\sigma^*(\tau)}{dt}H(\tau)+\delta(\tau)\sigma^*(\tau)\right)d\tau=\int_0^t J(t-\tau)\frac{d\sigma^*(\tau)}{dt}H(\tau)d\tau+\int_0^t J(t-\tau)\delta(\tau)\sigma^*(\tau)d\tau=$$
$$=\int_{0^+}^t J(t-\tau)\frac{d\sigma(\tau)}{dt}d\tau+J(t-0)\sigma^*(0)$$

Which coincides with equation (44b) since $\sigma_0 = \sigma^*(0)$. In a similar manner equation (43b) is obtained.

In the previous calculation we used the property of the Dirac delta function that

$$\int_a^b f(x)\delta(x-c)dx=f(c)$$

if a < c < b.

EXERCISE

Determine the relaxation modulus of a standard linear solid in relation to its value at T_g. Assume that the only dependency with temperature is introduced through the value of the relaxation time, governed by an Arrhenius type thermal activation equation, $\tau_R = C\, e^{-\Delta H/RT}$, where C and the activation energy, ΔH, are constants, R is the gas constant and T the absolute temperature. Compare the result with that from the WLF equation.

Solution:

From equation (46) we can write

$$G(t,T) = E_H + E_V e^{-\frac{t}{\tau_R(T)}} = G\left(\frac{t}{\tau_R(T)}\right) = G\left(te^{\frac{\Delta H}{RT}}\right)$$

therefore,

$$G(t,T) = G\left(te^{\frac{\Delta H}{RT}}\right) = G\left(te^{\frac{\Delta H}{RT}-\frac{\Delta H}{RT_g}+\frac{\Delta H}{RTg}}\right) = G\left(t*e^{+\frac{\Delta H}{RTg}}\right)$$

where

$$t^* = te^{\frac{\Delta H}{R}\left(\frac{1}{T}-\frac{1}{T_g}\right)}$$

then in this case

$$a_T = e^{\frac{\Delta H}{R}\left(\frac{1}{T}-\frac{1}{T_g}\right)}$$

and

$$\ln a_T = \frac{\Delta H}{R}\left(\frac{1}{T}-\frac{1}{T_g}\right)$$

The figure shows the equation obtained and that from the WLF model.

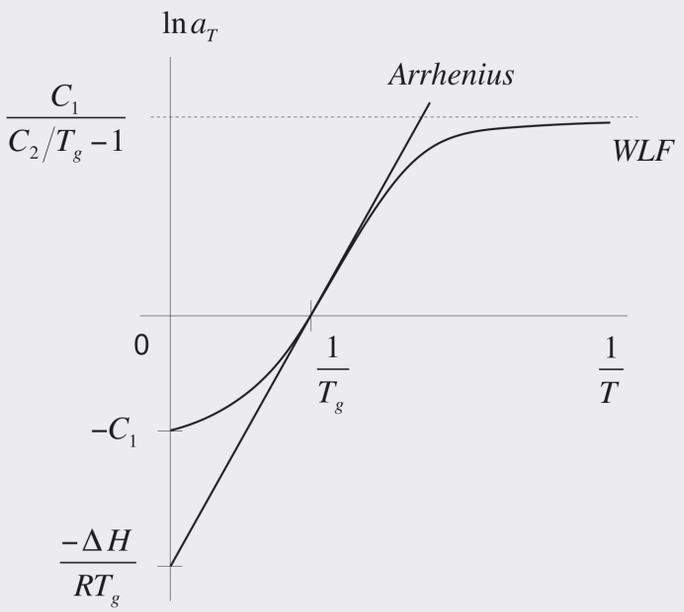

5 CHAPTER References

Abrahams, M.
Mechanical behaviour of tendon In vitro
Medical and biological engineering 5 (5) (1967); 433-443

Alexander R. McN
Rubber-like properties of the inner hinge-ligament of pectinidae
J Exp Biol 44, (1966), 119-130

Alexander R. McN
Viscoelastic properties of the mesogloea of jellyfish
Journal of Experimental Biology 41, (1964), 363-369

Amiel D, Frank C, Harwood F, Fronek J, Akeson W.
Tendon and ligaments: A morphological comparison.
J Orthop Res 1 (1984) :257–265.

Andersons, J., Sparnins, E., Joffe, R. and Wallstrom, L
Strength distribution of elementary flax fibres
Compos. Sci. Technol. 65,, (2005), 693–702

Arruda E.M., Boyce M.C.
A three-dimensional constitutive model for the large stretch behaviour of rubber elastic materials
J Mech Phys Solids 41, (1993), 389-412

Ball R.C., Doi M., Edwards S.F., Warner M.
Elasticity of entangled networks
Polymer 22, (1981), 1010-1018

Barber E.J.W.
Prehistoric Textiles
Princeton Univ. Press (1992)

Barnett V.
Probability plotting methods and order statistics
Applied Statistics 24 (1), (1975), 95-108

Bazant, Z.P and Planas, J.
Fracture and Size Effect in Concrete and Other Quasibrittle Materials
CRC press, Boca Raton (1997)

Bendit E.G.
A quantitative X-ray diffraction study of the alpha-beta transformation in wool keratin
Text Res J 30 (1960), 547-555

Beste L.F., Hoffman R.M.
Resilience of fibres and fabrics: Quantitative study
Text Res J 20 (1950), 441-453

Bledzki A.K., Gassan J. (1999)
Composites reinforced with cellulose based fibres
Prog Polym Sci 24, 221-274

Boltzmann L.
Zur Theorie der Elastischen Nachwirkung
Sitzungsberichte der Akademie der Wissenschuften II 70, (1874), 275-306

Brinckmann J.
Collagens at a glance.
Top. Curr. Chem. 247 (2005) :1–6

Buehler M.J.
Nature designs tough collagen: Explaining the nanostructure of collagen fibrils
PNAS 103 (33), (2006); 12285-12290

Buehler, M. J.
Nanomechanics of collagen fibrils under varying cross-link densities: atomistic and continuum studies.
J. Mech. Behav. Biomed. Mater. 1 (2008): 59–67.

Bustamante C., Smith S.B., Liphardt J., Smith D.
Single-molecule studies of DNA mechanics
Current Opinion in Structural Biology 10(3), (2000). 279-285.

Chawla, K. K.
Fibrous Materials.
Cambridge UP , HRS (2016).

Cowan PM, McGavin S, North ACT.
The polypeptide chain configuration of collagen.

Nature 176 (1955): 1062–64.
Cowin, S.C., Doty, S. B.
Tissue Mechanics.
Springer, New York, USA, (2007)

Danilatos G., Feughelman M.
Dynamic mechanical properties of α-keratin fibers during extensión
J Macromol Sci – Phys B16 (1979), 581-602

Dorrington K., Grut W., McCrum N.G.
Mechanical state of elastin
Nature, London 255, (1975), 476-478

Drummy L.F., Farmer B.L., Naik R.R.
Correlation of the β-sheet crystal size in silk fibers with the protein amino acid sequence
Soft Matter 3 (2007), 877-882

Drymon, M. M.
Disguised As the Devil: How Lyme Disease Created Witches and Changed History.
Wythe Avenue Press. p. 114. ISBN 0-615-20061-3. (2008)

Edwards S.F., Vilgis Th.
The effect of entanglements in rubber elasticity
Polymer 27, (1986), 483-492

Eichner R., Rew P., Engel A., Aebi U.
Human epidermal keratin filaments: Studies on their structure and assembly
Ann N Y Acad Sci 455 (1985),381-402

Elices M., Llorca, J
Fiber Fracture,
Elsevier Science (2002)

Elices M., Pérez-Rigueiro J., Plaza G.R., Guinea G.V.
Usos médicos de la seda
Investigación y Ciencia (2011), Agosto, 28-35

Elices M., Pérez-Rigueiro J., Plaza G.R., Guinea G.V.
Finding inspiration in Argiope trifasciata spider silk fibers
JOM 57(2) (2005), 60-66

Elices M., Plaza G.R., Pérez-Rigueiro J., Guinea G.V.
The hidden link between supercontraction and mechanical behavior of spider silks
Journal of the Mechanical Behavior of Biomedical Materials 4(5) (2011), 658-669

Eppell, S. J., B. N. Smith, H. Kahn, and R. Ballarini.
Nano measurement with micro-devices: mechanical properties of hydrated collagen fibrils
J. Roy. Soc. Interface. 3 (2006) :117–121

Farag R. Elmogahzy Y.
Tensile properties of cotton fibres
en Handbook of Tensile Properties of Fibers (A.R. Bunsell Ed.) (2009), Chap. 3

Feltwell J.
The Story of Silk
St. Martin Press, NY (1990)

Feughelman M.
Mechanical Properties and Structure of Alpha-Keratin Fibres
Sydney: University of New South Wales Press (1997)

Feughelman M.
The creep of wool fibres in wáter
J Text Inst 45 (1954), T630-T641

Feughelman M., Robinson M.S.
Some mechanical properties of wool fibers in the “Hookean” región from zero to 100% relative humidity
Text Res J 41 (1971), 469-474

Fidelis, M. E. A., Pereira, T. V. C. , Gomes, , Silva, F. D. A. and Filho, R. D. T.
The effect of fiber morphology on the tensile strength of natural fibers
Journal of Materials Research and Technology, 2, (2013) 149-157

Flory P.J.
Statistical Mechanics of Chain Molecules
Hanser Publishers, Munich (1989)

Fung YC.
Stress–strain history of soft tissues in simple elongation
en Biomechanics, its Foundations and Objectives
(YC Fung, N Perrone, M Anliker, Eds.), (1972), 181–208, Englewood Cliffs, NJ: Prentice-Hall.

Garrido M.A., Elices M., Viney C., Pérez-Rigueiro J.
Active control of spider silk strength: Comparison of drag line spun on vertical and horizontal surfaces
Polymer 43(4) (2002), 1537-1540

Gatesy J., Hayashi C., Motriuk D., Woods J., Lewis R.
Extreme diversity, conservation, and convergence of spider silk fibroin sequences
Science 291 (2001), 2603-2605.

Gosline J.M., French C.J.
Dynamic mechanical properties of elastin
Biopolymers 18, (1979), 2091-2103

Guinea G.V., Rojo F.J., Elices M.
Brittle failure of dry spaghetti
Eng. Failure Anal. 11 (2004), 705

Guinea G.V., Pérez-Rigueiro J., Plaza G.R., Elices M.
Volume constancy during stretching of spider silk
Biomacromolecules 7(7) (2006), 217
3-2177

Guinea G.V., Elices M., Pérez-Rigueiro J., Plaza G.R.
Structure and properties of spider and silkworm silk for tissue engineering in Silk Biomaterials (s.c. Kundu Ed.) cap. 9 (2023).

Guinea G.V., Elices M., Pérez-Rigueiro J., Plaza G.R.
Stretching of supercontracted fibers: A link between spinning and the variability of spider silk
Journal of Experimental Biology 208(1) (2005a), 25-30

Guinea G.V., Elices M., Real J.I., Gutiérrez S., Pérez-Rigueiro J.
Reproducibility of the tensile properties of spider (Argiope trifasciata) silk obtained by forced silking
Journal of Experimental Zoology Part A – Compartive Experimental Biology 303A (2005b), 37-44

Hakimi O., Knight D.P., Vollrath F., Vadgama P.
Spider and mulberry silkworm silks as compatible biomaterials
Compos Pt B: Eng 38 (2007), 324-337

Harley, R., D. James, A. Miller, and White. J. W.
Phonons and the elastic moduli of collagen and muscle
Nature. 267 (1977) :285–287.

Hazen A.
Flood Flows: A Study of Frequencies and Magnitudes
John Wiley & Sons, New York (1930)

Hebert J.J., Thibodeaux D.P., Shofner F.M., Singletary J.K., Patelke D.B.
A new single fiber tensile tester
Text Res J 65, (1995), 440-444

Heim, A. J., W. G. Matthews, and T. J. Koob.
Determination of the elastic modulus of native collagen fibrils via radial indentation
Appl. Phys. Lett. 89 (2006) :181902.

Hingorani RV, Provenzano PP, Lakes RS, Escarcega A, Vanderby R.
Nonlinear viscoelasticity in rabbit medial collateral ligament
Ann Biomed Eng 32 (2004) :306–312.

Hudspeth M., Nie X. Chen W., Lewis R.
Effect of loading rate on mechanical properties and fracture morphology of spider silk
Biomacromolecules 13(8) (2012), 2240-2246

James H.M., Guth E.
Theory of the elastic properties of rubber
J Chem Phys 11, (1943), 455-481

Jefferies R., Jones D. M., Roberts J. G., Selby K., Simrnens S. C., Warwicker J. O.
Current ideas on the structure of cotton
Cell Chem Tech 3, (1969), 255-274

Johnson T.P.M., Socrate S., Boyce M.C.
A viscoelastic, viscoplastic model of cortical bone valid at low and high strain rates
Acta Biomaterialia 6, (2010), 4073-4080

Kadler K. (1994)
Extracellular matrix. 1: Fibril-forming collagens
Protein Profile 1, 519-638

Kerr T.
The structure of the growth rings in the secondary wall of the cotton hair
Protoplasma 27(1), (1937), 229-241

Kolken H. M. A., Lietaert K., Sloten T., et al.
Mechanical perfomance of auxetic meta-biomaterials.
Journal of the Mechanical Behaviour of Biomedical Materials 404 (2020) 103658

Lakes, R.
Viscoelastic Materials
Cambridge U.P. (2009)

Landau L.D., Lifshitz E.M:
Theory of Elasticity (3ª Ed.)
Pergamon Press (1986)

Le Bourhis E.
Glass: Mechanics and Technology
John Wiley & Sons (2008)

Lee, C.H, Singla, A. Lee, Y.
Biomedical applications of collagen
International Journal of Pharmaceutics, 221 (2001), 1-22

Leikina E, Mertts MV, Kuznetsova N, Leikin S.
Type I collagen is thermally unstable at body temperature
Proc. Natl. Acad. Sci. USA 99 (2002) :1314–18

Letai A., Fuchs E.
The importance of intramolecular ion pairing in intermediate filaments
Proc Natl Acad Sci USA 92 (1995), 92-96

Maher, B.
Tissue engineering: How to build a heart
Nature, 499 (2013), 20–22, doi:10.1038/499020ª

Martel A., Burghammer M., Davies R.J., Riekel C.
Thermal Behavior of Bombyx mori Silk: Evolution of Crystalline Parameters, Molecular Structure, and Mechanical Properties
Biomacromolecules 8 (2007), 3548-3556

Meredith R.
A comparison of the tensile elasticity of some textile fibers
J Textile Inst 36(7), (1945), 147-164

Meyer K.H., Ferri C.
Sur l'élasticité du caoutchouc
Helv Chim Acta 18, (1935), 570-589

Morton W.E., Hearle J.W.S.
Physical Properties of Testile Fibres, 3rd edition
The Textile Institute, Manchester (1993)

Motriuk-Smith D., Smith A., Hayashi C.Y., Lewis R.V.
Analysis of the conserved N-terminal domains in major ampullate spider silk proteins
Biomacromolecules 6 (2005), 3152-3159

Murphy A.R., Kaplan D.
Biomedical applications of chemically-modified silk fibroin
J Mater Chem 19 (2009), 6443-6450

Nakazawa Y., Asakura T.
High-Resolution 13C CP/MAS NMR Study on Structure and Structural Transition of Antheraea pernyi Silk Fibroin Containing Poly(l-alanine) and Gly-Rich Regions
Macromolecules 35 (2002), 2393-2400

New Scientist (2020).
January 15, page 7, January 29, page. 9.

Ng B.H., Chou S.M., Lim B.H., Chong, A.
Strain rate effect on the failure properties of tendons
Proc Inst Mech Eng H. 218 (3) (2004):203-6.

Nimni, M. E., Cheung, D., Strates, B., Kodama M. and Sheikh K.
Chemically modified collagen: A natural biomaterial for tissue replacement
Journal of Biomedical Materials Research, 21 (1987), 6, 741–771

Nissenbaum A.
8000 Years Collagen from Nahal Hemar Cave.
Archaeology and Natural Sciences 5 (1997): 5-9 (en hebreo).

Oesser, S., Proksch, E., Schunck, M.
Prophylactic treatment with a special Collagen Hydrolysate deceases cartilage tissue degeneration in the knee joints
Osteoarthritis and Cartilage 16 (2008):72

Onions W.J.
Wool, an Introduction to its Properties, Varieties, Uses and Production
London: Ernest Benn Ltd. (1962)

Orgel JPRO, Irving TC, Miller A, Wess TJ.
Microfibrillar structure of type I collagen in situ
Proc. Natl. Acad. Sci. USA 103 (2006) :9001–5

Parenteau-Bareil , R., Gauvin , R. and Berthod F.
Collagen-based biomaterials for tissue engineering applications
Materials 3, (2010) 1863-1887; doi:10.3390/ma3031863

Pauling L., Corey R.B.
Two rippled-sheet configurations of polypeptide chains, and a note about the pleasted sheets
Proc Natl Acad Sci USA 39 (1953) 253

Pauling L., Corey R.B., Branson H.R.
The structure of proteins: Two hydrogen bonded helical configurations of the polypeptide chain
Proc Natl Acad Sci USA 37 (1951), 205-211

Pérez-Rigueiro J., Elices M., Llorca J., Viney C.
Effect of degumming on the tensile properties of silkworm (Bombyx mori) silk fiber
Journal of Applied Polymer Science 84(7) (2002), 1431-1437

Perez-Riguero, J., Elices, M., Llorca, J. & Viney, C.
Tensile properties of Argiope trifasciata drag line silk obtained from the spider's web
J Appl Polym Sci 82 (2001), 2245-2251

Pérez-Rigueiro J., Elices M., Llorca J., Viney C.
Tensile properties of silkworm silk obtained by forced silking
Journal of Applied Polymer Science 82(5) (2001), 1928-1935

Pérez-Rigueiro J., Viney C., LLorca J., Elices M.
Mechanical properties of silkworm silk in liquid media
Polymer 41(23) (2000), 8433-8439

Perez-Riguero, J., Viney, C., Llorca, J. & Elices, M.
Silkworm silk as an engineering material
J Appl Polym Sci 70 (1998), 2439-2447

Pérez-Rigueiro J., Elices M., Plaza G.R., Real J.I., Guinea G.V.
The effect of spinning forces on spider silk properties
Journal of Experimental Biology 208(14) (2005), 2633-2639

Peters L., Woods H.J.
Protein fibres
en Mechanical Properties of Textile Fibres (MeredithR., Ed.), North-Holland, Amsterdam (1956)

Planas J., Guinea G.V., Elices M.
Constitutive model for fiber-reinforced materials with deformable matrices
Phys Rev E 76 (2007), 041903.1-9

Plaza G.R., Guinea G.V., Pérez-Rigueiro J., Elices M.
Thermo-hygro-mechanical behavior of spider dragline silk: Glassy and rubbery states
Journal of Polymer Science Part B – Polymer Physics 44(6) (2006), 994-999

Plaza, G. R., Pérez-Rigueiro J., Riekel C., Perea G.B., Agulló-Rueda F, Burghammer M., Guinea G.V., Elices M.
Relationship between microstructure and mechanical properties in spider silk fibers: two regimes in the microstructural changes.
Soft Matter 8, (2012), 6015–6026

Ramshaw JAM, Shah NK, Brodsky B.
Gly-X-Y tripeptide frequencies in collagen: A context for host-guest triple-helical peptides
J. Struct. Biol. 122 (1998) :86–91

Rogers G.E.
Genetic engineering for novel fibers
J Text Inst 91 (2000), 24-31

Romero de Ávila, M.D., Escudero, R., Ordóñez, J.A., Cambero, M.I.
Weibull analysis characterizes the breaking properties of dry-cured ham slices
Meat Science 97 (2014), 451-458

Sasaki, N., and Odajima, S.
Stress-strain curve and Young's modulus of a collagen molecule as determined by the x-ray diffraction technique
J. Biomech. 29 (1996):655–658.

Sasser P.F., Shofner F.M., Chu Y.T., Shofner C.K., Townes M.G.
Interpretations of single fiber, bundle, and yarn tenacity data
Text Res J 61, (1991), 681-690

Schechtman, H., Bader, D. L
In vitro fatigue damage of human tendons
J. Biomech. 30 (8) (1997): 829-835.

Schwartz P. (Ed.)
Structure and Mechanics of Textile Fiber Assemblies
Woodhead Pub. Cambridge (2008)

Shen, Z.L., Dodge, M.R., Kahn, H., Ballarini, R., Eppell, S.
Stress-Strain Experiments on Individual Collagen Fibrils
Biophysical Journal 95 (2008), 3956-3963

Shoulders M.D. and Raines R.T.
Collagen Structure and Stability
Annu. Rev. Biochem.78 (2009), 929–58

Simpson W.S., Crawshaw G.H.
Wool: Science and Technology
Woodhead Pub. Ltd. (2002)

Smart J., Williams J.C.
A comparison of single-integral non-linear viscoelastic theories
J. Mech. Phys. Solids (1972), 20, 313-324

Smith, C.A. and Wood, E.J.
Biological Molecules
Chapman and Hall, Londres (1991)

Soderhall, C., I. Marenholz, T. Kerscher, F. Ruschendorf, J. Esparza-Gordillo, M. Worm, C. Gruber, G. Mayr, M. Albrecht, K. Rohde, H. Schulz, U. Wahn, N. Hubner, and Y. A. Lee.

Variants in a novel epidermal collagen gene (COL29A1) are associated with atopic dermatitis
PLoS Biology 5 (2007):1952-1961.

Sparrow J.T.
The Fracture of Cotton
Ph.D. Thesis, Univ. of Manchester (1973)

Speakman J.B.
Intracellular structure of the wool fibre
J Text Inst 18 (1927) T431-T453

Termonia Y.
Molecular modeling of the stress/strain behaviour of spider dragline in Structural Biological Materials (M. Elices Ed.) Pergamon Press (2000)

Thibodeaux D.P., Hebert J.J., Abd El-Gawad N.S., Moraitis J.S.
Quality measurements – relating bundle strength to mantis single fiber strength measurements
Cotton Sci 2, (1998), 62-67

Treloar L.R.G.
The Physics of Rubber Elasticity (3ª Ed.)
Clarendon Press (1975)

Treloar L.R.G.
Stress-strain data for vulcanised rubber under various types of deformation
Trans Faraday Soc 40 (1944), 59-70

Van der Rijt, J. A. J., K. O. van der Werf, M. L. Bennink, P. J. Dijkstra, and J. Feijen.
Micromechanical testing of individual collagen fibrils
Macromol. Biosci. 6 (2006) :697–702

Vincent J.
Structural Biomaterials
Princeton U.P. (1990)

Vollrath F., Porter D.
Spider silk as archetypal protein elastomer
Soft Matter 2 (2006), 377-385

Ward I. M., Sweeney J.
An Introduction to the Mechanical Properties of Solid Polymers (2ª Ed.)
Wiley (2004)

Ward, A.G., Courts, A.
The Science and Technology of Gelatin
New York: Academic Press. ISBN 0-12-735050-0 (1977).

Warner, S.B.
Fiber Science
Prentice Hall (1995)

Weibull, W.
A statistical distribution function of wide applicability
J. Appl. Mech.-T. ASME, 18, (1951), 293–297

Weibull W.
A statistical theory of the strength of materials
Ingeniors Ventenskaps Akademien Handlingar, 151, (1939)

Weis-Fogh T.
Thermodynamic properties of resilin, a rubber-like protein
J Mol Biol 3, (1961), 520-531

Weiss JA, Gardiner JC.
Computational modeling of ligament mechanics.
Crit Rev Biomed Eng 29 (2001) 303-71

Wenger,M.P.E., Bozec,L., Horton,M.A., Mesquida, P.
Mechanical Properties of Collagen Fibrils
Biophysical Journal 93 (2007), 1255–1263

Wineman A.S., Rajagopal K.R.
Mechanical Response of Polymers
Cambridge U.P. (2000)

Work R.W., Young C.T.
The amino acid compositions of major and minor ampullate silks of certain orb-web-building spiders (Araneae, Araneidae)
J Arachnol 15 (1987), 65-80

Wu P.D., Giessen E. van der
On improved network models for rubber elasticity and their applications to orientation hardening in glassy polymers
J Mech Phys Solids 41, (1993), 427-456

Zener C.
Elasticity and Anelasticity of Metals
Univ. Chicago Press (1948)

Zhou Z., Confalonieri F., Medina N., Zivanovic Y., Esnault C., Yang T., Jacquet M., Janin J., Dugwet M., Persso R., Li Z.G.
Fine organization of Bombyx mori fibroin heavy chain gene
Nucleic Acids Res 28 (2000), 2413-2419

SUBJECT INDEX